MODELLING CHANGES IN MULTI-DECADAL STREAMFLOW CONTRIBUTIONS – BOLOGNA GLACIER, SELWYN MOUNTAINS, NWT, CANADA

A Thesis Submitted to the
College of Graduate and Postdoctoral Studies
In Partial Fulfillment of the Requirements
For the Degree of Master of Science
In the Department of Geography and Planning
(Centre for Hydrology)
University of Saskatchewan, Saskatoon

By

Emily R. Anderson

Permission to Use

In presenting this thesis in partial fulfilment of the requirements for a Postgraduate degree from the University of Saskatchewan, I agree that the Libraries of this University may make it freely available for inspection. I further agree that permission for copying of this thesis in any manner, in whole or in part, for scholarly purposes may be granted by the professor or professors who supervised my thesis work or, in their absence, by the Head of the Department or the Dean of the College in which my thesis work was done. It is understood that any copying or publication or use of this thesis or parts thereof for financial gain shall not be allowed without my written permission. It is also understood that due recognition shall be given to me and to the University of Saskatchewan in any scholarly use which may be made of any material in my thesis.

Requests for permission to copy or to make other use of material in this thesis in whole or part should be addressed to:

Head of the Department of Geography and Planning
117 Science Place
University of Saskatchewan
Saskatoon, SK Canada
S7N 5C8

Abstract

Climate warming can result in glacier contraction and changes in the coverage of snow, firn, and glacier ice that impact the energy balance and affect the timing and magnitude of streamflow generation. The impact of glacier-climate co-variability on streamflow in Canada's northern continental regions remains undocumented. This study evaluates changes in glacier snow accumulation, ablation, and hydrological regime with changing climate for the Bologna Glacier in the Ragged Range (Selwyn Mountains) headwaters of the South Nahanni River, Northwest Territories. The Bologna Glacier basin was instrumented in 2014 with two meteorological stations that measured air temperature, relative humidity, precipitation, wind speed, and radiation on and off the glacier surface. These short term observations were used to spatially and temporally downscale and bias correct ECMWF Interim Re-Analysis (ERA-Interim) atmospheric reanalyses to construct a meteorological record from 1980 to 2015. Both the rainfall ratio and the average daily maximum summer temperatures were found to be increasing significantly over the study period. Total spring precipitation was found to be decreasing significantly over the time period. The Cold Regions Hydrological Modelling Platform (CRHM) was used to construct a physically based glacier hydrology model that incorporated a new glacier module: an energy balance snow and ice ablation model coupled with a blowing snow and avalanche model to characterize the mass balance of glacier snow and ice. To set up the model, the Bologna Glacier basin was discretized into Hydrological Response Units (HRUs) representing the spatial distribution of hydrological processes, parameters, and driving meteorology. HRUs were delineated by metrics including elevation, slope, aspect, firn limit, and land cover type, using a digital elevation model and Landsat satellite imagery from 1984 and 2014. Reconstructed meteorological data were used to force the model to run over three decades with the former (1984) and contemporary (2014, 2015) glacier geometry and firn limit configuration to determine the effect of climate warming, reduced glacier cover, and increased ice exposure on headwater streamflow generation, which was found to be substantial. Analysis of satellite imagery showed that the glacier area decreased by 14% from 1984 to 2014 (30 years) and that firn coverage was reduced from 82% to 47% over the same time period. Firn coverage entirely disappeared by 2015, as observed during the field trip in August of that year. There was a shift in CRHM-modelled discharge contribution from substantial firn melt contributions to substantial ice melt contributions between the historical and contemporary model configurations.

Results indicate that both annual discharge and ice melt contributions to streamflow increased significantly over the study period. Overall, there was a substantial contribution to streamflow from glacier melt and wastage in all three model configurations. The envelope of annual mass balance was determined to be -9.0 m to -20.3 m water equivalent. The envelope of modelled summertime wastage contribution to measured streamflow at the Virginia Falls gauge in the South Nahanni River was determined to be 2.9 to 6.0%.

Acknowledgements

My relationship with the lands I have written and researched on are bound by Treaty 6 and Treaty 11. These lands are the traditional and contemporary territories of the First Nations signatories of these treaties as well as the Métis homeland. I feel honoured to have done my field research in Nahanni National Park Reserve, home of the Dehcho First Nation, on Treaty 11 territory.

I extend my sincere gratitude to my supervisors, Dr. John Pomeroy and Mike Demuth, for their expertise, guidance, and mentorship throughout my graduate studies. Thank you to my committee member, Dr. Dirk de Boer, and external examiner, Dr. Karl-Erich Lindenschmidt, who provided valuable suggestions for my research. I appreciated the participation of Dr. Alec Aitken, who acted as my committee chair and provided helpful advice throughout my studies.

Many individuals at the Centre for Hydrology provided invaluable support and guidance throughout this project. Special thanks to Kevin Shook for his thoughtful explanations and analytical support, as well as his guidance as I transition to the next stage of my career. Thanks to May Guan for her efforts in the field and her companionship on the road. Thanks to Dr. David Atkinson and Eric Courtin from the University of Victoria for sharing their field data. For help with the model, thanks go to Dhiraj Pradhananga, Tom Brown, and Logan Fang. Thanks to Joni Onclin and Phyllis Baynes, who provided administrative support throughout my time at the Centre. I have been fortunate to have had such a supportive group of peers. To my fellow students: thank you for your help and guidance throughout my graduate studies and, most of all, for your friendship.

This project could not have been completed without funding from the University of Saskatchewan, the Changing Cold Regions Network, the Northern Scientific Training Program, the W. Garfield Weston Foundation for Northern Research, and the Canadian Federation of University Women.

I am grateful for the unwavering support and encouragement from my family, Pat, Ken, and Rachael Anderson, and from my boyfriend, Matt Kozun. Thank you to Pat Keyser for her friendship and for sharing her home with me during my studies. Finally, thank you to Joyce Brooks, who encouraged us to follow our dreams.

To Mom and Dad

Table of Contents

List of Tables

List of Figures

List of Abbreviations

AO	Arctic Oscillation
ASTER	Advanced Spaceborne Thermal Emission and Reflection Radiometer
AWS	Automatic Weather Station
BNI	Bologna North Ice
BNN	Bologna North Nunatak
CDED	Canadian Digital Elevation Model
CDEM	Canadian Digital Elevation Data
CFSR	Climate Forecast System Reanalysis
CRHM	Cold Regions Hydrological Model
CS	Campbell Scientific
CV	Coefficient of Variation
DEM	Digital Elevation Model
EBGM	Energy Balance Glacier Melt model
EC	Environment Canada
ECMWF	European Centre for Medium-Range Weather Forecasts
ELA	Equilibrium Line Altitude
ERA-Interim	ECMWF Interim Re-Analysis
ET	Evapotranspiration
ETM+	Enhanced Thematic Mapper Plus
GDB	Geospatial Database
GIS	Geographic Information System
GLIMS	Global Land Ice Measurements from Space
GLS	Generalized Least Squares
GMSLR	Global Mean Sea Level Rise
GNE	Greater Nahanni Ecosystem
GPS	Global Positioning System
GTOPO30	Global 30 Arc-Second Elevation Dataset
IPCC	Intergovernmental Panel on Climate Change
JISAO	Joint Institute for the Study of the Atmosphere and Ocean
LiDAR	Light Detection and Ranging

LSS	Late Summer Snowline
MK	Mann-Kendall
MSC	Meteorological Service of Canada
NARR	North American Reanalysis
NCEP	National Centers for Environmental Protection
NNPR	Nahanni National Park Reserve
NOAA	National Oceanic and Atmospheric Administration
NRCan	Natural Resources Canada
NTDB	National Topographic Data Base
OLI	Operational Land Imager
PDO	Pacific Decadal Oscillation
SAGA	System for Automated Geoscientific Analysis
SOI	Southern Oscillation Index
STRM	Shuttle Radar Topography Mission
SW	Shortwave Radiation
SWE	Snow Water Equivalent
TM	Thematic Mapper
UNESCO	United Nations Educational, Scientific and Cultural Organization
V-A Scaling	Volume-Area Scaling
WATCH	Water and Global Change
w.e.	Water Equivalent
WFD	WATCH Forcing Data
WFDEI	WATCH Forcing Data ERA-Interim
WGMS	World Glacier Monitoring Service
WSC	Water Survey of Canada
YG	Yukon Government

1 INTRODUCTION

Mountain glaciers are highly sensitive to changes in climate (Kaser et al., 2004; Haeberli et al., 2007; IPCC, 2013). Glacier coverage has been widely shown to be diminishing around the globe in recent years (Zemp et al., 2014). Because glaciers are relatively small bodies of ice, compared to ice sheets and ice shelves, they are effective indicators of climate change and demonstrate a climate change signal on a human time scale (Zemp et al., 2014). Mountain glaciers and ice caps – not including the Greenland or Antarctica ice sheets – are predicted to be the main contributors to sea level rise throughout the 21st century (Meier et al., 2007; IPCC, 2013), and glacier discharge can have a significant effect on the magnitude and timing of streamflow, with significant implications for downstream communities and ecology (Fountain and Tangborn, 1985; Demuth and Pietroniro, 2003; Petts et al., 2006).

Glaciers have a diurnal, seasonal, and annual influence on streamflow (Meier and Tangborn, 1961; Stahl and Moore, 2006). They act as hydrological storage by retaining snowfall in wet, cool periods and releasing it as streamflow it in hot, dry periods (Jansson et al., 2003). In this way, they regulate seasonal and annual streamflow. Changes to glacier coverage can significantly alter discharge (Chen and Ohmura, 1990b). As glacier volume decreases due to warming, discharge will initially increase until the volume reaches a certain threshold, at which time it will continuously decrease (Braun and Esher-Vetter, 1996; Collins, 2008; IPCC, 2014).

There is unequivocal evidence of rapid climate change in northern high latitudes, where temperature increases are the most severe around the globe (Liu et al., 2007; IPCC, 2013). The cryosphere in this region has experienced some of the most rapid changes on Earth (Derksen et al., 2012). Glacier change in the Arctic has been widely studied (Hodgkins et al., 2009; Gardner et al., 2011; Sharp et al., 2014; etc.); however, there is a lack of research in the northern continental interior of Canada. Glaciers of Nahanni National Park Reserve in the Ragged Range of the Northwest Territories have been rapidly diminishing over the past three decades (Demuth et al., 2014). These headwater glaciers feed the South Nahanni River, which eventually drains into the Mackenzie Delta. The effect of glaciers and glacier change on streamflow regimes in the northern continental region of Canada is so far unknown. This research will provide a baseline analysis of glacier-hydrological regimes in this environmentally significant frontier region.

1.1 Scholarly and Societal Relevance

Scholarly: This is a contribution to scholarly research given the rapid environmental change occurring in northern high latitudes and a lack of understanding of the effect of climate change on glaciers in this cold continental region. The contribution to global mean sea level rise from glaciers has the highest uncertainty of any other contributing component (Figure 1.1). This research aims to aid in closing the gap in this uncertainty.

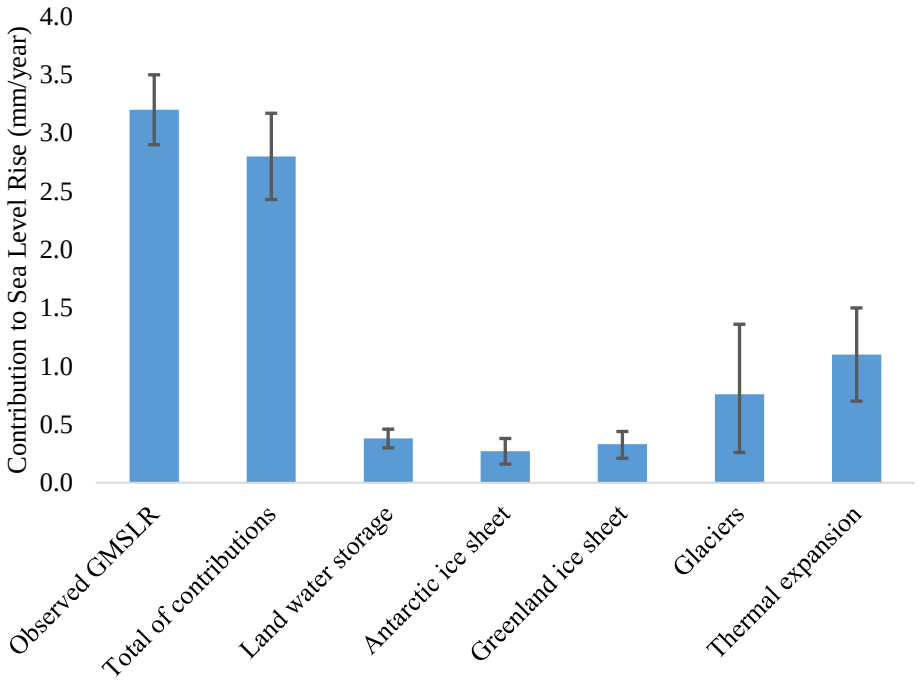

Figure 1.1: Global Mean Sea Level Rise (GMSLR), 1993 – 2010. Data source: Table 13.1, page 1151 in IPCC WG I (Church et al., 2013).

Societal: Glaciers are widely recognized to be robust indicators of climate change (IPCC, 2013). This research will aid in understanding the progression of climate change in the northern continental region of Canada. Such an understanding will contribute to mounting evidence of significant climate change in Canada, with implications for the environment and society alike. Regional effects of the glaciers of Nahanni National Park Reserve are also significant, as perennial snow and ice influence the local climate as well as the ecosystems reliant on the characteristics of local rivers (Letréguilly, 1988; Petts et al., 2006). Local wildlife and vegetation depend on this climate, and the Dehcho First Nation continues to rely on the land for hunting (Parks Canada, 2002).

1.2 Purpose and Objectives

There is unequivocal evidence of rapid climate change in northern latitudes, with average temperatures in the Arctic rising at almost twice the global average over the past few decades (Liu et al., 2007). Over the past four decades, increasing surface air temperatures in this region have led to an accelerating loss of glacier volume (Derksen et al., 2012). It is projected that high latitude glaciers will continue to experience the highest ice volume loss (Radić et al., 2013; Sharp et al., 2014). A 2008 glacier inventory of the Ragged Range in the Northwest Territories showed that regional glacier coverage has decreased by 30% since 1982, with the complete loss of 60 glaciers (Demuth et al., 2014). Glaciers influence streamflow on diurnal to decadal timescales, and given the significant change in glacier coverage, it is hypothesized this glacier loss has influenced streamflow regimes. The purpose of this research is to evaluate how glacier cover and glacier change affect streamflow in the northern continental region of Canada.

Purpose: To evaluate the impact of climate change, reduced glacier cover, and increased ice exposure on headwater streamflow generation from the Bologna Glacier.

Objectives:

1. Quantify recent changes in glacier configuration and climate.
2. Calculate the basin water budget and glacier mass balance.
3. Determine whether there are trends in hydro-meteorological and glaciological variables that control streamflow and whether they are influenced by changing glacier configuration.
4. Evaluate how changing glacier configuration affects local and regional basin hydrology.

2 LITERATURE REVIEW

This section provides background information on glaciers and their fluctuations, followed by a discussion of the current state of knowledge of glacier hydrology and changing glacier-hydrological regimes. Methods for evaluating glacier contribution to streamflow are described. The review highlights gaps in the literature and provides a foundation for this research.

2.1 Background

2.1.1 Glaciers and their Fluctuation

A glacier forms when snow remains in an area without entirely ablating during the warm or dry period of the year. The deposition of new seasonal layers year after year will gradually compact and compress the underlying layers, transforming them into firn and eventually into ice (Benn and Evans, 1998). Firn is transformed into glacier ice when the interconnecting air and water passages between grains are compressed, a process called *pore close-off* (Cuffey and Paterson, 2010). A region's climate will determine the process that transforms snow into glacier ice and the time it takes for this process to occur (Benn and Evans, 1998). Glaciers gain and lose ice mass through multiple processes, including gaining mass through snowfall, blowing snow deposition, and avalanching, and losing mass through wind erosion of snow, calving of ice, melting, and sublimation (Benn and Evans, 1998; Cuffey and Paterson, 2010). A glacier is divided into two zones: the *accumulation zone* in which mass gain exceeds mass loss and the *ablation zone* in which mass loss exceeds mass gain. The two zones are divided by an equilibrium line where the mass balance is in equilibrium or zero (Cogley et al., 2011). The glacier equilibrium line altitude (ELA) is defined as the average elevation of the equilibrium line, where ablation is equal to accumulation (Hoinkes, 1970; Benn and Lehmkuhl, 2000; Cuffey and Paterson, 2010).

This layered mass of snow, ice, and firn eventually becomes large enough such that it will deform under the force of gravity. Glaciers flow under the influence of gravity by sliding, deformation of the ice, and deformation of the glacier bed. Mass is transferred from the accumulation zone to the ablation zone by these processes. A glacier is in equilibrium when the rate of glacier flow balances the rates of accumulation and ablation (Benn and Evans, 1998).

2.1.2 Glacier Wastage and Melt

Glaciers contribute to streamflow via seasonal snowmelt and glacier melt. These processes are often poorly defined in the literature. To understand glacier influence in a basin, it is essential to define terminology related to glacier contribution to streamflow and to differentiate the terms "wastage" and "melt," as defined in Comeau et al. (2009). The distinction between the two terms is important when considering the potential effects of declining glacier cover on streamflow. The derivation of these terms are detailed below, as in Comeau et al. (2009):

Glacier mass balance, $\frac{dm}{dt}$, can be defined by the inputs and outputs of the system:

$$\frac{dm}{dt} = P_s - M_s - M_i - S - R \tag{2.1}$$

Where P_s is snowfall; M_s is snowmelt, M_i is ice melt, S is sublimation, and R is losses and/or gains due to avalanches, blowing snow redistribution, and ice calving. This equation is simplified assuming that (1) sublimation is negligible and (2) that there are no gains or losses from blowing snow or avalanching or any losses from ice calving:

$$\frac{dm}{dt} = P_s - M_s - M_i \tag{2.2}$$

At the end of a hydrological year (September 30th), the input of snow that remains on the glacier ($P_s - M_s$) is added to the glacier system and will metamorphose into firn and eventually ice under subsequent layers of new snow, provided it does not melt the following year. If the glacier is in equilibrium ($\frac{dm}{dt} = 0$), then:

$$M_i = P_s - M_s \text{ when } \frac{dm}{dt} = 0 \tag{2.3}$$

The annual glacier ice melt (M_i), is equal to the annual input into the glacier system ($P_s - M_s$). If the glacier has positive mass balance ($\frac{dm}{dt} > 0$), then:

$$M_i < P_s - M_s \text{ when } \frac{dm}{dt} > 0 \tag{2.4}$$

Here, annual glacier ice melt is less than the annual input into the glacier system. Melt is therefore defined as "the ice melt volume that is equal to, or less than, the water equivalent

volume of snow that accumulates into the glacier system in a hydrological year" (Comeau et al. 2009). If the glacier has negative mass balance ($\frac{dm}{dt} < 0$), then:

$$M_i > P_s - M_s \text{ when} \frac{dm}{dt} < 0 \tag{2.5}$$

Here, annual glacier ice melt is greater than the annual input into the glacier system and the annual glacier ice melt includes both melt ($P_s - M_s$) and the additional annual ice melt causing the negative net mass balance. Wastage is therefore defined as "the volume of ice melt that exceeds the water equivalent annual volume of snow accumulation into the glacier system, causing an annual net loss of glacier volume" (Comeau et al. 2009):

$$\text{Wastage} = M_i - (P_s - M_s) \text{ when } \frac{dm}{dt} < 0 \tag{2.6}$$

$$\text{Melt} = P_s - M_s \tag{2.7}$$

According to these definitions, a glacier will affect total streamflow in a basin via wastage contributions only. Melt will have a significant effect on streamflow timing given that this volume of snow is stored in the glacier system until ice melt occurs in late summer months. When considering melt as a percentage contribution to streamflow, it can only be evaluated on a seasonal, not annual, scale. Similarly, La Frenierre and Mark (2014) defined melt as "water generated from melting ice in the ablation area exclusive of glacier mass balance state."

An additional significant consequence of ice cover is that glaciers will have localized influences on climate which can affect snow accumulation and melt, on and off the glacier (Letréguilly, 1988; Hannah et al., 2000; Oerlemans, 2010; Petersen and Pellicciotti, 2011). Hannah et al. (2000) observed strong topographic controls on the microclimate of the Taillon Glacier in the French Pyrénées and that the magnitude and partitions of the energy balance components varied widely with time and weather conditions. The presence of ice also affects katabatic wind flow, which reduce snowmelt rates on and downwind of the ice. Petersen and Pellicciotti (2011) found that katabatic wind flow was the main controller of the temporal and spatial variability of lapse rates over the Juncal Norte Glacier in Chile. Under the definitions of wastage and melt, it is important to consider the feedback effects of the presence of the glacier itself – the

corresponding impact the energy balance and katabatic wind flow will have on glacier accumulation and melt.

2.2 Glacier Storage

Glaciers are natural reservoirs of water that have a significant influence on the hydrology of alpine basins over varying time scales. The glacier itself acts as a storage body for water in the solid form as ice, firn, and snow, in addition to the storage of water held in snow and firn, crevasses, englacial pockets and conduits, supraglacial channels and ponds, subglacial cavities and conduits, and basal sediments (Jansson et al., 2003). The various storage capacities of glaciers are shown over short, intermediate, and long term timescales in Figure 2.1. These storage capacities have significant influence on the storage and release of water and many studies have reported on the significant influence of glacier discharge on streamflow ranging from diurnal to annual timescales (e.g. Meier and Tangborn, 1961; Fountain and Tangborn, 1985; Schuster and Young, 2006). It is essential to understand and quantify the retention and release of water by glaciers considering the significant implications for downstream agricultural, domestic, and industrial needs as well as determining consequences for sensitive hydroecological environments (Chen and Ohmura, 1990b; Petts et al., 2006; Moore et al., 2009). The following sections will describe glacier storage on three timescales, with a focus on the impact of storage on catchment hydrology.

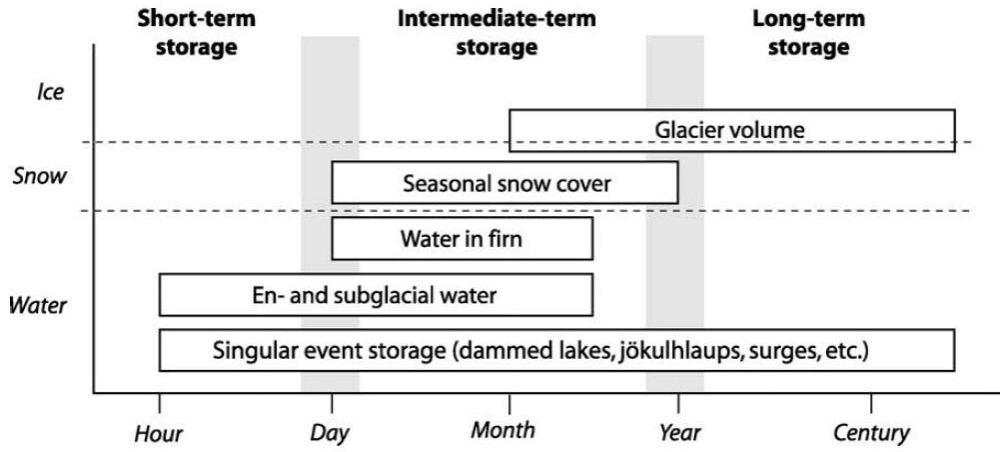

Figure 2.1: Mechanisms of glacier storage at various time scales (From Jansson et al., 2003, reproduced with permission of Elsevier. Copyright © 2003)

2.2.1 Long-term Storage

Glaciers act as storage of water in the form of ice and snow over years, centuries, and longer. Variation in climate over these timespans will result in a net storage or release of water (Jansson et al., 2003). Glaciers moderate annual runoff volumes by retaining precipitation in cool, wet years and releasing flow in warm, dry years (Meier and Tangborn, 1961; Chen and Ohmura, 1990b). The regulating ability of a glacier produces predictable streamflow downstream of the headwaters, the stability of which has implications for water supply, hydroelectric facilities, freshwater habitat, and flood hazards (Fleming and Clarke, 2005; Moore et al., 2009). This effect is observed even in basins with a lower percentage of glacier cover (Hock et al., 2005).

Variations in glacier cover have been found to affect the seasonal and annual coefficients of variation (CV) of streamflow (Fountain and Tangborn, 1985; Moore, 1992; Demuth and Pietroniro, 2003; Fleming and Clarke, 2005). Annual variability is typically lower for glacierized basins than for non-glacierized basins (Jansson et al., 2003). Several studies have found that a moderate coverage will have the lowest CV and a basin with either higher or lower coverage will experience more annual variability (Fountain and Tangborn, 1985; Demuth and Pietroniro, 2003; Hock et al., 2005). Chen and Ohmura (1990b) reported that annual glacier runoff variability is at a minimum for moderate glacier cover (40%) and increasing or decreasing glacier cover will lead to increased variability.

2.2.2 Intermediate-term Storage

Seasonal runoff is regulated by a high volume of precipitation stored in winter and released in summer (Meier and Tangborn, 1961). This produces a distinctive hydrograph for glacier-fed rivers where peak runoff is delayed until late summer (Meier, 1969; Fountain and Tangborn, 1985). The presence of ice will help retain local and even regional seasonal snow volumes further into the melt season compared to non-glacierized basins (Hannah et al., 2000; Oerlemans, 2010).

Glaciers act as regulators of a relatively unlimited supply of meltwater after the snowpack has been exhausted (Meier, 1969; Fountain and Tangborn, 1985). During dry summer months, glaciers sustain flow, which compensates for a reduction in streamflow from other sources

(Radić and Hock, 2014). Even basins with a very low percentage glacier coverage will exhibit this pattern in late summer (Stahl and Moore, 2006).

The rate of meltwater production from glaciers in the summer is primarily controlled by incoming solar radiation and the glacier surface albedo (Meier, 1969). The albedo of dry snow is roughly 80% whereas firn and clean ice are roughly 50% and 40% respectively (Oerlemans and Knap, 1998; Schuster et al., 2006). During May and June, melt rates remain moderate because of the high albedo of snow. In July and August, the rising transient snowline exposes firn and glacier ice and high melt rates occur due to the lower albedo (Meier, 1969). Because of this, glaciers contribute the highest volumes to streamflow in the late summer months. Firn cover has also been observed to have a strong influence on melt rates (e.g. Braun and Escher-Vetter, 1996). Since firn is permeable, it can act as a storage body for precipitation, further delaying runoff (Fountain, 1996; Jansson et al., 2003). This storage capacity ceases if the firn pack entirely disappears from a glacier's surface.

2.2.3 Short-term Storage

Short-term storage includes volumes of water stored in snow, firn, and en- and subglacial storage. This can have a significant effect on the diurnal variations in glacier runoff. Figure 2.2 shows a typical curve of evolving diurnal variations for Peyto Glacier (Schuster and Young, 2006). In June and early July, diurnal variations in energy and melt are buffered by the snowpack (Fountain, 1996). From mid-July onwards, as radiation and exposed glacier ice area increases, the amplitude of the diurnal variation increases (Braun and Escher-Vetter, 1996; Schuster and Young, 2006). These fluctuations are also a result of the continuously developing drainage system, which increases the efficiency with which meltwater is removed from the glacier (Singh and Singh, 2001; Schuster and Young, 2006). The combined impact is observed in the diurnal cycle of glacier discharge where, as the ablation season progresses, the amplitude of the diurnal discharge peaks increases significantly and the timing of the peak shifts (Hock et al., 2005). Daily peak discharge can exceed daily minimum discharge by several hundred percent (Hock et al., 2005).

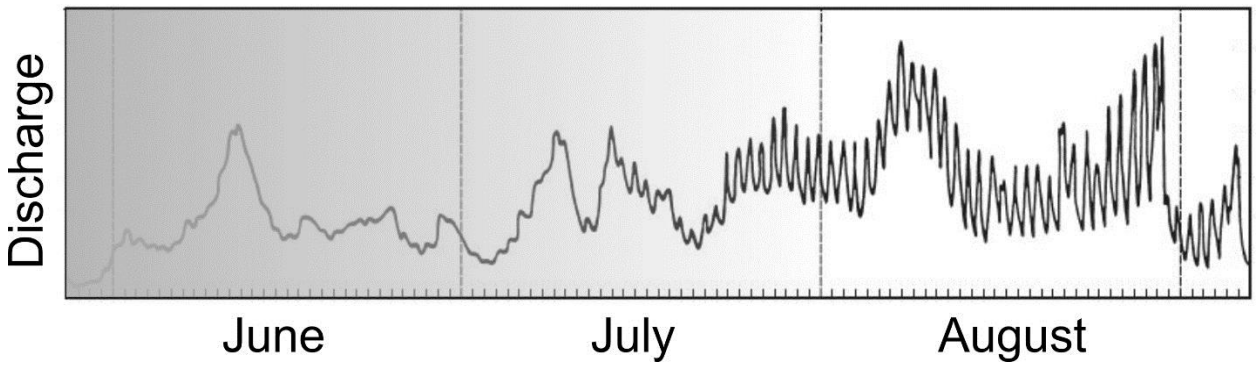

Figure 2.2: Typical discharge pattern (hourly resolution) for a mountain glacier in the temperate latitudes (northern hemisphere), illustrating the evolution of a fully developed diurnal signal (adapted from Schuster and Young (2006) by M. N. Demuth, Natural Resources Canada, reproduced with permission)

2.3 Impact of Climate Change on Glacier Streamflow

Climate change can influence the capacity of glaciers to store and release water on all timescales. Rapidly increasing temperatures are significant because glacierized basins are most sensitive to changes in temperature (Singh et al., 2006), whereas basins with little glacier cover are more sensitive to changes in precipitation (Braun et al., 2000; Fleming and Clarke, 2003). However, glacier response to climate change is relatively slow, and a glacier's current configuration depends on the conditions of the previous year and, with decreasing influence, the climate extending back decades and centuries (Meier, 1969). Glacier response lags current temperature increases and glaciers will continue to diminish even with no further climate warming (IPCC, 2013; Mernild et al. 2013). The primary impact of a warming climate on glacier runoff is initially higher melt rates, which causes increased streamflow (Hock et al., 2005).

In the long term, rising temperatures can cause a decrease in the net volume of a glacier, contributing to a transient increase in glacier discharge and an increase in sea level. Glaciers comprise a relatively small proportion of the global cryosphere (IPCC, 2013). However, numerous studies attribute rising sea levels largely to global glacier and ice sheet mass losses and glacier contributions will continue to dominate sea level rise into the next century (Arendt et al., 2002; Meier et al., 2007; Hock et al., 2009; Radić et al., 2013).

On an intermediate term basis, climate change influences regional accumulation and ablation, which will affect seasonal contributions to flow. Climate warming in glacierized basins will reduce the relative volume of precipitation falling as snow and influence the timing of peak runoff towards spring (Demuth and Pietroniro, 2003; Barnett, 2005; IPCC, 2014). There has been a well-documented increase in runoff contribution as glaciers experience consecutive seasons of high melting followed by sustained discharge decline once a certain threshold of glacier contraction is reached (Braun and Esher-Vetter, 1996; Collins, 2008; Comeau et al., 2009; IPCC, 2014). Many glaciers, including those in the Canadian Cordillera, may have already passed this threshold (Demuth and Pietroniro, 2003; Stahl and Moore, 2006; Demuth et al., 2008; Marshall et al., 2011).

Higher melt rates caused by a warming climate can affect the diurnal cycles of glacier discharge (e.g. Braun and Escher-Vetter, 1996; Schuster et al., 2006). Short term diurnal cycles of glacier contributions can be exacerbated by early loss of seasonal snow cover and higher temperatures (Lafrenière and Sharp, 2003). Increased exposure of glacier ice, well developed drainage channels, and reduced firn and snow cover contribute to these altered regimes (Hock et al., 2005; Schuster and Young, 2006). Additional feedback effects further intensify the cycle, as shown in Figure 2.3 (Hock et al., 2005).

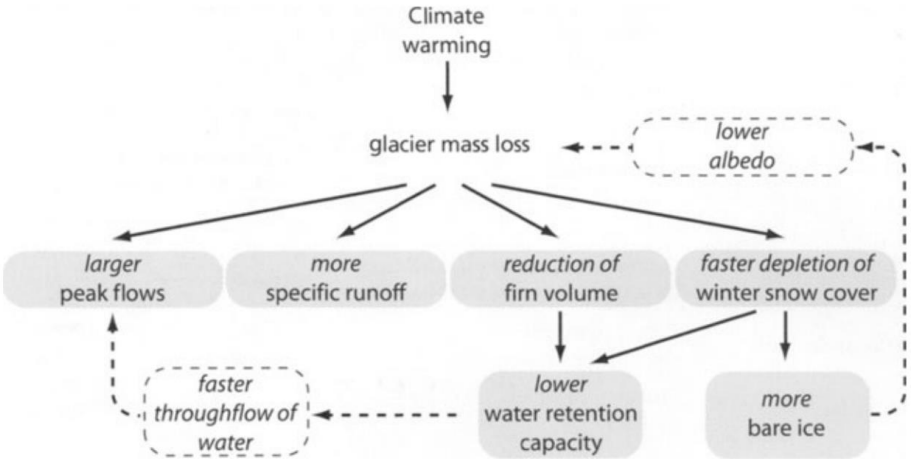

Figure 2.3: Short term effects of climate warming on glacier discharge (From Hock et al., 2005, reproduced with permission of Springer. Copyright © 2005)

2.4 Evaluating Glacier Contribution to Streamflow

Evaluating glacier contribution to streamflow is essential to determine the impact of the presence of glaciers in a watershed. It is also increasingly important to understand the effects of glacier retreat due to climate change and the corresponding effects on streamflow. Methods for estimating the contribution of snowmelt and glacier wastage to streamflow can be grouped into five broad categories: direct discharge measurement, glaciological approaches, hydrological balance, hydrochemical tracers, and hydrological modelling. It is important to note that not all methods can differentiate between glacier melt and wastage. Direct discharge measurement, hydrological balance equations, and hydrochemical tracers do not differentiate between glacier melt and wastage while glaciological methods (those that include mass balance measurements) and hydrological modelling can differentiate between melt and wastage (La Frenierre and Mark, 2014). Often a combination of techniques are used to provide a comprehensive assessment of a glacier-climate system.

2.4.1 Direct Discharge

This method measures proglacial streamflow immediately downstream of the glacier and compares it to measurements taken further downstream (e.g. Gascoin et al., 2011). While this is the simplest method to quantify glacier contribution to streamflow, monitoring presents logistical difficulties given potential problems in accessing the glacier tongue and the dynamic channel conditions of the proglacial stream (La Frenierre and Mark, 2014). This method assumes that the gauge directly downstream of the tongue measures all the glacier meltwater discharge (none is lost to groundwater) and that all flow derived from the tongue is of glacial origin. It cannot distinguish between melting ice, melting seasonal snow, direct precipitation runoff, or groundwater contributions from outside the basin (Gascoin et al., 2011).

2.4.2 Glaciological

Glaciological methods attempt to quantify glacier contribution to streamflow by quantifying the volume of ice melting from a glacier and determining the proportion of flow downstream derived from the glacier (e.g. Demuth et al., 2008). Glacier volume loss can be determined via mass balance measurements or remote sensing.

The most common way to quantify glacier volume change is with direct mass balance measurements (Østrem and Brugman, 1991). Benn and Evans (1998) define glacier mass balance as "the difference between gains and losses (expressed in terms of water equivalent) measured over a specified time period, usually one year." The annual mass balance, b_n, is the sum of the winter balance, b_w, and summer balance, b_s:

$$b_n = b_w + b_s \tag{2.8}$$

Specific annual mass balance is the net mass balance at a specific point on a glacier, expressed per unit area (Benn and Evans, 1998; Cogley et al., 2011). This can be subdivided into surface, englacial, and basal mass balance; however, a fundamental assumption is that the surface balance will represent the accumulation and ablation rates of the glacier (Collier, 1958; Cuffey and Paterson, 2010).

Glacier mass balance is a key indicator of climate change as these fluctuations reflect a direct response to climate forcing (Demuth and Keller, 2006; Kaser et al., 2006). Fluctuations in the advance or retreat of glacier margins can also signify a delayed adjustment and thus glacier records can provide both short and long term perspectives on climate change (Dyurgerov and Meier, 2000; Demuth and Keller, 2006). Successive years of non-zero mass balances indicate climate forcing and increasing differences in successive years signal accelerating change (Haeberli et al., 2007). Glacier mass balance measurements have been used extensively to attempt to quantify streamflow regime changes (e.g. Moore and Demuth, 2001; Demuth and Pietroniro, 2003).

This method has some limitations given that mass balance and discharge monitoring programs are rarely simultaneous (Hock et al., 2005). Mass balance measurements tend to be sparse and relatively brief, especially in the Arctic and at high elevations (Agnew et al. 2002). Measurements have been extrapolated to characterize glacier volume change in an entire watershed (e.g. Hopkinson and Young, 1998; Demuth et al., 2008; Huss et al., 2011). Fleming and Clarke (2003) note that "mass balance is not a comprehensive and unique descriptor of the potential streamflow effects of glacioclimatic variability." For example, an increased amplitude in the mass balance cycle (resulting in no net change to ice mass) may increase streamflow generation. Additionally, a focus on mass balance–proglacial runoff relationships may exclude

streamflow contributions that are non-glacial including groundwater, vegetation, lake, and wetland cover, and precipitation runoff.

An additional drawback of using measurements from direct mass balance studies to assess hydrological contributions is that measurements tend to be sparsely distributed and geographically biased (Mernild et al., 2013). This results in a bias of global glacier mass balance measurements toward small glaciers instead of those containing the most ice (Cogley and Adams, 1998; WGMS, 1998). However, this bias is being reduced as a result of the World Glacier Monitoring Service (WGMS) and Global Land Ice Measurements from Space (GLIMS) collaborating with observing practitioners and stakeholders (M. N. Demuth, WGMS Canadian National Correspondent, personal communication).

Remote sensing techniques can be used to estimate changes in glacier volume, from which glacier mass can be determined based on an assumption of surface densities. This method is referred to as the geodetic technique (Cogley et al., 2011). This technique has been successful because many glaciers currently exhibit high ice exposure, meaning that any changes in volume can easily translate to mass loss. The geodetic (mass balance) method proves to be an advantageous technique because the spatial and temporal scale of analysis may be larger than that of the direct, or glaciological, method of measuring mass balance. The unique spectral properties of snow and ice allow for accurate delineation of glaciers; however, debris covered ice can introduce higher complexity (Quincey et al., 2014). Multi-temporal satellite digital elevation models (DEMs), including the Shuttle Radar Topography Mission (STRM) and Advanced Spaceborne Thermal Emission and Reflection Radiometer (ASTER) have been used to estimate elevation changes of glaciers, which can indicate changes in thickness and size (Paul and Haeberli, 2008; Radić et al., 2013). These methods tend to produce low-quality DEMs, which can be related to historical DEMs (e.g. Khromova et al., 2003; Bolch et al., 2008; Svobodo and Paul, 2009) but they are not suitable for inter-annual change detection (M. N. Demuth, personal communication). Glacier hypsometry has been detected using airborne light detection and ranging (LiDAR) technologies (Hopkinson and Demuth, 2006; Hopkinson et al., 2010). Remote sensing images are frequently used to delineate historical and contemporary glacier boundaries (e.g. DeBeer and Sharp, 2007; Demuth et al., 2008; Kargel et al., 2014).

Many studies have used remotely sensed data along with empirical volume-area scaling relationships to attempt to quantify the volume of ice wastage. This method has been widely applied in the Canadian Cordillera (e.g. DeBeer and Sharp, 2007; Demuth et al., 2008; Comeau et al., 2009; Barrand and Sharp, 2010; Marshall et al., 2011). Volume-area scaling uses an empirical scaling equation based on glacier area to determine glacier volume. Chen and Ohmura (1990a) performed volume-area scaling in the early 1990s for which Bahr et al. (1997, 2015) later provided the physical basis. Glacier volume, V (10^6 m^3), of an alpine valley glacier is related to its area, A (10^6 m^2), by:

$$V = cA^{\gamma} \tag{2.9}$$

The scaling parameters c and γ are equal to 28.5 and 1.375 (for valley glaciers), respectively, calibrated on world-wide observations of glaciers (Chen and Ohmura, 1990a; Bahr et al., 1997). These values are considered to be global averages (Chen and Ohmura, 1990a) and caution should be used when applying these empirical relationships (Marshall et al., 2011). For example, the highly erodible limestone and dolstone that dominates the Canadian Rocky Mountains results in higher glacier volumes for a given observed area-wise change (M. N. Demuth, personal communication). The relationship was originally derived empirically, though the value of γ has been supported in the derivation of the parameter from the underlying physics in Bahr et al. (1997, 2015). The dimensionless scaling coefficient, *c*, cannot be derived and is more sensitive, therefore it can be regionally adjusted (Clarke et al., 2009). One caution of using a subset of the global parameters for *c* is that the accuracy of the scaling relationship is also a function of the size of the sample used in estimating the scaling parameters. Therefore, limitations exist for using a scaling relationship calibrated with local parameters (Farinotti and Huss, 2013). The scaling parameter can vary by glacier, region, time, slope, climate parameters, or other factors and the error in the calculated volume is proportional to the error in the scaling parameter (Bahr et al., 2015). Arendt et al. (2006) used a subset of all nontidewater glaciers to find a value for *c*, and discussed the limitations of the method in applying the equation to a single glacier. Barrand and Sharp (2010) calculated the volume of an ensemble of Yukon glaciers using various values of c from the literature including Chen and Ohmura (1990a), Bahr et al. (1997), Arendt et al. (2006), and DeBeer and Sharp (2007) and found that the resulting volume estimates varied by up to 44%.

Estimates of glacier volume and volume change using volume-area scaling can be over or underestimated due to errors in glacier surface area measurement and in the scaling relationship itself (DeBeer and Sharp, 2007; Demuth et al., 2008; Marshall et al., 2011). Area estimation depends on the accuracy with which glacier margins can be identified given image resolution, snow conditions, contrast between ice and surrounding terrain, and debris-covered ice (DeBeer and Sharp, 2007). Caution should be used when applying the relationship to individual glaciers; Meier et al. (2007) estimate an error of 50% in applying the relationship to a single ice mass. High error for individual glaciers can be a result of complex eroded bed topography or unusual ice flow regimes (Marshall et al., 2011). This error is reduced to approximately 25% in applying the relationship globally or regionally to an ensemble of glaciers (Meier et al., 2007). Similarly, Marshall et al. (2011) found errors up to 57% for individual glaciers but obtained "reasonable results" for an ensemble. The scaling relationship applied to a large glacier population, should reduce the uncertainty since "the error associated with the regression equation for Bahr et al.'s power law is randomly distributed" (Demuth et al., 2008). Farinotti and Huss (2013) determined that an appropriate population is several hundred glaciers for "recovery of the true total volume within 40%." This population size is also appropriate for determining volume change of a glacier population between two time points. For comparing volume change over a period of time, it is assumed that the scaling parameters do not vary over time (Farinotti and Huss, 2013).

2.4.3 Hydrological Balance

This method quantifies components of the water balance equation to determine glacier melt from discharge. The water balance equation for a glacierized watershed is:

$$Q_t = P - E - G_W + \Delta S + \Delta G \tag{2.10}$$

Where Q_t is total proglacial discharge, P is precipitation, E is evaporation and/or sublimation, G_W is groundwater recharge, ΔS is the change in storage resulting from changes in surface water and sub-surface storage (that is not groundwater), and ΔG represents snow storage changes from perennial snow patches (not on a glacier), and gain (snowpack converting to firn) or loss of glacier ice volume (Mark and Seltzer, 2003).

2.4.4 Hydrological Modelling

Modelling of glacier hydrology has significantly contributed to understanding the processes of glacier hydrology and the effects of climate change on glacier change (Hock and Jansson, 2005). All hydrological models require some form of hydroclimatic and spatial data, as well as parameters to govern the algorithms used by the model. Glacier models require glaciological data to describe the glacier within the model. Parameters can be determined from deductive, inductive, or abductive reasoning (Pomeroy et al., 2013). The deductive approach uses measured values from the basin to derive parameters. The inductive approach uses calibration against discharge measurements to determine parameters. The abductive approach assigns parameters from a similar basin where there exists a wider body of data to draw from. Data availability and the type of model determines what system of parameterization is used, and often a combination of these methods is used to parameterize the model. The spatial distribution of models can be lumped, distributed, or semi-distributed (Pomeroy et al., 2016). Lumped models have low spatial resolution and typically use a single set of parameters to represent an entire basin. Semi-distributed models group landscape classifications and resolve hydrological processes given specific parameters for each classification type. Fully distributed models use a gridded representation of the landscape to resolve hydrological processes for each cell, transferring mass and energy between the cells. Hydrological models can be categorized into two types: conceptual models and physically based models.

Conceptual models use a set of statistics and calibration to represent hydrological processes. These models tend to be more simplistic, requiring less input data, but are prone to equifinality, where different sets of parameters can lead to the same modelled result (Beven and Freer, 2001). Because they use empirical relationships, conceptual models cannot be easily transferred in time or space. A common conceptual model used in modelling glaciers is the temperature-index model (sometimes called the degree day model). Temperature-index models use an empirical relationship between air temperatures and melt rates to quantify melt in a basin (Ohmura, 2001; Hock, 2003). These models were initially the most widely used technique for calculating snow and ice melt because air temperature measurements are prevalent and relatively simple to interpolate and forecast (Hock, 2005). A limitation of conceptual models is that there are often no measurements to calibrate the temperature index, making these models inappropriate for remote areas due to the uncertainty in the parameters. This type of model is also inappropriate

for studying the effects of changes in climate on glacier energy balance and discharge since the empirical relationships cannot be determined for future climates. Most importantly, the temperature-index relationship is not derived from physical processes. Net radiation, not temperature, is the primary energy source for melt (Wendler and Weller 1974), which means that the temperature-index model is inherently flawed. However, this type of model has been widely applied in glacier modelling for multiple purposes: Oerlemans et al. (1998) modelled glacier mass balance, Braithwaite and Zhang (1999) modelled glacier snow and ice response to climate change, and numerous operational runoff models have been developed including the HBV model (Bergström, 1976), the UBC model (Quick and Pipes, 1977), and the HYMET model (Tangborn, 1984). Jost et al., (2012) applied the HBV-EC hydrological model, which uses a temperature-index snowmelt algorithm, to determine the contribution of glacier runoff to streamflow in the upper Columbia River basin.

Physically based models use governing physical principals to represent hydrological processes. They typically require more input data but can produce results with a high temporal resolution and low uncertainty. Physically based models have a limited need for calibration, which makes them ideal for applications in ungauged basins (Pomeroy et al., 2007). These models are also capable of producing results at a much higher time step than conceptual models (e.g. sub-daily, hourly). This is essential for some glacier investigations because glaciers can have a drastic effect on the amplitude of discharge due to the diurnal melt cycles prevalent in glacierized basins. Physically based models can also provide higher spatial resolution. This is an important consideration in glacier modelling as there is often high spatial heterogeneity in alpine glacierized basins in terms of both glacier cover and diverse topography (Hock et al., 2005). Physically based glacier models are often based on calculating the energy balance of the glacier to determine glacier melt (e.g. Holmgren, 1971; Escher-Vetter, 1985). More recently, Sicart et al. (2011) used a distributed energy balance model at the Zongo Glacier in Bolivia to analyze seasonal variations in mass balance and meltwater discharge. Naz et al. (2014) used a spatially distributed hydrologic model with glacier dynamics and determined that the effect of glacier decline on streamflow response in the upper Bow River basin was significant.

Uncertainty in hydrological modelling stems from numerous sources: errors in the applicability of the model structure and governing equations, errors in parameters, and insufficient input

glaciological or climate data. Uncertainty in modelling can be evaluated by determining parameter sensitivity. Another common problem with many glacier hydrology models is the tendency to hold glacier area constant throughout the model run. Many models also lack glacier dynamics to move glacier ice from the accumulation to the ablation zone. While some glacier models with ice dynamics have been developed (e.g. MacGregor et al., 2000; Le Meur and Vincent, 2003; Kessler et al., 2006), they have not been coupled with hydrological models and therefore cannot be applied to partially glacierized basins. The lack of ice dynamics can be a significant problem in glacier modelling as changing glacier area and ice-firn configuration has been shown to have a significant effect on basin discharge over time.

2.5 Gaps in Literature

Given the unequivocal evidence for advanced warming in northern regions and the global recognition of the importance of water resources (IPCC, 2014), there is a fundamental need to evaluate the impact of climate on streamflow trends northern regions (e.g. Spence, 2002). Mountain glaciers have been shown to be key indicators of climatic variability as they are highly sensitive to small changes in climate on a relatively small timescale (Oerlemans, 1989; Cogley and Adams, 1998; Kaser et al., 2004; Haeberli et al., 2007). Climate change has critical consequences for glacier-fed rivers including the potential for a permanent decrease in runoff due a reduction in glacier size, which limits meltwater contributions and increases variability in seasonal and annual runoff (Braun and Esher-Vetter, 1996; Collins, 2008; Comeau et al., 2009; IPCC, 2014). A geographically diverse network is needed to provide broad insight into the impact of glacier-climate relationships on downstream hydrology and ecology (Agnew et al., 2002). The impact of glaciers and glacier change on streamflow in the northern continental region of Canada remains unknown. The study of this region will provide insight into these potentially shifting regimes and will contribute to a more complete representation of glacier change in Canada.

3 METHODS

A framework of the methods for this project is shown in Figure 3.1. A hydrological model was implemented for the Bologna Glacier basin. The model was driven with meteorological data spatially and temporally downscaled from atmospheric reanalyses. Spatial delineation of the basin used remote sensing products and field observations. The model – parameterized using field observations and past studies on similar basins – was run over a 36 year period (hydrological years 1980 – 2015) under three glacier configurations (1984, 2014, 2015). An additional analysis used satellite imagery and field observations to illustrate how the glacier surface coverage evolved over 30 years (1984 – 2015). Model output was assessed for temporal trends over the study period and a water budget and mass balance were calculated for the three model configurations. An analysis determined whether there are teleconnections of temperature, precipitation, and model output with large scale atmospheric patterns. The numerical analysis for this project fully utilized tools in the R package "CRHMr" by Shook (2016a).

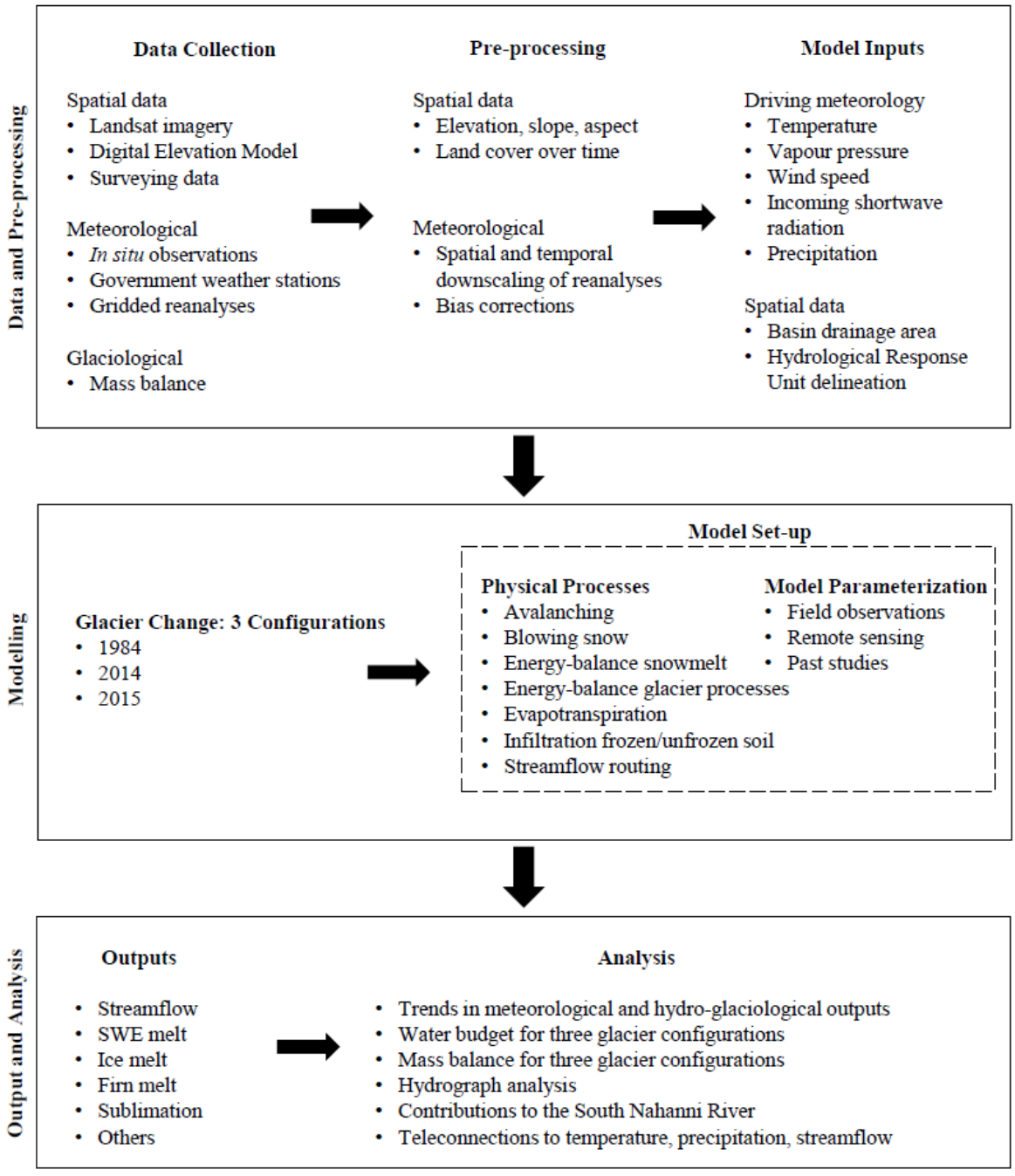

Figure 3.1: Methods framework for this study

3.1 Study Area

Nahanni National Park Reserve (NNPR), NWT is located in the Mackenzie River basin, approximately 350 km west of Fort Simpson (Figure 3.2). The Park is a UNESCO World Heritage Site, with a globally unique landscape and intrinsic ecological value, and is a travel area for the Dene Nation (Parks Canada, 2004; Demuth et al., 2014). The Park covers 30,055 km^2 and ranges from 180 to 2773 m elevation, covering a large portion of the Greater Nahanni Ecosystem (GNE).

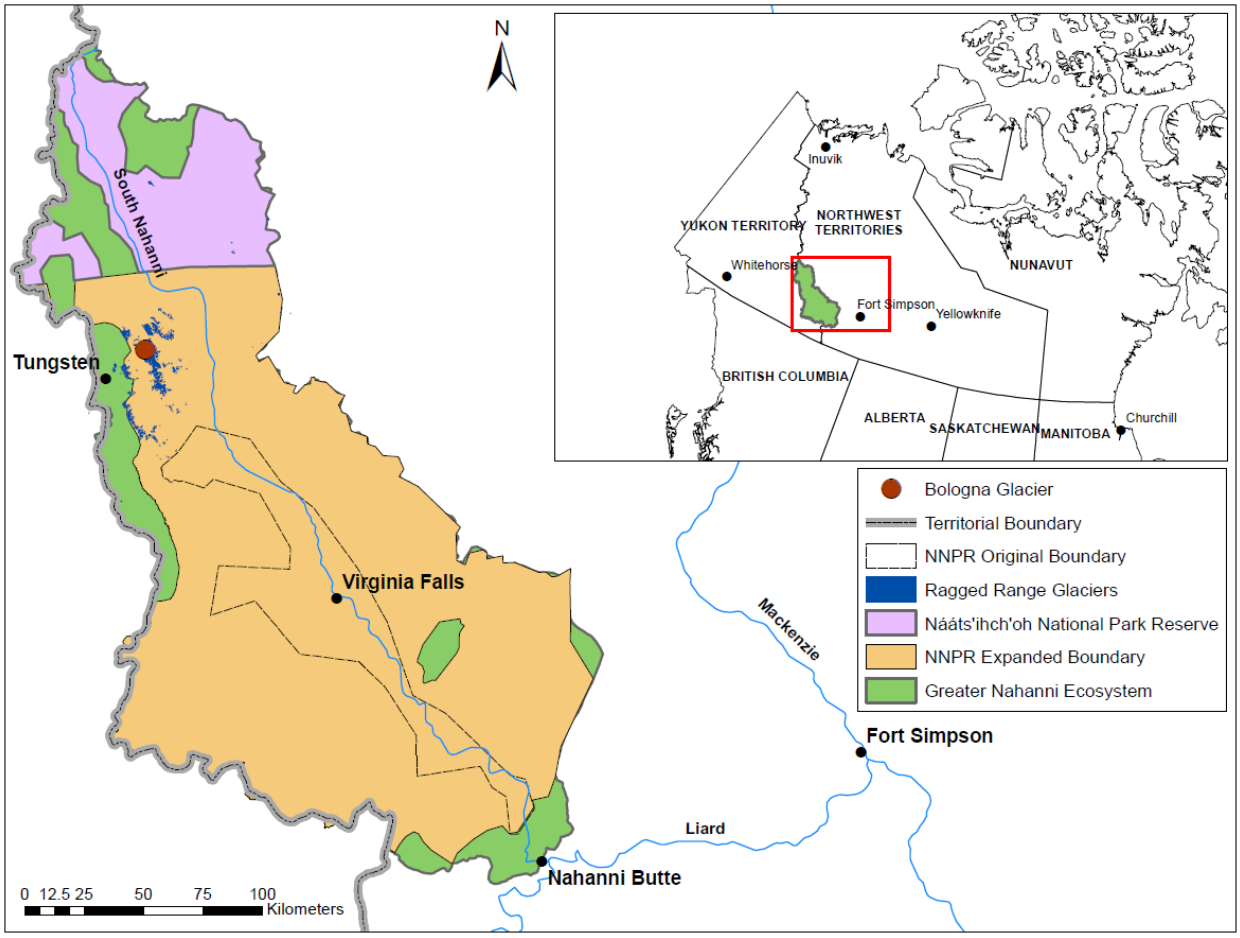

Figure 3.2: Location of the Bologna Glacier within Nahanni National Park Reserve and the Greater Nahanni Ecosystem

The cold continental climate of this region has long winters and high snowfall at the upper elevations (Halliwell and Catto, 2003), which feeds large icefields and hundreds of small glaciers in the Ragged Range (Demuth et al., 2014). These glaciers make up the headwaters of the South Nahanni River, a tributary to the Liard River. The Liard River flows northeast to join the Mackenzie River at Fort Simpson, flowing north and eventually emptying into the Beaufort Sea and the Arctic Ocean. The region had no glacier studies prior to the inventories by Demuth et al. (2014) and mass balance studies established in 2007. Mentions of glaciers of the Ragged Range in the literature are scarce (Bostock, 1948; Demuth, 1998; Williams and Ferrigno, 2002).

Demuth et al. (2014) conducted a glacier inventory and change detection analysis of glaciers of the Ragged Range, comparing coverage in 1982 to 2008; 263 glaciers were delineated for change detection. Glaciers occupied approximately 262 km^2 in 1982, and coverage decreased by roughly 30 percent to 184 km^2 in 2008. The largest icefield in this region is the Brintnell-Bologna Icefield, with an area of 28.5 km^2.

The Bologna Glacier, shown in Figure 3.3, is located at 62°N, 128°W and is one of the two main outlet glaciers of the Brintnell-Bologna Icefield. It is currently the only glacier in the region with *in situ* monitoring. The glacier is 16 km^2 in size. The relief is 800 m and the aspect is primarily north-northwest facing. Mean annual temperature is -6.5°C and total annual precipitation averages 600 mm water equivalent over the past 36 years. These values were determined from the corrected ERA-Interim reanalyses to be described in Section 3.2.2. Figure 3.4 shows that the glacier mass balance was negative in the first two years of measurement, consistent with mass balance measurements throughout the Cordillera (Demuth et al., 2017). Additional images of the study site can be found in Appendix E.

Figure 3.3: Bologna Glacier (reproduced with the permission of Margaret J. Demuth, 2006)

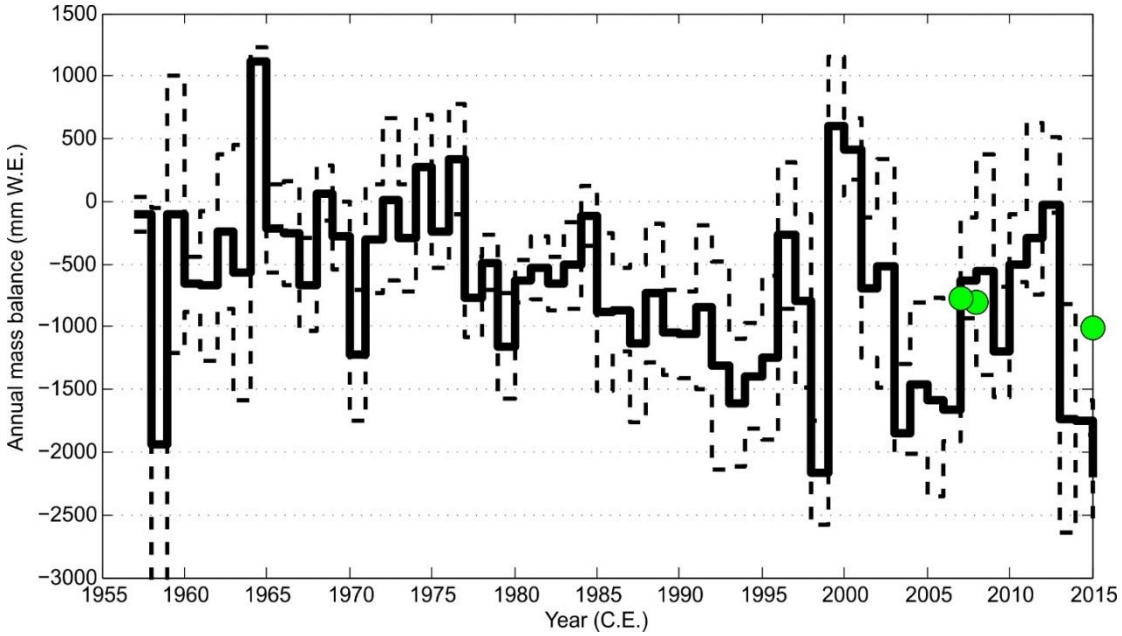

Figure 3.4: Regional annual glacier mass balance for northwestern America, 1957-2015. Dashed lines represent the 95% confidence interval. Available measurements for the Bologna Glacier are superimposed (reproduced with the permission of M. N. Demuth, Natural Resources Canada).

3.1.1 Field Data

3.1.1.1 Mass Balance Data

Mass balance observations for the Bologna Glacier exist for 2006, 2007, and 2015. Figure 3.5 shows the distribution of mass balance stakes over the Bologna Glacier.

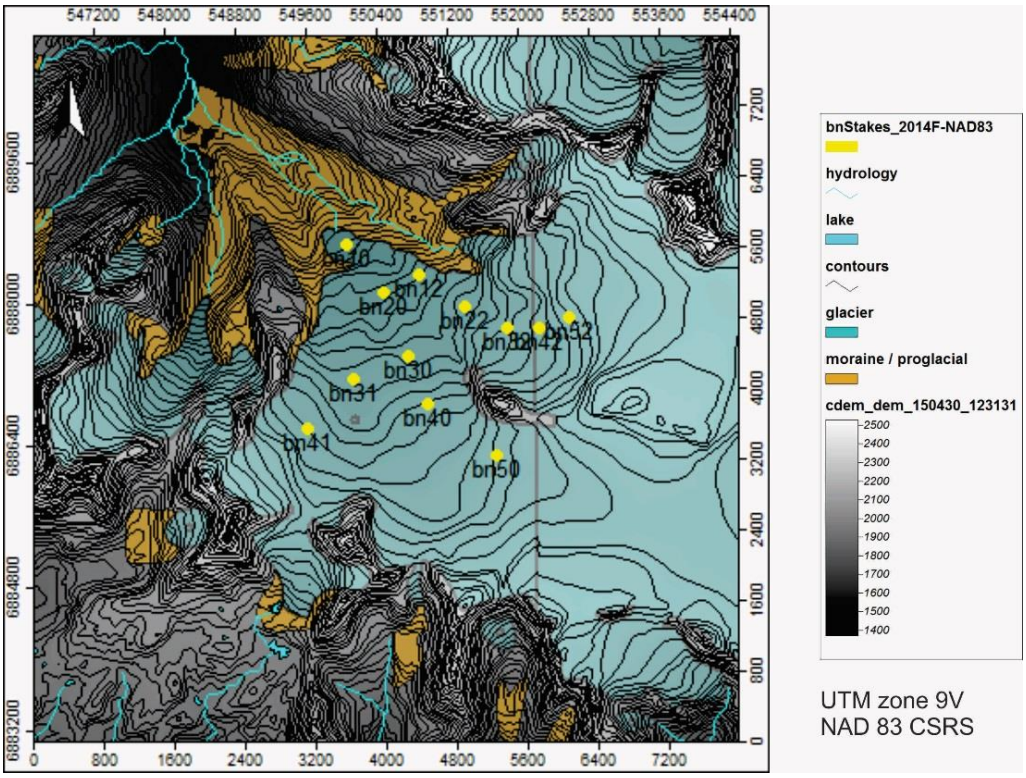

Figure 3.5: Mass balance stake locations on the Bologna Glacier (reproduced with the permission of M. N. Demuth, Natural Resources Canada, 2015)

3.1.1.2 Meteorological Station Data

Two automatic weather stations (AWS) were installed in August of 2014 (Figure 3.6): University of Saskatchewan installed an AWS on the Nunatak surrounded by the glacier (Nunatak Station) and University of Victoria installed an AWS in the ablation zone of the glacier (Ice Station). The station positions are shown in an oblique view photograph shown in Figure 3.7. The Ice Station is 375 m northeast of the Nunatak Station and 51 m lower than the Nunatak Station. Both are situated near the central flowline of the glacier, at roughly the midpoint between the highest and lowest elevation. The Nunatak Station sits at the downstream point of an exposed rocky peak. It is subject to high winds and slight shading from the peak of the Nunatak. The Ice Station is situated on the glacier ice in the ablation zone with little shading from surrounding terrain.

Both stations experienced some degree of malfunction in their first year of operation. Problems with the power supply for the Nunatak Station caused the station to suspend logging in February of 2015. Ice melt and anchoring problems let to the partial collapse of the Ice Station in July of 2015. Both stations were repaired during the August 2015 field campaign and continue to collect observations. The Ice Station has telemetry; therefore, the observations are readily available. The Nunatak Station observations must be downloaded directly from the station. Station details are given in Table 3.1.

Figure 3.6: Nunatak (L) and Ice (R) Stations (reproduced with the permission of May Guan, 2015)

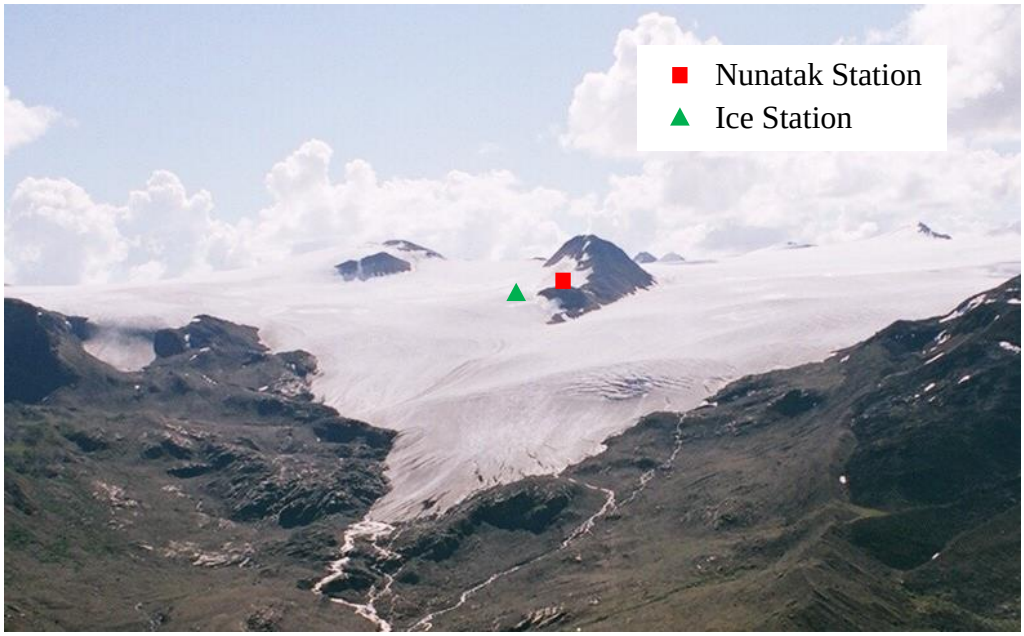

Figure 3.7: Ice and Nunatak Station locations on the Bologna Glacier (reproduced with the permission of Margaret J. Demuth, 2006)

Table 3.1: Specifications for the Nunatak and Ice AWS Stations

	Nunatak Station		Ice Station	
Location	62°2’ N 128°0’W		62°2’ N 128°0’W	
Elevation	2159 m		2108 m	
Period	August 2014 – February 2015		August 2014 – July 2015, August 2015 – June 2016	
Total Months	6		24	
Frequency	15 Minute, Daily		Hourly	
Measurements	2.5 m temperature and relative humidity	Rotronic HC-S3-XT	1.4 m/4.3 m/9.2 m temperature and relative humidity	Rotronic HC-S3-XT-L
	2.9 m wind speed and direction	R. M. Young 05130AP-10	1.4 m/4.3 m/9.2 m wind speed and direction	R. M. Young 05103AP-10-L
	Snow depth	Campbell Scientific SR50A	Incoming and outgoing radiation	Kipp & Zonen CNR4-L
	Incoming shortwave radiation	Apogee CS300	Surface temperature	Apogee SI-111-L
	Tipping bucket rain gauge	Texas Electronics TR-525M	Snow depth	Campbell Scientific SR50A
	20 cm/100 cm snow temperature	Campbell Scientific Type E Thermocouple	Tipping bucket rain gauge	Texas Electronics TE525M-L
			Multi-level temperature probe	Campbell Scientific 109AM-L
			Snow water equivalent sensor	Campbell Scientific CS725
			Barometric Pressure Sensor	Vaisala CS106

Station observations were compared to determine whether there is a correlation between the two datasets. Discrepancies can either demonstrate the differences in microclimate between the two stations or indicate instrumentation malfunction. Figure 3.8 shows regressions of the Ice Station observations and Nunatak Station observations for temperature, vapour pressure, wind speed, and incoming shortwave (SW) radiation for the period of time when both stations were logging (August 2014 to February 2015). The 15-minute Nunatak Station observations were resolved into hourly observations and these values were compared to the hourly Ice Station observations. Vapour pressure was converted from relative humidity using air temperature. Because the wind speed measurements were at different heights (Table 3.1), the 9.2 m Ice Station wind speed was converted to a 2.9 m wind speed, matching that of the Nunatak Station. The Ice Station had a mast with three measurement heights, which were used to calculate the aerodynamic roughness height, $z_{0,}$ of the glacier in the ablation zone (Appendix A). The aerodynamic roughness height was found to be $3x10^{-3}$ m, which is consistent with the literature (Van den Broeke, 1997; Smeets et al., 2008; Sicart et al. 2014). It is evident that there is good agreement between the Ice and Nunatak Station temperature and relative humidity. Wind speed at the Nunatak Station is higher than that of the Ice Station, consistent with field observations. Incoming shortwave radiation is higher at the Nunatak Station than the Ice Station. Observed rainfall from the tipping bucket gauges were compared as cumulative values, as shown in Figure 3.9, in a double mass curve. The double mass method uses a fixed proportion derived from comparing two cumulative variables over the same time period (Searcy and Hardison, 1950). The Ice Station appears to catch more rain. Figure 3.9 shows that the slope of the double mass curve is not constant. This change in slope is most likely due to the limited quantity of observations from the Nunatak station as it collected very little summer data (August and September 2014). There were no instrumentation changes and the record did not extend over multiple seasons so the slope change cannot be explained by seasonality.

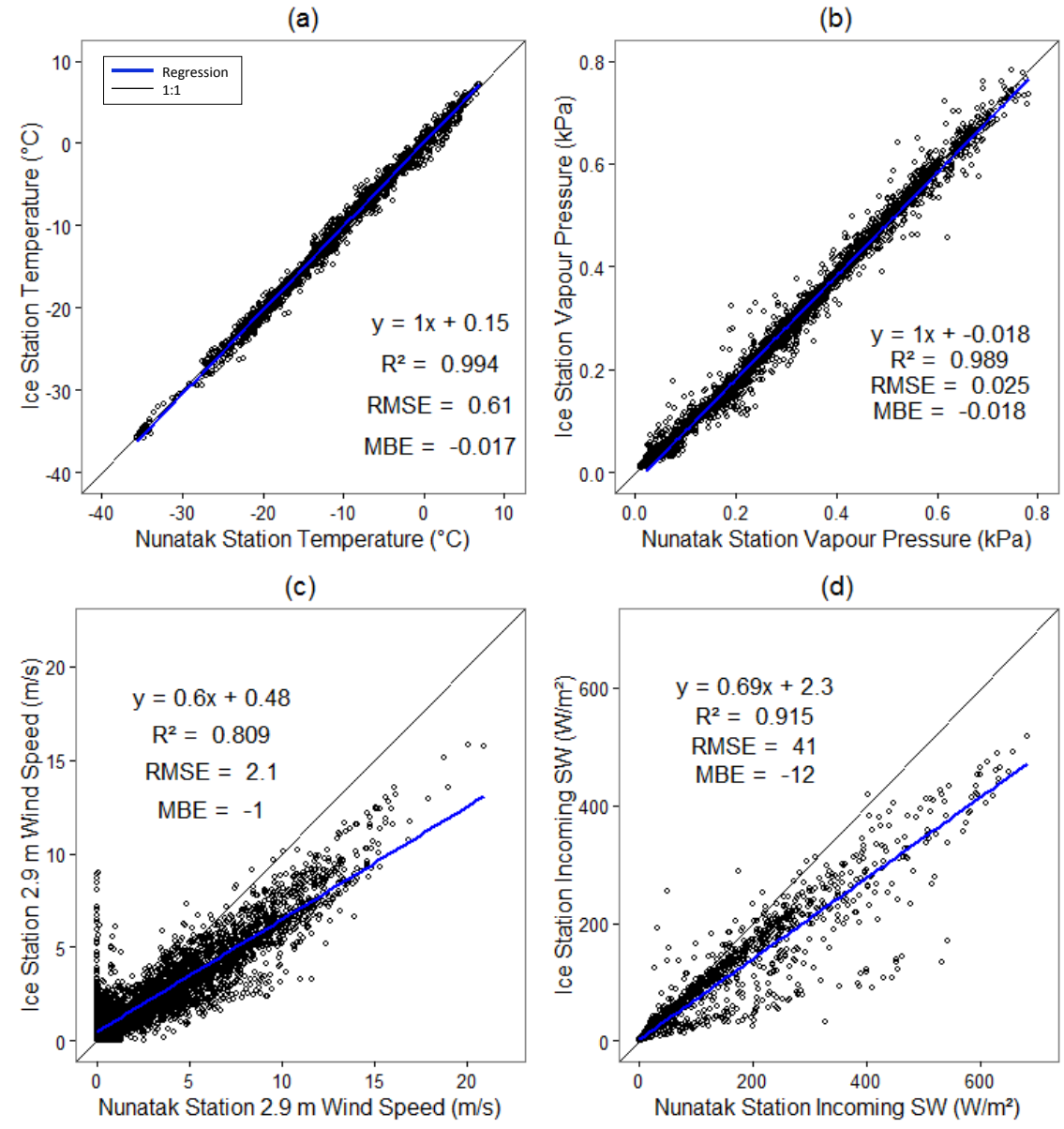

Figure 3.8: Comparison of Ice Station and Nunatak Station hourly observations (August 2014 to February 2015) for (a) temperature; (b) vapour pressure; (c) wind speed; and (d) incoming shortwave radiation

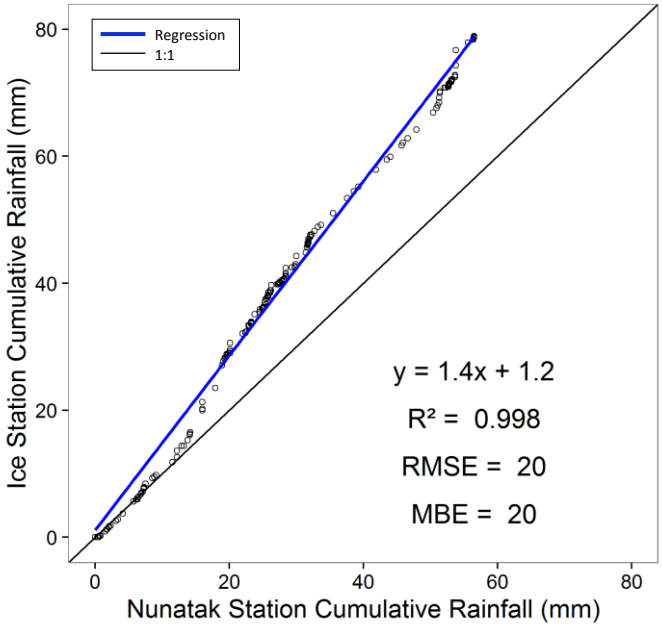

Figure 3.9: Double mass curve for Ice and Nunatak Station Rainfall (August 2014 to February 2015)

3.1.1.3 Surveying Data

Delineating glacier margins from digital imagery is dependent on the accuracy with which glacier margins can be identified and digitized: a function of image resolution, snow conditions, and the contrast between ice and adjacent terrain (DeBeer and Sharp, 2007). Cloud cover and shadows can obscure ice margins, increasing error. Debris-covered ice can obscure identification of the true ice margin; however, differences in illumination at the glacier margins can assist in delineating the boundary (Demuth et al., 2008).

By surveying the Bologna Glacier margins in the field, it was apparent that the margin of the glacier is differentiable from the surrounding terrain, even when the ice cover is darker due to slight coverage from glacial till, fine debris, or algae. Margins were surveyed using rapid-static Global Positioning System (GPS) techniques and were differentially corrected with respect to a base station location. The base station position was determined using Natural Resources Canada's (NRCan) Precise Point Positioning online service. The surveying base station and roaming antenna shown are in Figure 3.10. Twenty-eight locations were surveyed for their position and elevation. Horizontal accuracy was within 0.020 m and vertical accuracy was within

0.040 m, at 95% confidence. Locations surveyed included the AWS locations, mass balance stake locations, and current glacier margins. Sites were selected such that they would be recognizable from remote sensing imagery.

Figure 3.10: GPS base station (L); surveying the margins (R) (reproduced with the permission of M. N. Demuth, Natural Resources Canada, 2015)

3.2 Meteorological Record

A long term meteorological record at the Bologna Glacier was required to run the model. The AWS stations provide observations starting in late 2014, which is insufficient to test for long term temporal trends in driving meteorology and glacier-hydrological variables. To construct a meteorological record, a gridded reanalysis product was chosen. This product was tested for accuracy in high-elevation northern locations to determine whether it could adequately capture local weather conditions in settings similarly situated to the Bologna Glacier. Once the validity of the product was verified, the reanalyses were spatially and temporally downscaled to best represent meteorological conditions at the Bologna Glacier.

3.2.1 Regional Stations

The closest high-elevation northern stations to the Bologna Glacier are those at Tungsten, NWT and Macmillan Pass, YT. Each location has an Environment Canada (EC) station and Macmillan Pass also has a station set up by Yukon Government (YG). Station details and proximity to the Bologna Glacier are given in Table 3.2. The R package for downloading and extracting Meteorological Service of Canada (MSC) meteorological observations, "MSCr" by Shook (2015), was used to extract data from the Environment Canada Historical Data archive (http://climate.weather.gc.ca). The Yukon Government observations were retrieved from the Water Resources Branch in the Department of Environment (Tyler Williams, personal communication). The Tungsten station is situated at a mine site in a wide valley. The Macmillan Pass stations are both situated in a high-elevation site near the Macmillan Pass air strip. The precipitation gauge at the Macmillan Pass YG station is a stand pipe with a pressure transducer. It does not have a wind shield but is surrounded by sparse, low vegetation which should reduce wind-induced undercatch. While the mouth of the standpipe is wide, snow capping occurs under certain conditions, which prevents accurate snowfall measurements, as shown in Figure 3.11. The precipitation gauge at the Macmillan Pass EC station was a Belfort potentiometric weighing gauge with an Alter shield, which was then replaced by a first generation OTT Pluvio with an Alter shield on September 29, 2002 (Bob Kochtubajda, personal communication). The Macmillan Pass EC site is shown in Figure 3.12. Specifications for the other instrumentation at these sites could not be located.

Figure 3.11: Stand pipe precipitation gauge at the Macmillan Pass Yukon Government station under snow capping conditions (reproduced with the permission of Yukon Government)

Figure 3.12: Macmillan Pass Environment Canada Station, 1999 (reproduced with the permission of Bob Kochtubajda)

Table 3.2: Station details for Macmillan Pass, YK and Tungsten, NWT

Station Name	Climate ID	Location	Elevation	Distance from Bologna Glacier	Vertical Elevation Difference from Nunatak Station	Variables Available	Time Step	Years of Record
Macmillan Pass EC	2100693	63°14’ N 130°02’W	1379 m	164 km	-780 m	Temperature	Hourly	1998-present
						Dew point temperature	Hourly	
						Relative humidity	Hourly	
						Wind speed and direction	Hourly	
						Pressure	Hourly	
						Precipitation	Daily	
Macmillan Pass YG	N/A	63°14’ N 130°02’W	1379 m	164 km	-780 m	Temperature	Hourly to 3-Hourly	2007-present
						Precipitation	Daily	1995-present
Tungsten EC	22003922	61°57’N 128°15’W	1143 m	12 km	-1016 m	Temperature	Daily	1966-1990
						Precipitation	Daily	

3.2.1.1 Wind Undercatch Corrections

Wind undercatch of solid and mixed precipitation is one of the highest contributors to gauging errors (Goodison et al., 1998). Undercatch corrections for the precipitation observations at Macmillan Pass and Tungsten were made where possible. Table 3.3 shows the gauges and shields used at the stations. The gauge and shield type for Tungsten could not be found. It was determined that a correction was not required for the Belfort gauge at Macmillan Pass because prior to 2003, 71% of the precipitation observations were missing and therefore the observations prior to 2003 were eliminated from this analysis. Details of the undercatch correction equations can be found in Appendix A.

Table 3.3: Gauge and shield types for the Macmillan Pass and Tungsten meteorological stations and corresponding undercatch corrections

Station	Date	Gauge / Shield	Undercatch Correction
Macmillan Pass EC	1998 – 2002	Belfort potentiometric weighing gauge with Alter shield	Not required (not included in analysis as too much data is missing)
Macmillan Pass EC	2002 – present	OTT Pluvio1 with Alter shield	See Appendix A
Macmillan Pass YG	1995 – present	Stand pipe with pressure transducer, no shield	See Appendix A
Tungsten	1966 – 1990	Unknown	None

3.2.1.2 Precipitation Analysis

Table 3.4 shows the significant quantity of precipitation observations that are missing from the Macmillan Pass records: 41% from the 18 year EC record and 34% from the 20 year YG record. This high percentage of missing observations is problematic for comparisons with reanalyses. For the EC station, years where there was greater than 25% of the observations missing were removed from the analysis, leaving six years for analysis. For the YG station, there were a significant portion of observations missing from many years, therefore the EC observations (corrected for wind-induced undercatch) were used to infill missing YG observations. This reduced the percentage of missing observations and left six years for analysis.

Table 3.4: Missing precipitation observations from Macmillan Pass and Tungsten stations

Station	Years of Record	Percent of Original Precipitation Observations Missing	Years used for analysis (<25% of observations missing)
Macmillan Pass EC	1998-2015	41%	2003-2005, 2011-2013
Macmillan Pass YG	1995-present (precipitation)	34%	2003, 2005, 2010-2013
Tungsten EC	1966-1990	6% of 1980 to 1990 (overlap with ERA-Interim)	1980-1990

3.2.2 Atmospheric Reanalyses

Atmospheric reanalysis combines observations with a meteorological forecast model to produce gridded datasets of atmospheric variables with a high temporal resolution. It is a useful tool for acquiring long term meteorological records for applications in hydrological modelling, especially in remote, data-sparse locations (Krogh et al., 2015; Trubilowicz et al., 2016). The product chosen for this project had to meet the following constraints: (i) the product must include observations overlapping the time period of the AWS stations; (ii) the product must be available at northern latitudes; and (iii) the data must be available at a sub-daily time step. This eliminated several products available for southern latitudes with data extending only into the 1990s and early 2000s including Climate Forecast System Reanalysis (CFSR) from the National Centers for Environmental Protection (NCEP), several of the ECMWF products: ERA-15, ERA-20, ERA40, and products from Water and Global Change (WATCH) including WFD and WFDEI. The final products under consideration were ERA-Interim and North American Reanalysis (NARR) from NCEP. Metadata of the main products considered can be found in Appendix B. ERA-Interim is available at a resolution of 0.125 by 0.125 degrees, which, at the latitude of the study site (62°N), translates to a spatial resolution of 14 km in the north-south direction and 6.5 km in the east-west direction. NARR is available at a resolution of 32 km. Accessibility was also considered when selecting a product. ERA-Interim is readily available online by selecting the required time period and variables and can be unpacked using the R package "Reanalysis" by Shook (2016b). NARR data are cumbersome to download: the user can download one variable for an entire year for all

of North America or download all data types for three hours for all of North America. This structure is not easily applicable for the scale of modelling in this project.

ERA-Interim was selected as it is has been shown to be relatively successful in applications requiring hydrometric data (Betts et al., 2009; Zhao et al., 2012; Krogh et al., 2015; Vuichard and Papale, 2015). It is also relatively easy to acquire and unpack for analysis. After some early testing of the product, it proved to be relatively accessible and showed good results in initial comparisons to field observations (Section 3.2.2.1).

The European Centre for Medium Range Weather Forecast (ECMWF) Interim Re-Analysis (ERA-Interim) is a global atmospheric reanalysis starting in 1979 and is updated continuously to present day (Dee et al., 2011). ERA-Interim offers a wide variety of parameters for the surface of the earth at a three-hour time step. Daily surface data were retrieved from the ECMWF website (http://apps.ecmwf.int/datasets/data/interim-full-daily/levtype=sfc) in Network Common Data Format (NetCDF). ERA-Interim data assimilation and forecast method produces four analyses per day at 00:00, 06:00, 12:00, and 18:00 UTC and two ten day forecasts per day, initialized from the analyses at 00:00 and 12:00 UTC (Berrisford et al., 2011). The combination of the analyses and forecasts allow for the retrieval of three hour data. The R package "Reanalysis" was used to extract the data from the package (Shook, 2016b) for the variables in Table 3.5. To spatially downscale the gridded product, the grid point nearest to the selected station location was chosen. Temperature, dew point temperature, and 10 metre wind speed are instantaneous, varying, surface, and single level parameters, and were acquired at a three hour interval. Linear interpolation was used to acquire the hourly values for each parameter. Total precipitation and downward surface solar radiation are forecasted accumulated, surface, single level parameters. These variables are produced in three-hourly accumulated variables which needed to be de-accumulated to acquire total three hour precipitation. Three-hourly total precipitation was re-accumulated into total daily precipitation. For hourly radiation, the disaggregated three-hourly values are interpolated hourly values based on the extra-terrestrial hourly radiation using the package "Reanalysis" (Shook, 2016b).

Table 3.5: Meteorological variables extracted for ERA-Interim at 3-hourly intervals for 1979-2015

Parameter	Units	Variable Name
10 m eastward wind component	$m\ s^{-1}$	*u10*
10 m northward wind component	$m\ s^{-1}$	*v10*
2 m temperature	K	*t2m*
2 m dewpoint temperature	K	*d2m*
Downward surface solar radiation	$J\ m^{-2}$	*ssrd*
Total precipitation	m water	*tp*

The horizontal and vertical distances from the reanalysis locations to the station locations are shown in Table 3.6. A DEM was used to determine the vertical distance from the reanalysis location to the actual station elevations. It was necessary to compare the actual elevation to the simulated elevation to see whether there were large discrepancies between the two. ERA-Interim uses the DEM Global 30 Arc-Second Elevation (GTOPO30) (Dee et al., 2011). The DEM was acquired from the USGS (https://lta.cr.usgs.gov/GTOPO30) via the USGS EarthExplorer (http://earthexplorer.usgs.gov) on October 26, 2015 in a GeoTIFF file format. The DEM was completed in 1996 and has a resolution of 435 m in the east-west direction and 930 m in the north-south direction at the Bologna Glacier. The product is specified at a vertical accuracy of 30 m at 90% confidence (GTOPO30 supporting documentation).

Table 3.6: Proximity of each station location to the nearest reanalysis grid point

Station	Station Elevation	Location of Nearest Reanalysis Location	Horizontal Distance from Station to Nearest Reanalysis Location	Elevation of Nearest Reanalysis Location	Vertical Distance from Station to Reanalysis Location
Bologna Nunatak Station	2159 m	62.125°N 128.000°E	1419 m	2007 m	152 m
Bologna Ice Station	2108 m	62.125°N 128.000°E	1048 m	2007 m	101 m
Macmillan Pass EC/YG	1379 m	63.250°N 130.000°E	2517 m	1498 m	119 m
Tungsten	1143 m	62.000°N 128.250°E	5570 m	1746 m	603 m

3.2.2.1 Comparisons at Other Stations

To determine whether ERA-Interim was a viable choice to represent meteorology at a northern high-elevation study site, comparisons were first made to the nearest high-latitude stations described in Section 3.2.1: Macmillan Pass, YT and Tungsten, NWT.

Temperature: Figures 3.13, 3.14 and 3.15 show the regression between ERA-Interim hourly temperature and station hourly temperature at Macmillan Pass EC, Macmillan Pass YG, and Tungsten stations, respectively. It is evident that there is good agreement for temperature (R^2 = 0.95, 0.94, and 0.96, respectively).

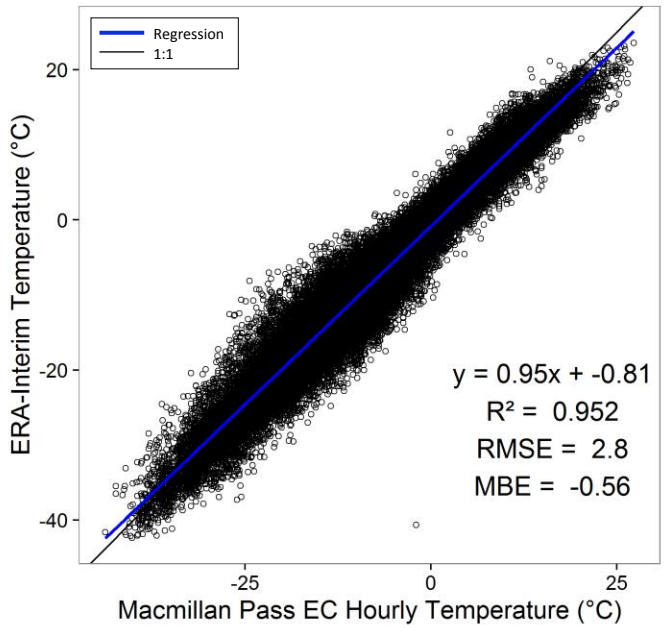

Figure 3.13: Hourly temperature for ERA-Interim compared to observations at the Macmillan Pass Environment Canada station

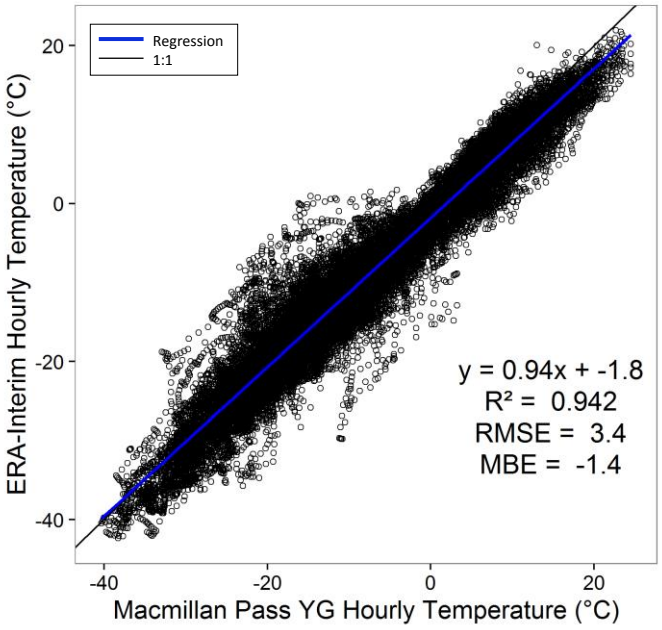

Figure 3.14: Hourly temperature for ERA-Interim compared to observations at the Macmillan Pass Yukon Government station

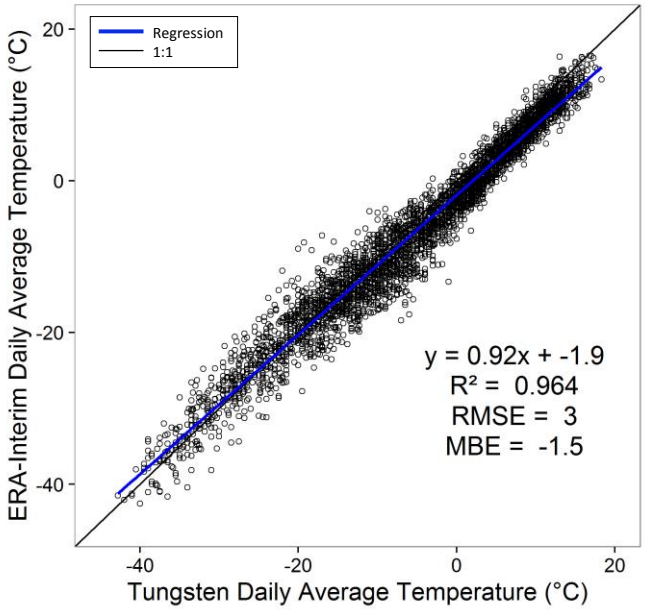

Figure 3.15: Hourly temperature for ERA-Interim compared to observations at Tungsten, NWT

Precipitation: Figures 3.16, 3.17, and 3.18 show regressions for the total daily, weekly, monthly, and annual precipitation from ERA-Interim and observations at Macmillan Pass EC, Macmillan Pass YG, and Tungsten, respectively. For the Macmillan Pass EC and YG stations, it is evident that there is no statistical correlation between the reanalyses and observed precipitation at a daily time step. However, the R^2 value increases as the time step increases. This indicates that although ERA-Interim may not provide accurate precipitation at a fine temporal resolution, the accuracy of total precipitation increases with increasing the time step. The same trend occurs for Tungsten, which has better agreement at an annual time step; however, the annual total ERA-Interim precipitation is significantly higher than the observed annual precipitation at Tungsten. This could be due to the significant distance between Tungsten and the nearest grid point location. The reanalysis location is 5.6 km from the Tungsten station in the horizontal direction and is 603 m higher in elevation. This significant difference in elevation could help to explain why precipitation at the reanalysis location is so much higher than that at the station. Additionally, the type of gauge at Tungsten was undocumented and therefore no wind undercatch corrections were applied. The lack of undercatch corrections likely caused lower measured winter precipitation than the actual winter precipitation. Figures 3.19, 3.20, and 3.21 show the double mass curves for

Macmillan Pass EC, Macmillan Pass YG, and Tungsten respectively. Precipitation predicted by ERA-Interim is much better at both of the Macmillan Pass stations. At the Tungsten station, ERA-Interim is significantly higher than the observations, which again may be attributed to the lack of wind undercatch corrections and the significant elevation difference between the reanalysis location and the station.

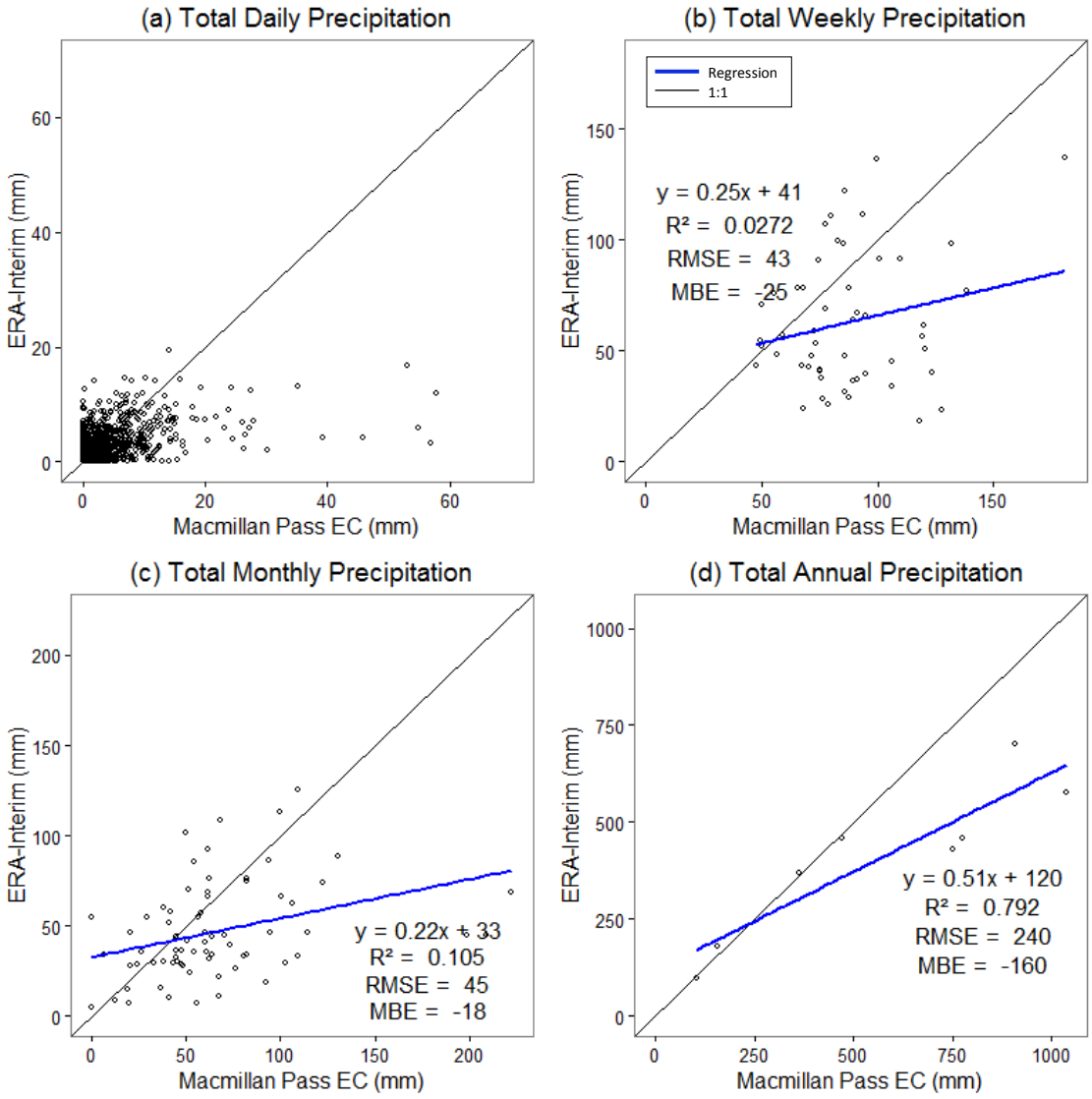

Figure 3.16: ERA-Interim compared to Macmillan Pass Environment Canada station for (a) total daily precipitation; (b) total weekly precipitation; (c) total monthly precipitation; (d) total annual precipitation

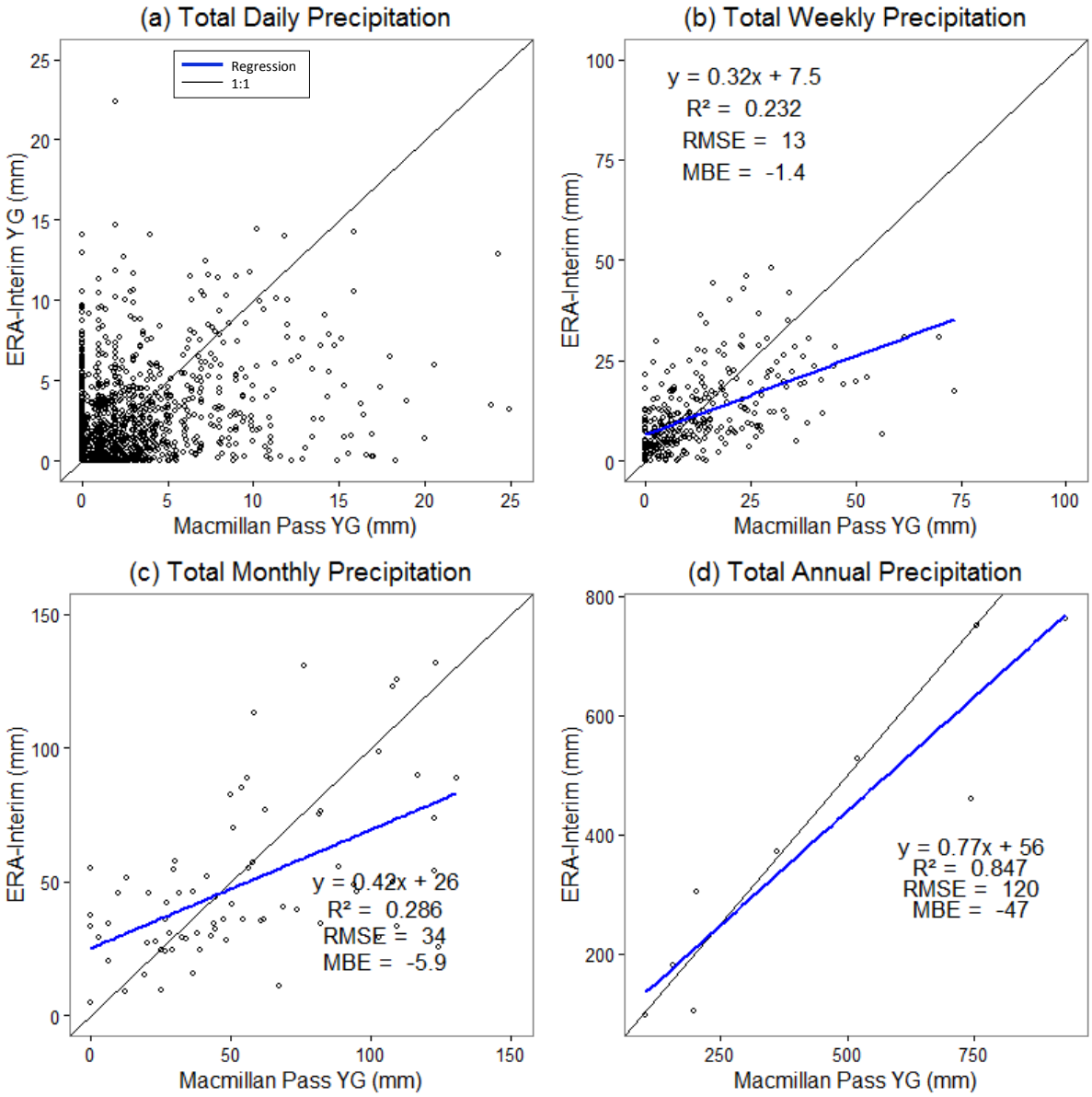

Figure 3.17: ERA-Interim compared to Macmillan Pass Yukon Government station for (a) total daily precipitation; (b) total weekly precipitation; (c) total monthly precipitation; (d) total annual precipitation

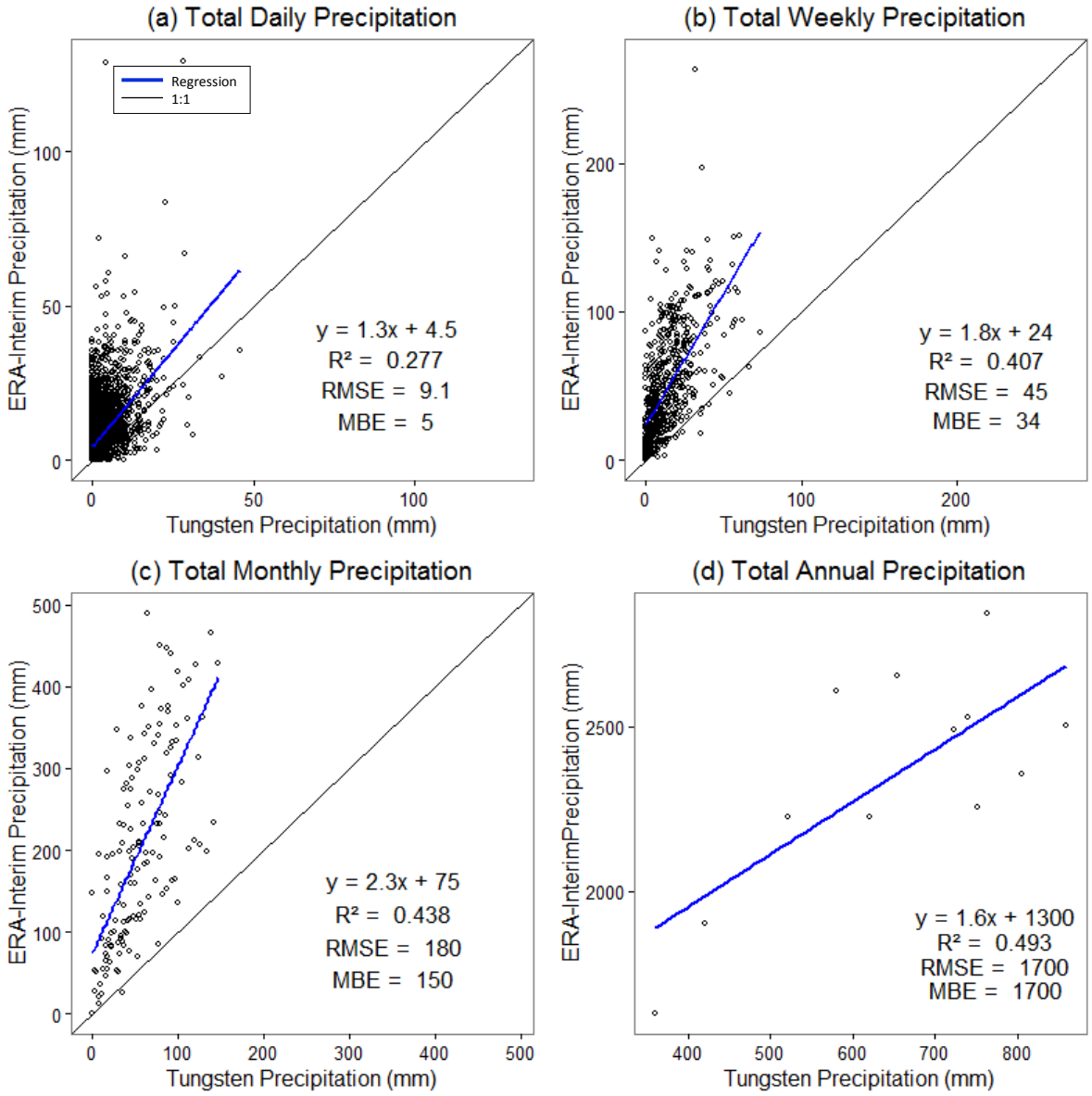

Figure 3.18: ERA-Interim compared to Tungsten, NWT for (a) total daily precipitation; (b) total weekly precipitation; (c) total monthly precipitation; (d) total annual precipitation

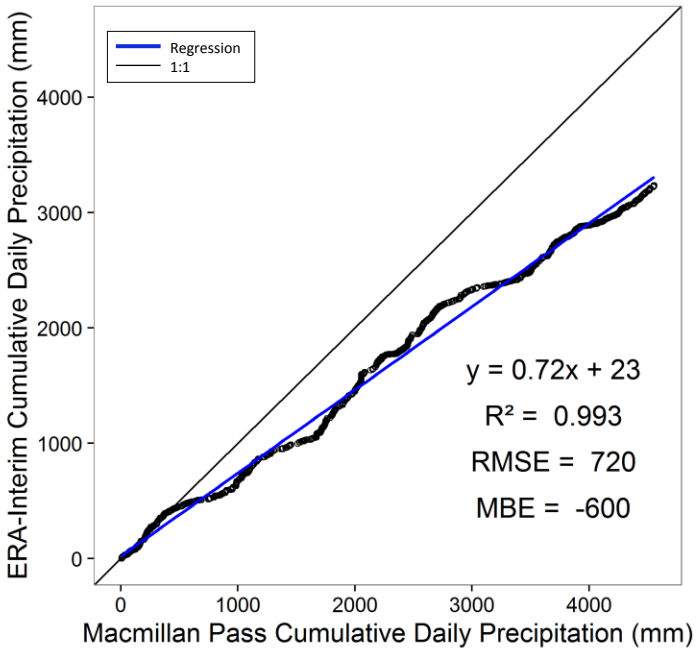

Figure 3.19: Double mass curve for ERA-Interim precipitation compared to Macmillan Pass Environment Canada precipitation

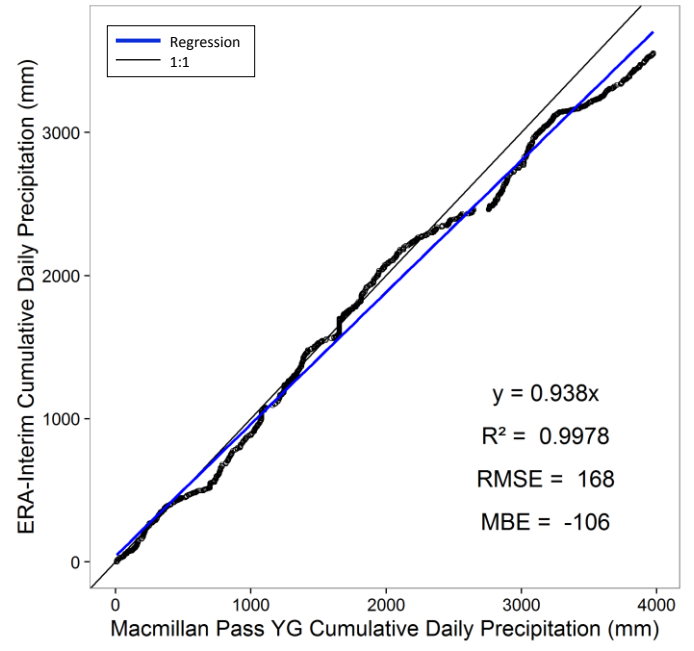

Figure 3.20: Double mass curve for ERA-Interim precipitation compared to Macmillan Pass Yukon Government precipitation

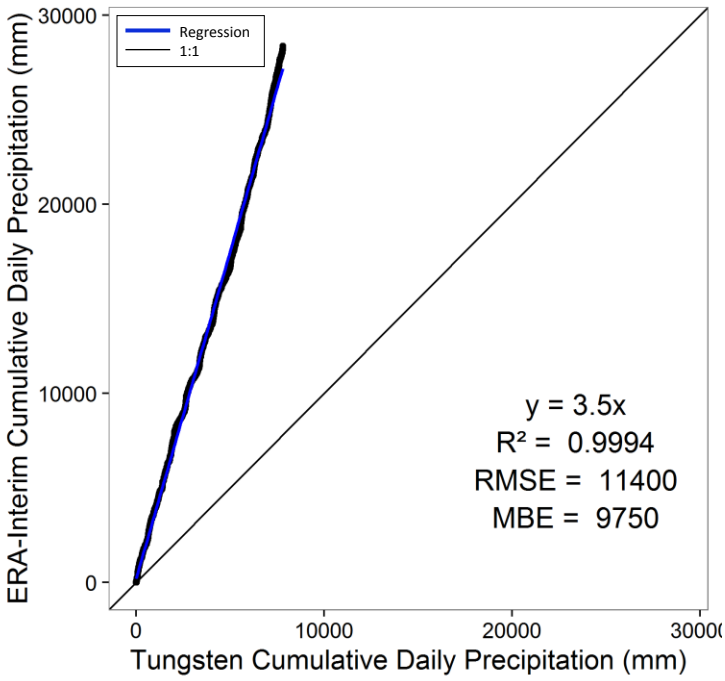

Figure 3.21: Double mass curve for ERA-Interim precipitation compared to Tungsten, NWT precipitation

3.2.2.2 Data Corrections

ERA-Interim must be downscaled (from grid scale to point scale) and bias corrected to local station observations to ensure that the record best represents the meteorology at the Bologna Glacier. Both the Ice and Nunatak Station were used for the bias corrections. Letréguilly (1988) showed that off-ice stations better represent local weather than on-ice glacier stations in glacierized basins: temperature at a gauge 200 km from Peyto Glacier in Alberta was better correlated to both mass balance and the ELA. Letréguilly (1988) speculated that this was, in part, due to the poor records at Peyto Glacier, given the challenges of remote data collection and given that the station was moved several times throughout the period of analysis. However, it was also determined that the microclimate created by the glacier itself can produce some bias in the meteorological observations, which exacerbated the problems with on-ice stations. A similar result was found at the McCall Glacier, where Klok et al. (2005) showed that mass balance was better correlated to observations at a ridge top station adjacent to the glacier rather than to stations placed on the glacier surface.

The Ice Station has a longer observation record that can describe conditions year-round. Therefore, in some cases described below, the Ice Station observations were first bias corrected to the Nunatak Station to create a "synthetic" Nunatak Station – effectively an off-ice station with the longest possible record. The synthetic station was then used to bias correct the reanalyses.

Temperature: Ice Station (BNI) observations were bias corrected (slope and offset) to the Nunatak Station (BNN) to create a synthetic Nunatak Station with a 24-month record. The slope and offset correction were found by plotting the synthetic Nunatak Station hourly temperature and ERA-Interim hourly temperature (Figure 3.22a). The synthetic Nunatak Station was then used to bias correct the ERA-Interim record with a multiplier of 0.69 and an offset of -2.2°C. After the correction, the mean bias error is effectively zero and the linear regression better fits the 1:1 line (Figure 3.22b). The corrected and uncorrected 36 year record is shown in Figures 3.23 and 3.24.

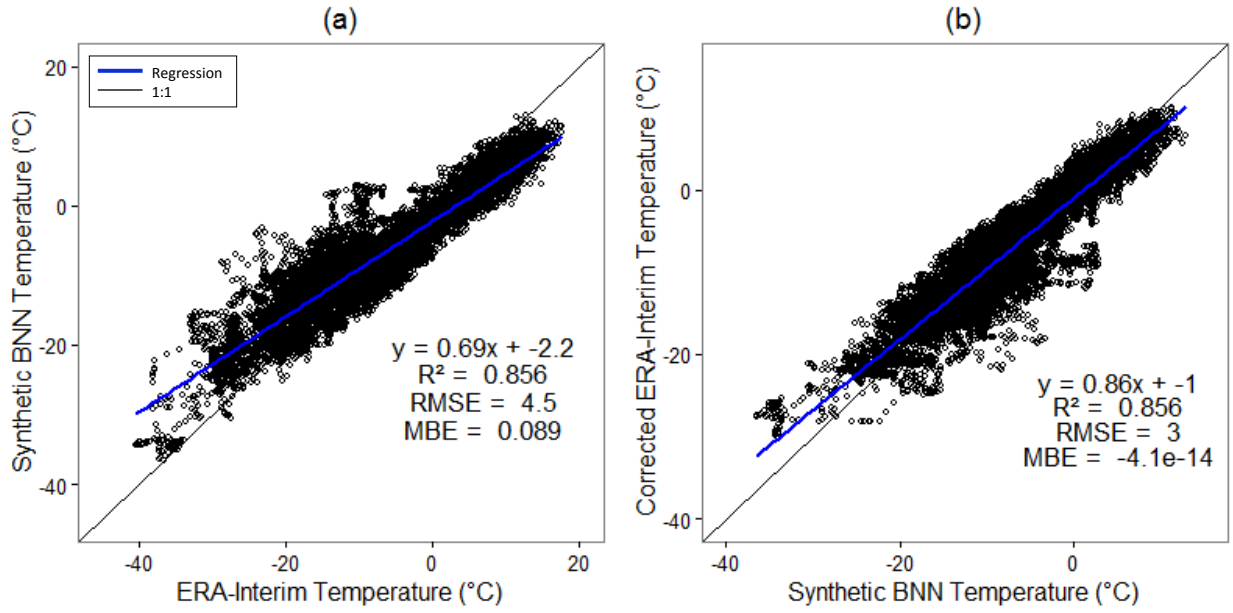

Figure 3.22: Hourly temperature comparisons for ERA-Interim and the Synthetic Nunatak Station: (a) plot used for correction; (b) correction applied

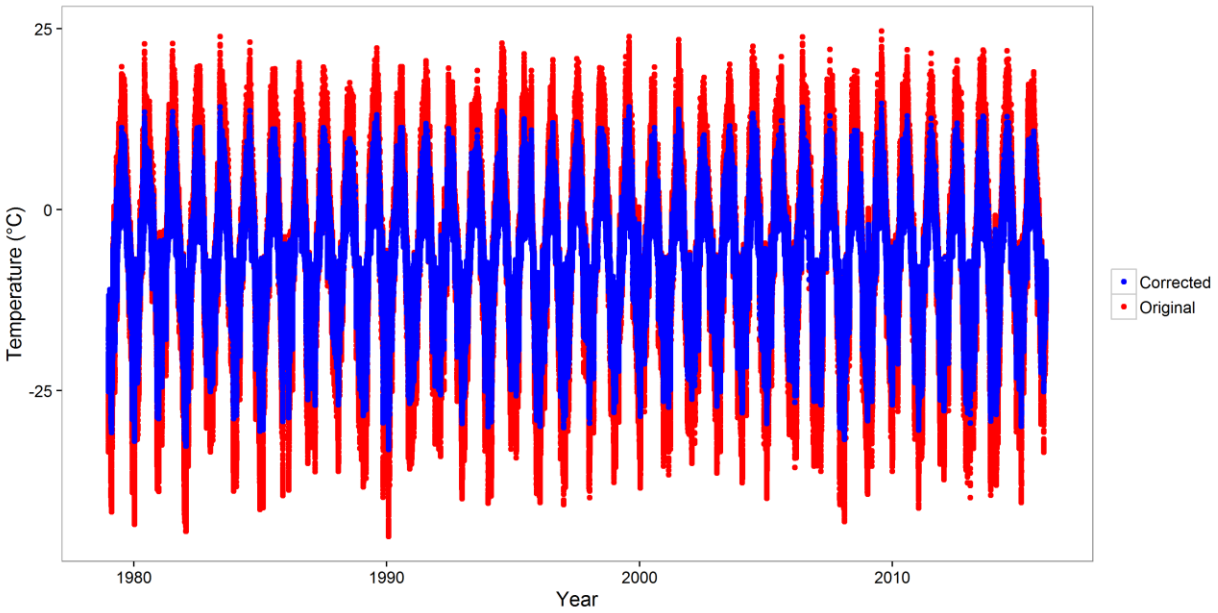

Figure 3.23: Corrected and original hourly temperature at the Bologna Glacier (1980-2015)

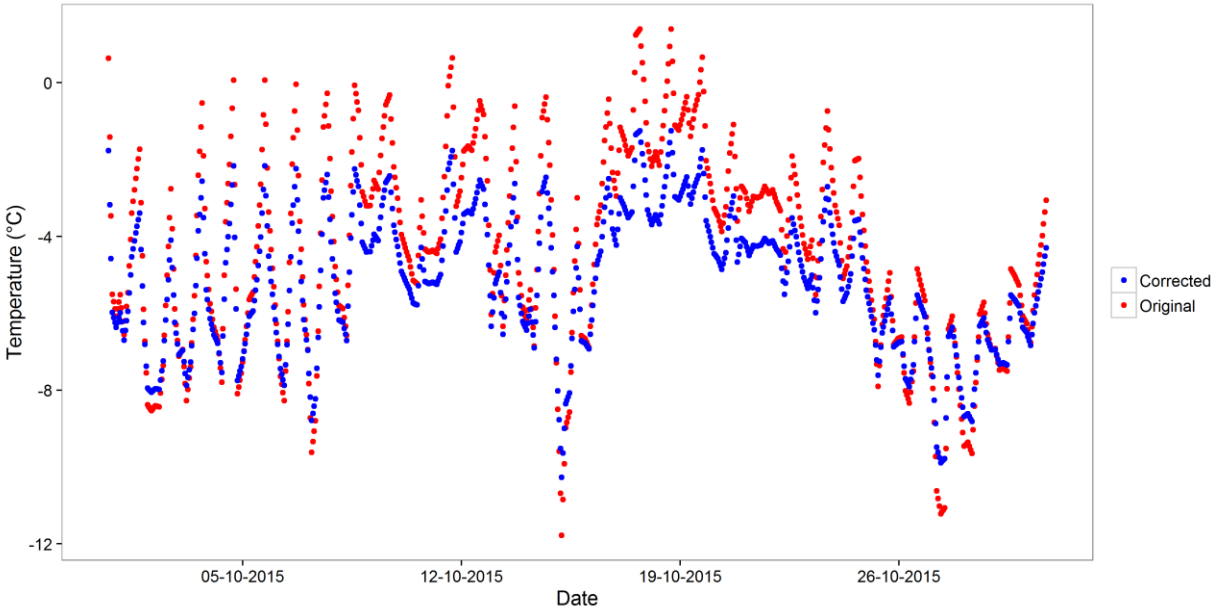

Figure 3.24: Corrected and original hourly temperature at the Bologna Glacier in October 2015

Vapour pressure: Relative humidity from both Bologna stations was converted to vapour pressure. ERA-Interim dew point temperature was converted to vapour pressure (Appendix A). Ice Station vapour pressure was corrected to the Nunatak Station to create a synthetic Nunatak Station with a 24-month record. Plotting the synthetic Nunatak Station against the ERA-Interim

record gives the slope correction of 0.6 (Figure 3.25a), used to correct the ERA-Interim record. The data were corrected slope only so as to prevent inducing negative vapour pressure values with an offset value. After the correction, the linear regression better fits the 1:1 line (Figure 3.25b). The corrected and uncorrected 36 year record is shown in Figures 3.26 and 3.27.

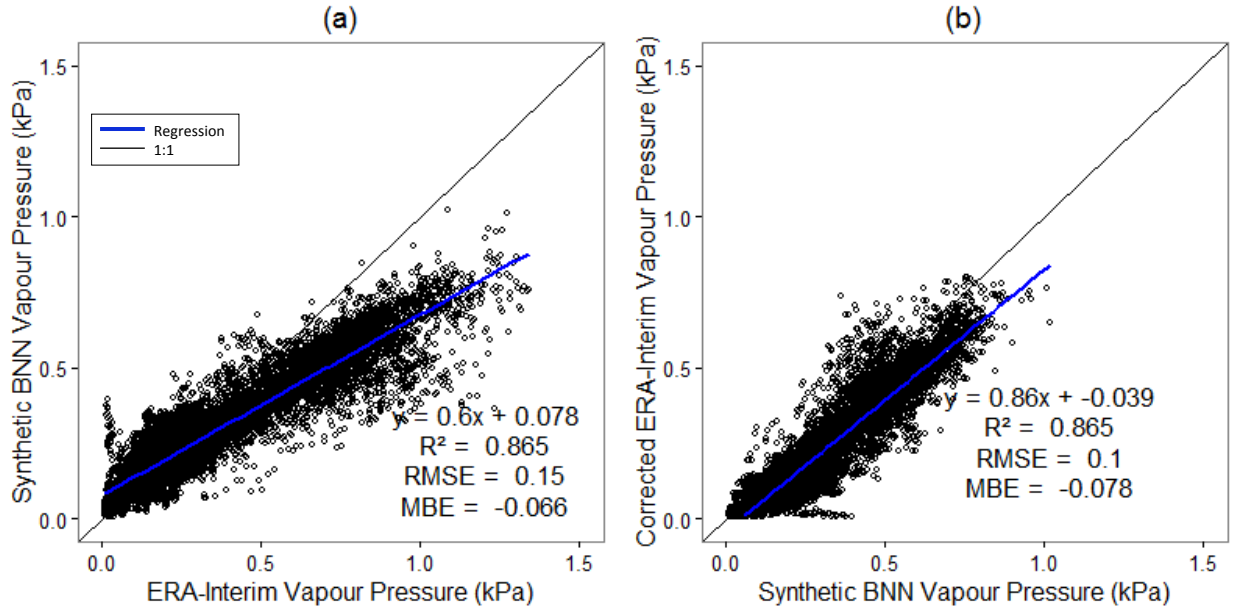

Figure 3.25: Hourly vapour pressure comparisons for ERA-Interim and the Synthetic Nunatak Station: (a) plot used for correction; (b) correction applied

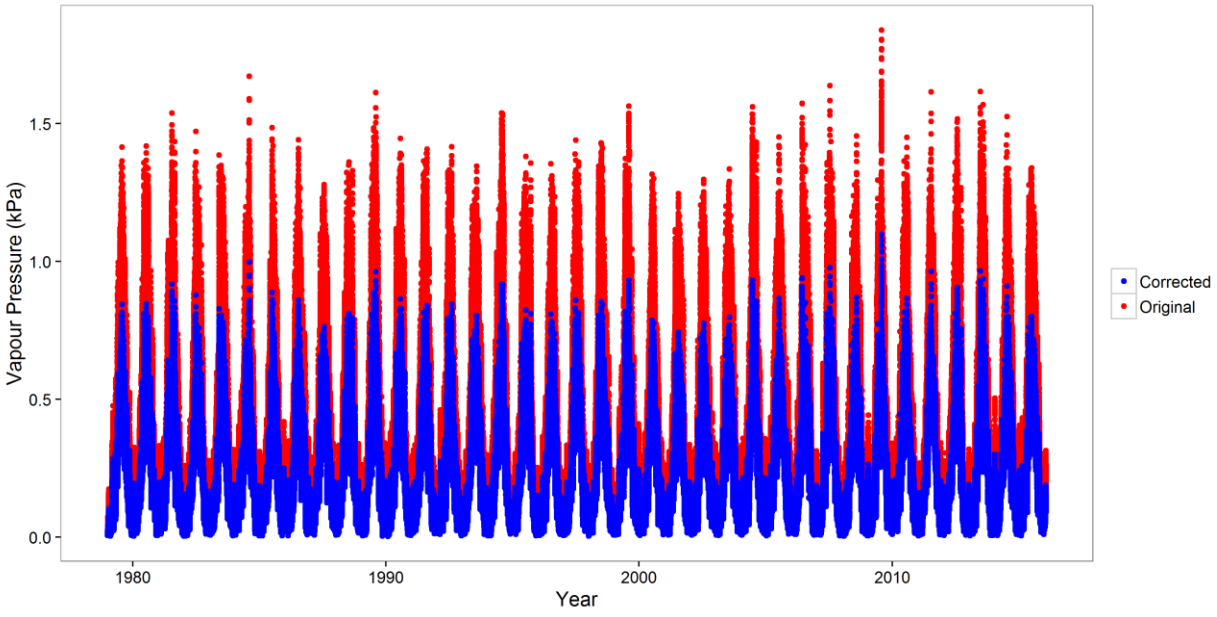

Figure 3.26: Corrected and original hourly vapour pressure at the Bologna Glacier (1980-2015)

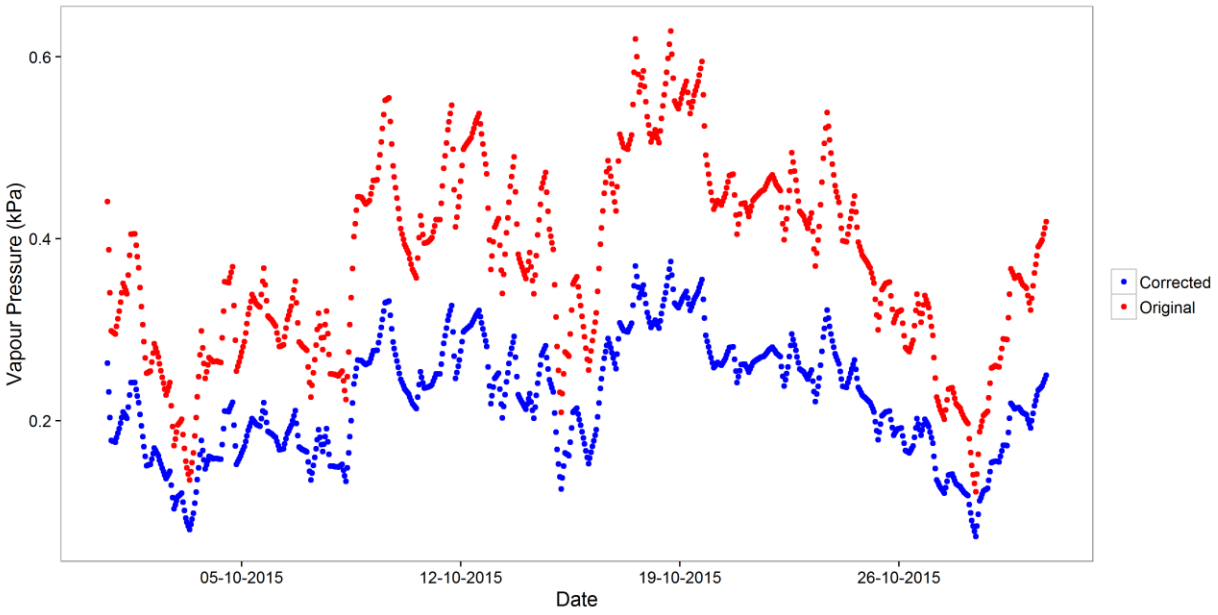

Figure 3.27: Corrected and original hourly vapour pressure at the Bologna Glacier in October 2015

Wind: Observations from the Ice Station were used to downscale the wind reanalyses. Because the Ice Station is situated on the glacier, it provided a better representation of the wind speed and direction over the glacier due to its full exposure to katabatic wind flow down the glacier. The terrain surrounding the Nunatak Station is highly complex and the wind observations are less representative of the basin than at the Ice Station. In addition, the Ice Station has a mast with three wind measurement heights, which allowed for the calculation of the aerodynamic roughness height of the glacier (Appendix A). Using the calculated roughness height, the 10 m wind speed could be calculated for the Ice Station more accurately than for the Nunatak Station, where the aerodynamic roughness height cannot be calculated. Wind roses for the Nunatak Station, Ice Station, and ERA-Interim reanalyses are shown in Appendix C. Figure 3.28a shows that there is no statistical correlation between the ERA-Interim 10 m wind speed and the Ice Station 10 m wind speed. The ERA-Interim wind speed was corrected by multiplying it by the ratio of the average ERA-Interim wind speed to the average Ice Station wind speed (multiplier = 1.82). A regression between the corrected ERA-Interim wind speed and Ice Station wind speed is shown in Figure 3.28b. The corrected and uncorrected 36 year record is shown in Figures 3.29 and 3.30.

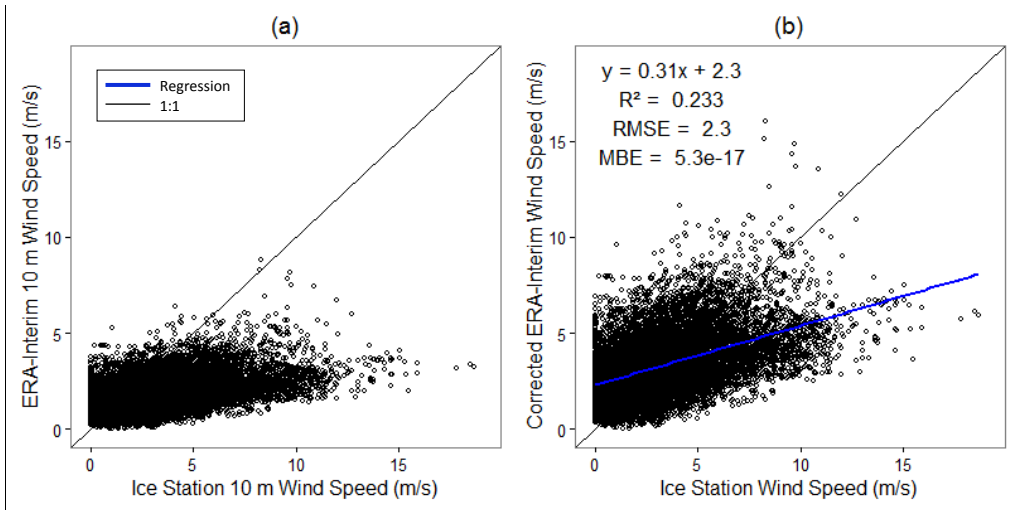

Figure 3.28: Hourly wind speed comparisons for ERA-Interim and the Ice Station: (a) uncorrected; (b) corrected

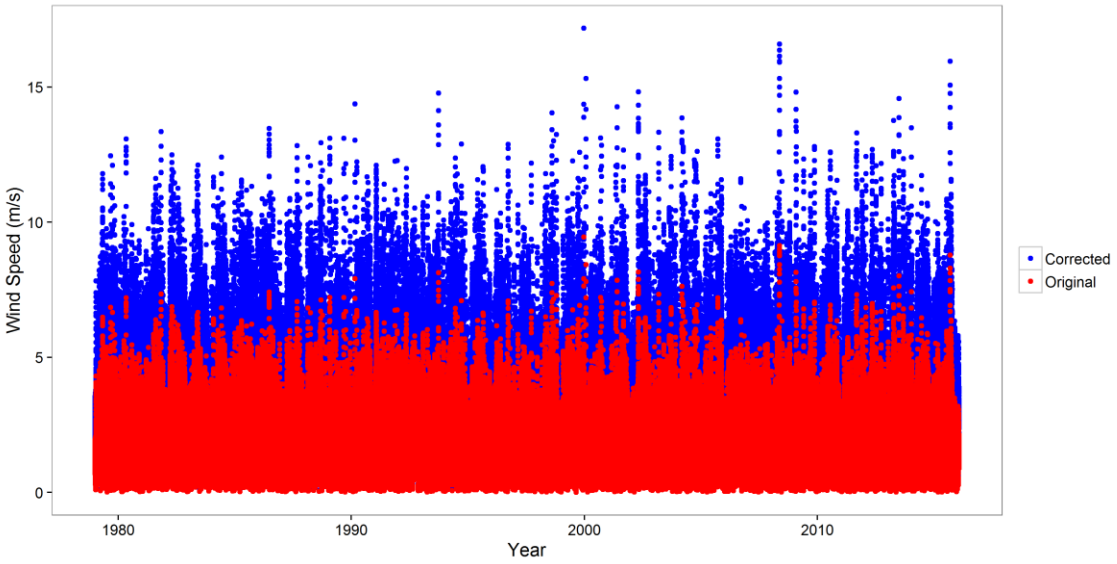

Figure 3.29: Corrected and original hourly wind speed at the Bologna Glacier (1980-2015)

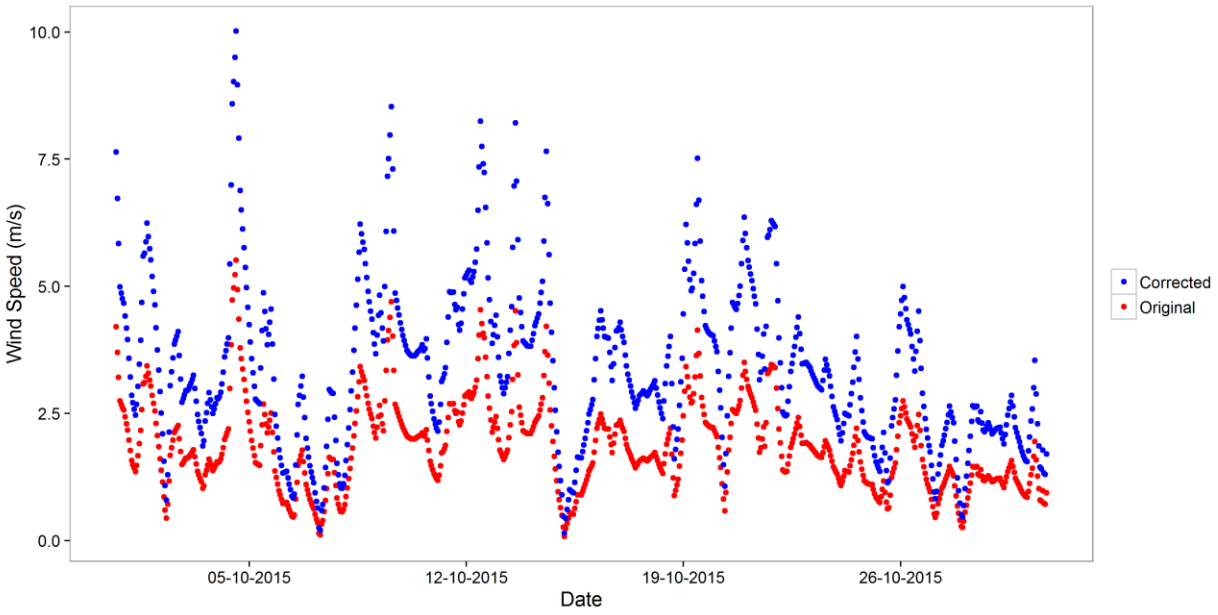

Figure 3.30: Corrected and original hourly wind speed at the Bologna Glacier in October 2015

Incoming Solar Radiation: Ice Station observations were bias corrected (slope only) to the Nunatak Station to create a synthetic Nunatak Station with a 24-month record. The observations were corrected for slope only so as to prevent inducing negative radiation with an offset value. The slope correction was found by plotting the synthetic Nunatak Station hourly shortwave radiation and ERA-Interim hourly shortwave radiation (Figure 3.31a). The synthetic Nunatak Station was then used to bias correct the ERA-Interim record with a multiplier of 0.96. The regression between corrected ERA-Interim incoming shortwave radiation and synthetic Nunatak Station shortwave radiation is shown in Figure 3.31b. The corrected and uncorrected 36 year record is shown in Figures 3.32 and 3.33.

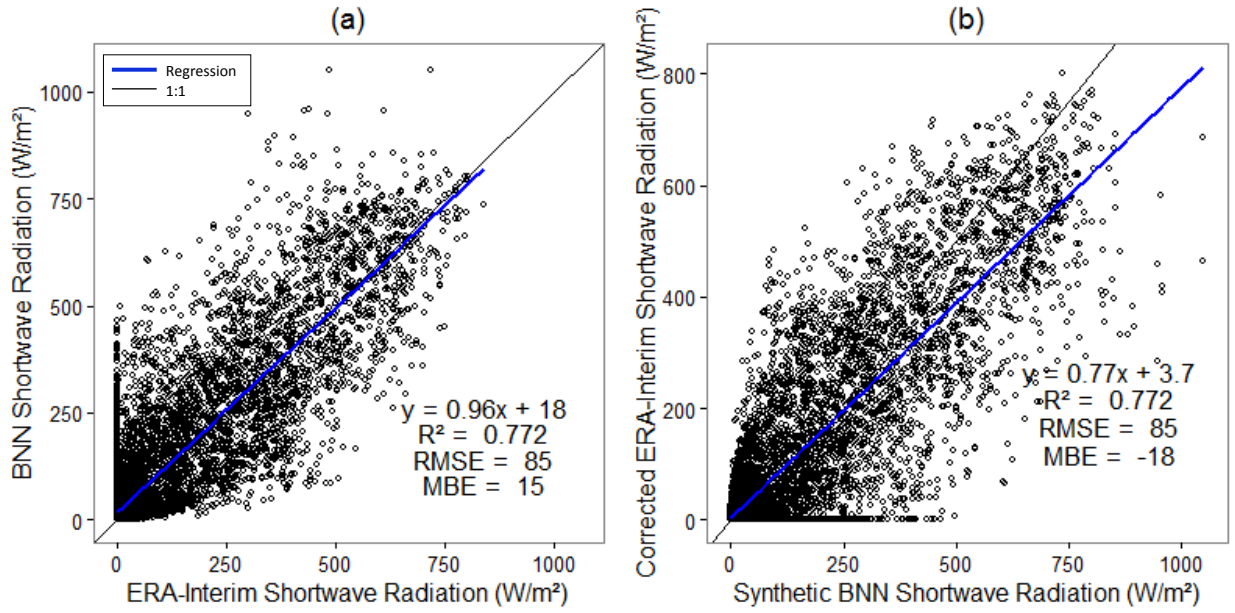

Figure 3.31: Hourly shortwave radiation comparisons for ERA-Interim and the Synthetic Nunatak Station: (a) plot used for correction; (b) correction applied

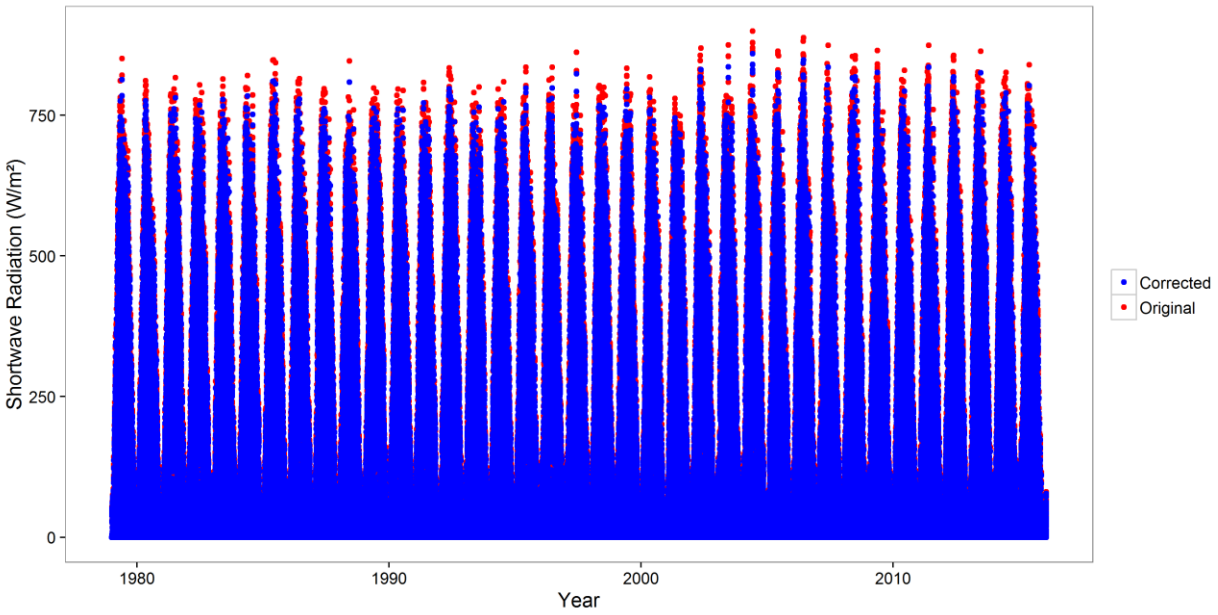

Figure 3.32: Corrected and original hourly shortwave radiation at the Bologna Glacier (1980-2015)

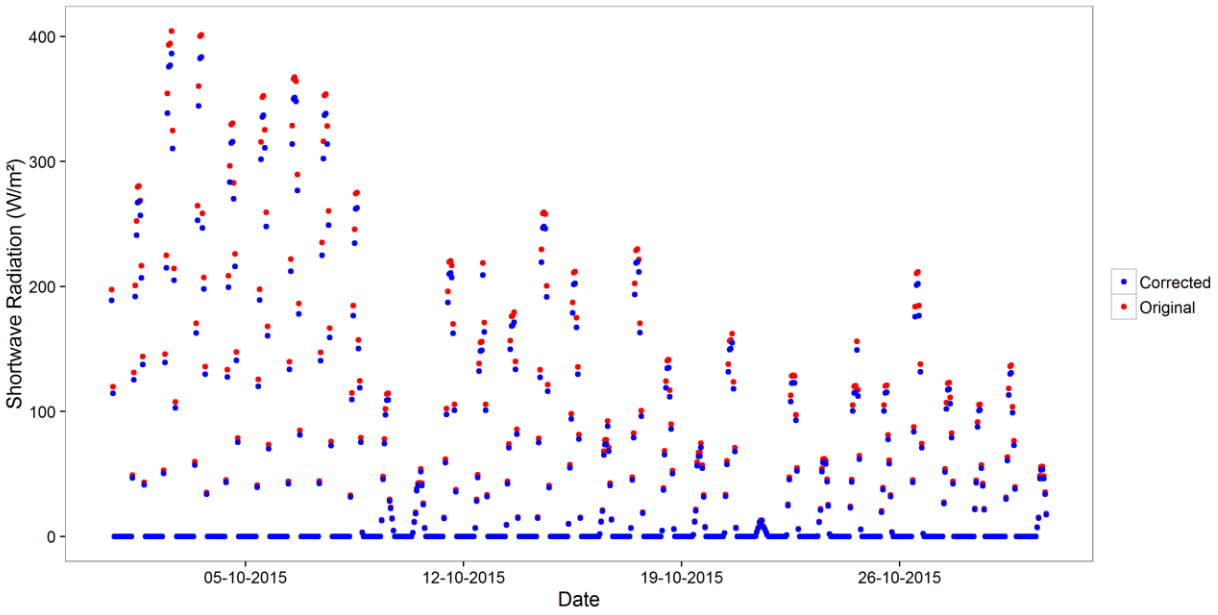

Figure 3.33: Corrected and original hourly shortwave radiation at the Bologna Glacier in October 2015

Precipitation: There is no snowfall gauge at the Bologna Glacier; therefore, precipitation was corrected to the tipping bucket gauge at the Ice Station. The Ice Station observations were used rather than the Nunatak Station as the Nunatak Station collected very few observations during the summer months. Additionally, the Ice Station gauge should predict rainfall at the glacier surface more accurately than the Nunatak Station gauge. The corrected temperature observations were used to identify a stretch of days where the mean daily temperature was greater than 2°C: July 3 – 18, 2015 – it was assumed that during this time, precipitation fell as rain only and was recorded by the tipping bucket gauge. Plotting ERA-Interim precipitation against observations during this stretch of days showed that there was no statistical correlation between the daily ERA-Interim precipitation and the daily Ice Station rainfall. Therefore, a double mass curve was plotted to compare ERA-Interim cumulative daily precipitation and Ice Station cumulative daily rain (Figure 3.34a). A linear regression forced through zero was used to obtain the regression equation to correct ERA-Interim precipitation. ERA-Interim total daily precipitation was multiplied by 0.75. The regression between the corrected cumulative ERA-Interim precipitation and the Ice Station cumulative rain is shown in Figure 3.34b. Figure 3.35 shows the total daily, weekly, and monthly ERA-Interim precipitation compared to Ice Station observations. The data used here included the summer months of 2015 – June, July, and the latter part of August after the station was repaired. It is evident that as the time period over which the precipitation data is

totalled increases from daily to weekly to monthly, the significance of the relationship between the two variables increases (R^2 = 0.22, 0.46, 0.83, respectively) The corrected and uncorrected 36 year record is shown in Figures 3.36 and 3.37.

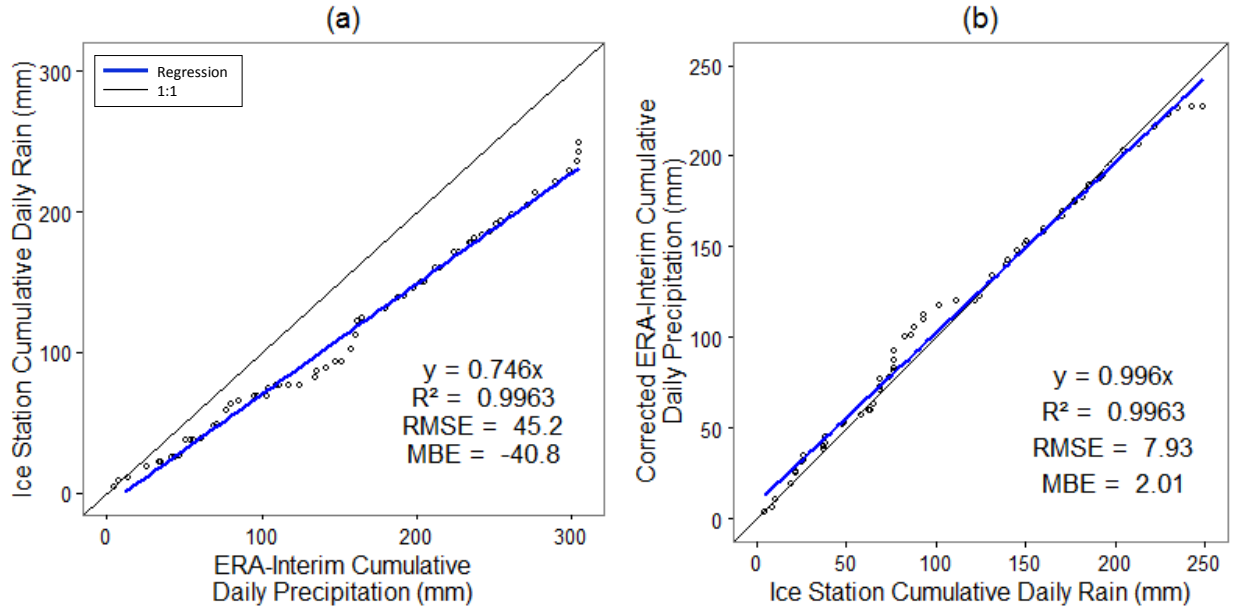

Figure 3.34: Cumulative precipitation comparisons for ERA-Interim and the Ice station: (a) plot used for correction; (b) correction applied

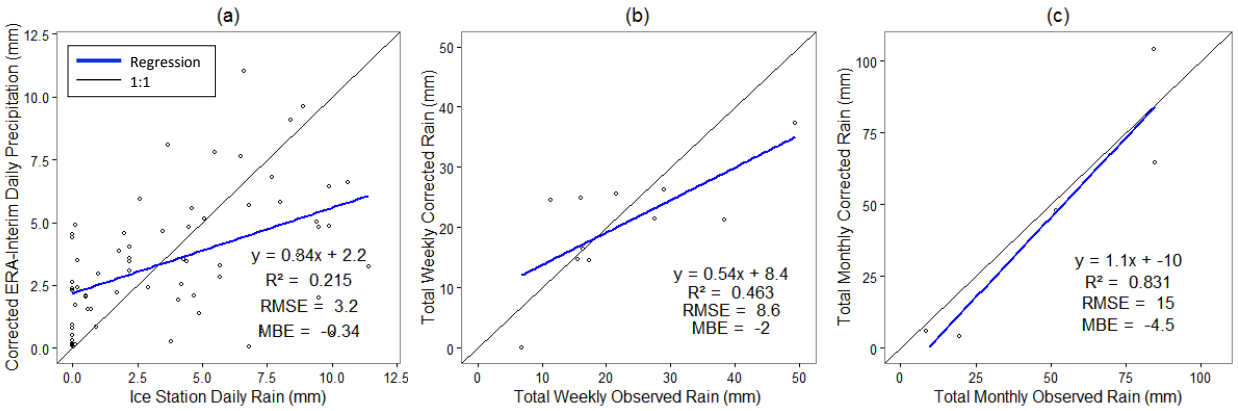

Figure 3.35: Corrected ERA-Interim compared to observations for (a) daily rainfall; (b) weekly rainfall; and (c) monthly rainfall from

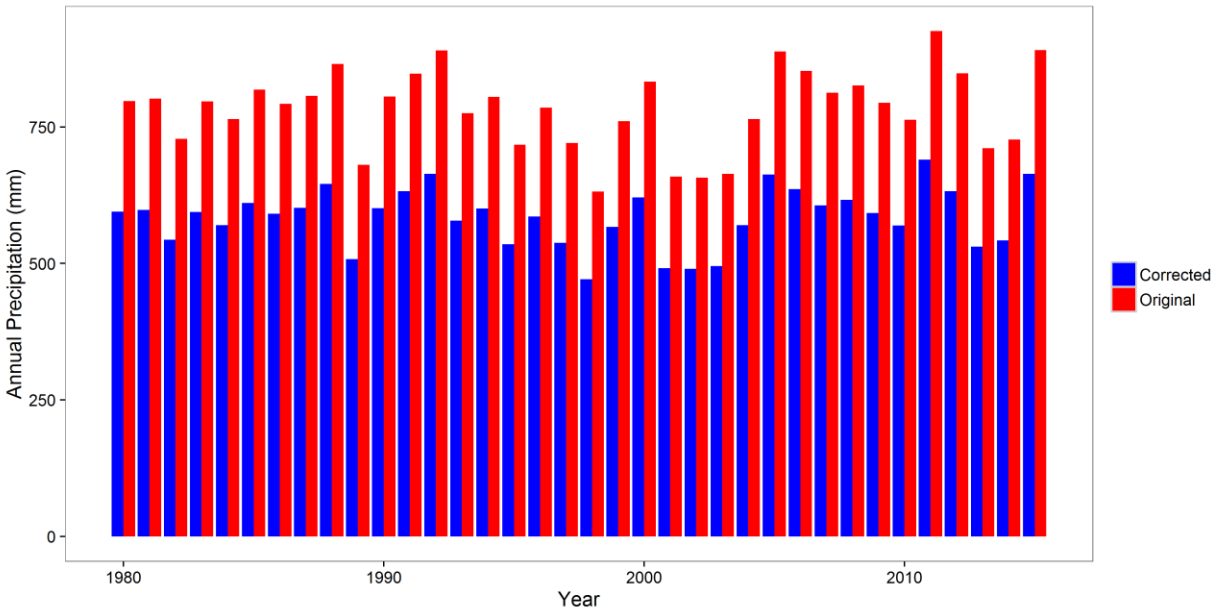

Figure 3.36: Corrected and original precipitation by hydrological year at the Bologna Glacier (1980-2015)

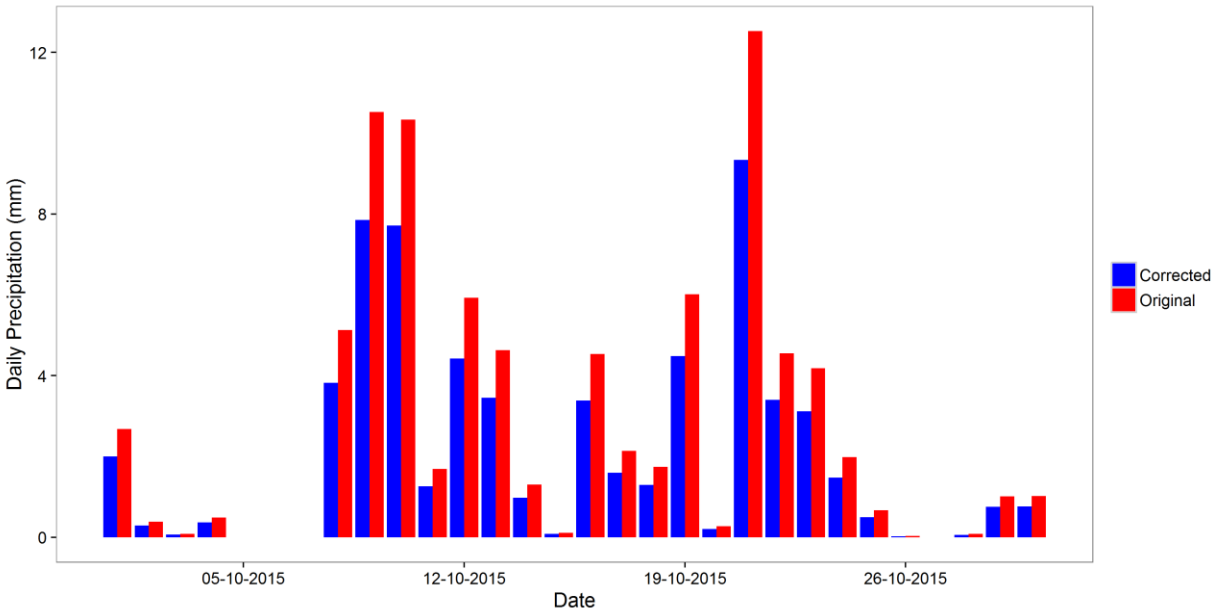

Figure 3.37: Corrected and original daily precipitation at the Bologna Glacier in October 2015

3.3 Hydrometric Data

Hydrometric measurements of stage and discharge are available from the Water Survey of Canada (WSC) (https://wateroffice.ec.gc.ca) for the South Nahanni River at Virginia Falls. The station location, time period available, and basic details are summarized in Table 3.7 and the daily discharge is shown in Figure 3.38. The measurements are available from 1962 to 2015. Approximately 6% of daily discharge measurements are missing; however, all gaps occur prior to 1973, which were not required for this study. The average daily discharge over this time period is 234 m³/s. The peak discharge is 2250 m³/s and occurred on July 27, 1972.

Table 3.7: Hydrometric measurements for the South Nahanni River above Virginia Falls

Station ID	Station Name	Station measurements	Latitude (°N)	Longitude (°W)	Drainage Area (km2)	Years Active	Daily time step
10EB001	South Nahanni River Above Virginia Falls	Daily discharge and stage	61°38'10"	125°47'49"	14500	52	1962 – 2015

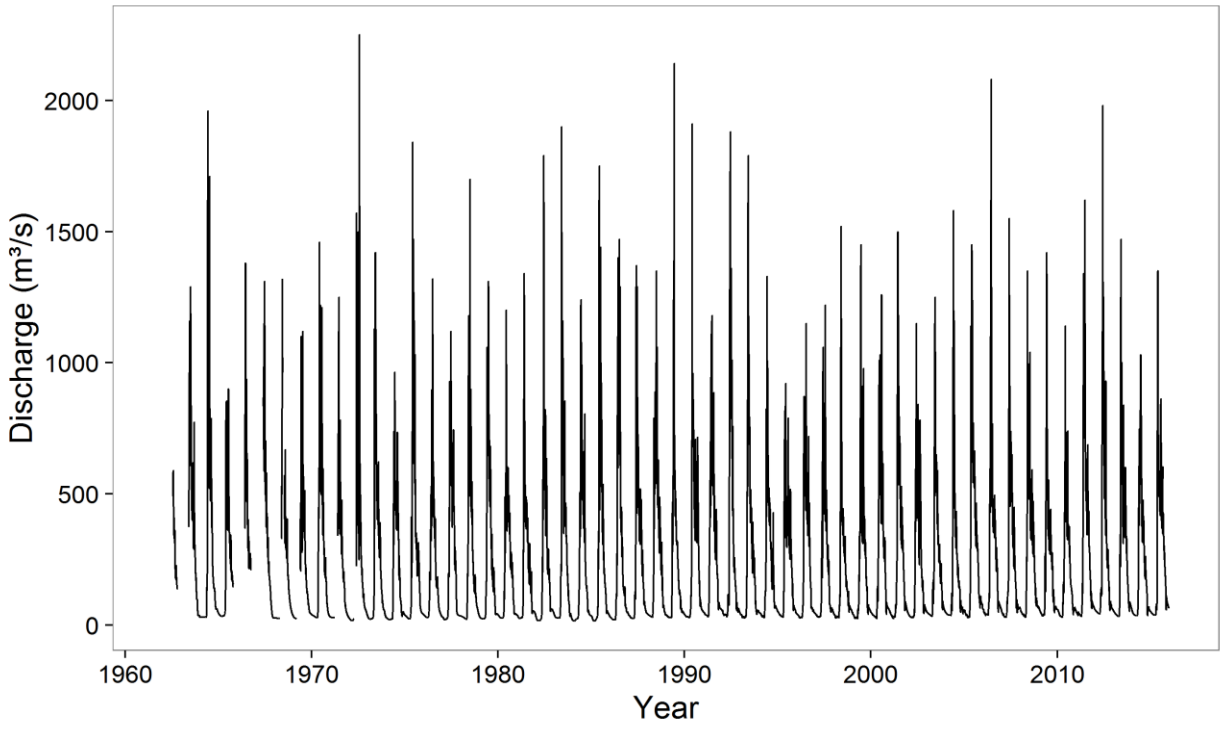

Figure 3.38: South Nahanni River discharge at the Virginia Falls gauge (1962 – 2015)

3.4 Hydrological Model Platform

The Cold Regions Hydrological Modelling Platform (CRHM) is an object-oriented, modular, flexible, physically based modelling platform used for diagnosing and predicting hydrological processes in cold regions (Pomeroy et al., 2007). Physically based models are advantageous compared to other types of models (e.g. conceptual, empirical, and statistical) because they represent the physical interactions of processes within the hydrological cycle. CRHM has been extensively applied throughout continental western Canada including British Columbia, the Yukon, the Canadian Rockies, the Canadian Prairies, and globally in Patagonia, the Pyrenees, the Alps, the Tibetan-Qinghai Plateau, and the Arctic in the Svalbard Archipelago, Norway (Ellis and Pomeroy, 2007; Dornes et al., 2008a; Ellis et al., 2010; Fang et al., 2013; López-Moreno et al., 2013; Zhou et al., 2014; Krogh et al., 2015; López-Moreno et al., 2016). This model was chosen because of its proven applicability in alpine cold regions and for its limited need for calibration, which means that it can be applied in ungauged basins (Pomeroy et al., 2007).

CRHM has several main components described in detail in Pomeroy et al. (2007). Those relevant to this project include: observations, parameters, modules, variables, and state variables. The observations include a 36 year meteorological record derived from ERA-Interim gridded reanalysis, as described in Section 3.2. The observations include hourly temperature, vapour pressure, wind speed, incoming solar radiation, and daily precipitation. Parameters describe the spatial characteristics of the basin as well as prescribed values governing relationships that control model function. Spatial parameters are based on measureable physiographic features, determined via observations or remote sensing analyzed using GIS tools. Spatial data are required to set up Hydrological Response Units (HRUs), which describe the spatial distribution of hydrological processes over the basin. These delineate basin area, vegetation cover, elevation, slope, and aspect. Other model parameters including those that govern model albedo, radiation, blowing snow, soil infiltration, routing, etc., are obtained via field observations or are transferred from scientific studies from similar climatic/landscape conditions (Dornes et al., 2008c; Pomeroy et al., 2013). The user selects modules containing algorithms to execute the hydrological/ physical processes required to construct the model. The model structure is then implemented globally by the CRHM platform. Both variables and state variables are created by the parameterization of the modules. Variables are the meteorological driving data including temperature, vapour pressure, wind speed, and precipitation. These differ from the observations

as the module declarations can alter the observations according to procedures that include lapsing temperature depending on elevation or adjusting precipitation for wind undercatch based on gauge type. State variables are the dynamic HRU properties, e.g., soil moisture, snow water equivalent, and albedo.

The next section will describe the modules selected to assemble the model, to delineate the basin, and to parameterize the model.

3.5 Model Construction and Parameterization

3.5.1 Module Selection

The model's modular platform allows users to select physical processes required to characterize the hydrology of a basin. The modules included to represent the Bologna Glacier basin are described below and are shown schematically in Figure 3.39. For more information on these and all CRHM modules, refer to the CRHM module manual (Centre for Hydrology, 2016).

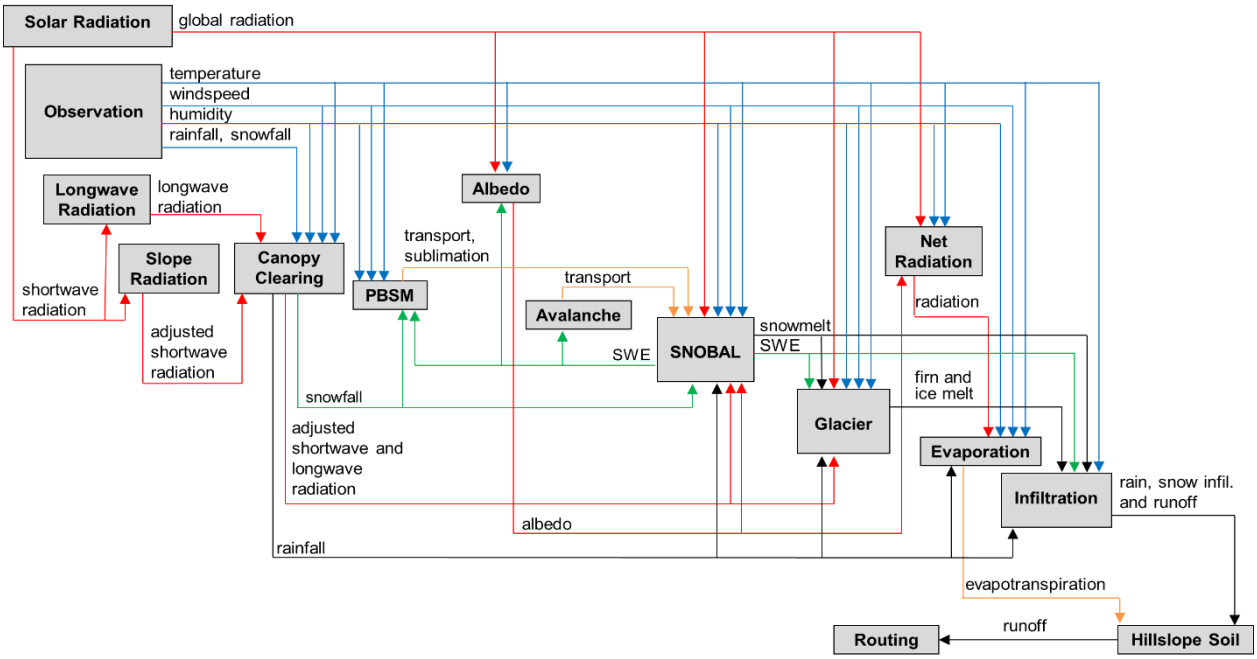

Figure 3.39: Modular design of the CRHM Platform: red lines indicate radiation terms; blue lines indicate climate observations; orange lines indicate mass transport; green and black lines indicate model output or calculated water equivalent, in solid and liquid forms, respectively (reproduced with the permission of Dhiraj Pradhananga, personal communication)

- The observation module, *obs*, reads meteorological forcing data from the observation files. Temperature, vapour pressure, wind speed, and shortwave radiation are provided at hourly intervals, and dictate the time step for the model. Precipitation is provided at a daily time step, and is input into the model at midnight each day. This module adjusts temperature relative to the elevation range using a prescribed lapse rate and adjusts precipitation with elevation.

- The global radiation module, *global*, uses geographic parameters including latitude, elevation, ground slope, and azimuth to calculate the theoretical global radiation, direct

and diffuse radiation, and maximum sunshine hours following the techniques described by Garnier and Ohmura (1968). This module provides inputs to the albedo, net radiation, longwave radiation, and slope radiation modules.

- The sunshine hour module, *calcsun*, uses the incoming shortwave observation, daily clear-sky direct and diffuse solar radiation, and maximum sunshine hours along with the HRU latitude to estimate the actual sunshine hours.

- The slope radiation module, *Slope_Qsi*, estimates incident shortwave radiation for a slope using the observed incoming shortwave radiation on a level surface and the calculated direct and diffuse solar radiation.

- The longwave radiation module, *longVT*, calculates longwave radiation using air temperature, vapour pressure, relative humidity, and the outputs from the global radiation module, following the method from Sicart et al. (2006), who proved this approach to be robust in finding the longwave radiation input to melting snow. This module provides inputs to the energy-balance snowmelt module.

- The soil module, *soil*, calculates the soil moisture throughout the year according to soil moisture balance and drainage calculations according to Leavesley et al. (1983), Dornes et al. (2008b), and Fang et al. (2010, 2013). The module handles two soil layers – a recharge layer and a lower layer – in addition to a groundwater layer and surface depressions. The algorithm calculates soil moisture balance, subsurface and groundwater discharge, groundwater storage, and runoff. Evaporation and subsurface runoff algorithms are executed after the infiltration module.

- The evaporation module, *evap*, calculates evapotranspiration during the snow-free period using either the Granger expression (Granger and Gray, 1989) or the Priestley and Taylor expression (Priestley and Taylor, 1972). For the Bologna Glacier basin, there is little vegetation and therefore this model employs the Granger method to quantify evapotranspiration as it does not require any vegetation-specific parameterization. The algorithm ensures continuity of mass by restricting water availability.

- The canopy clearing module calculates shortwave and longwave sub-canopy radiation at the snow surface according to Ellis et al. (2010). While there is no true canopy within the Bologna Glacier basin, this module is a requirement for the *Snobal* module described below.

- The albedo module, *Albedo_Richard*, estimates snow albedo throughout the snow covered period and during snowmelt following the work of Verseghy (1991).

- The all-wave radiation module, *netall*, is based on the work of Granger and Gray (1990): it models net radiation from calculated incoming shortwave radiation and the Brunt equation to determine evaporation during snow-free periods in the evaporation module. It uses temperature, vapour pressure, and actual sunshine hours.

- The snowmelt module, *Snobal*, employs the layered energy balance snowmelt model by Marks et al. (1999) to resolve the energy balance and calculate snowmelt.

- The blowing snow module, *pbsm*, follows the work of Pomeroy and Li (2000) to simulate snow transport via wind redistribution and the sublimation losses of snow due to wind throughout the winter period.

- The glacier module, *glacier*, is an energy balance snow and ice ablation module used to characterize the accumulation and melt of glacier ice, firn, and snow, in addition to characterizing infiltration of meltwater, surface, and groundwater flows. It was developed by Pradhananga and Pomeroy (unpublished) and is shown schematically in Figure 3.40. It couples new algorithms with existing modules for ice and snowmelt (*Snobal*), wind redistribution of snow (*pbsm*), routing, soil moisture balance, and infiltration. The model calculates snowmelt and ice/firn melt separately. Snowmelt is calculated using *Snobal*, as above, and ice and firn melt is characterized based on a single layer energy balance melt model (Gray and Landine, 1988; Ellis et al., 2010). The module incorporates firn densification according to Herron and Langway (1980), which considers densification processes including settling, sublimation, recrystallization, and diffusion to characterize the firn density and elevation change. Meltwater runoff through glacier snow cover, firn, and ice is characterized by a simple linear reservoir routing routine.

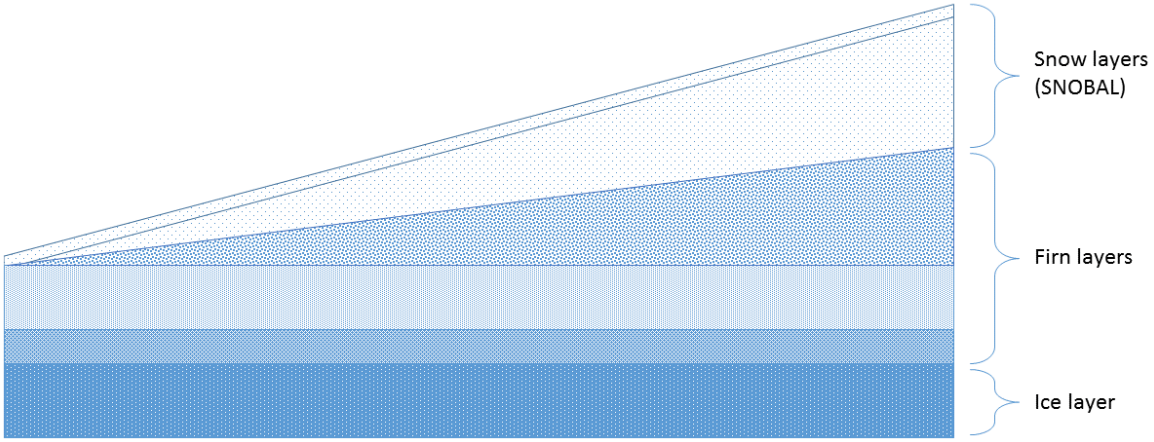

Figure 3.40: Schematic concept of the Energy Balance Glacier Melt model

The energy balance glacier melt model (EBGM) calculates the energy available for firn and ice melt, Q_M (MJ/d) using:

$$Q_M = Q_n + Q_h + Q_e + Q_p \tag{3.1}$$

where, Q_n (MJ/day) is net radiation, Q_h (MJ/day) is sensible heat, Q_e (MJ/day) is latent heat, and Q_p (MJ/day) is the advection energy from precipitation. The melt energy is then converted to a surface melt rate, M (mm/h), using:

$$M = \frac{Q_m}{\rho_w L_f} \tag{3.2}$$

where, ρ_w [kg/m^3] is the density of water and L_f (3.34 x 10^5 J/kg) is the latent heat of water fusion at freezing. Energy input due to precipitation is calculated by:

$$Q_p = \rho_w c_w R(T_p - T_s) \tag{3.3}$$

where ρ_w (kg/m^3) is the density of water, c_w (4.18kJ kg^{-1}K^{-1}) is the specific heat capacity of water, R (m/s) is the precipitation rate, and T_p and T_s are the temperatures of precipitation and the surface, respectively.

The model simulates the glacier mass balance of each HRU in terms of snow (SWE, mm), firn (FIRN, mm), and ice (ICE, mm) water equivalent. Snow redistribution by wind

and avalanche are also considered as these are significant factors in glacier mass balance. Glacier mass balance, MB, is given by:

$$MB = SWE + FIRN + ICE \tag{3.4}$$

Snow water equivalent, firn, and ice are expressed as:

$$SWE = SWE_0 + P + H_{in} - H_{out} - S - M \tag{3.5}$$

$$FIRN = FIRN_0 + V_{in} - V_{out} - S - M \tag{3.6}$$

$$ICE = ICE_0 + V_{in} - S - M \tag{3.7}$$

SWE_0, $FIRN_0$, and ICE_0 are the initial conditions of snow water equivalent, firn, and ice, respectively. P is precipitation, H_{in} and H_{out} are the horizontal mass transfers, V_{in} and V_{out} are the vertical mass transfers caused by firn densification, S is sublimation, and M is melt rate. All units are in millimetres. One limitation of this module is that it currently has no capacity to move ice and firn from upslope to downslope HRUs.

Elevation change, ΔE, is calculated from the mass balance components of changing ice, snow, and firn volumes:

$$\Delta E = \frac{\Delta SWE}{\rho_s} + \frac{\Delta FIRN}{\rho_f} + \frac{\Delta ICE}{\rho_i} \tag{3.8}$$

- The avalanche module, *SWESlope*, calculates snow redistribution due to gravity from higher elevation HRUs to lower elevation HRUs based on snow depth and slope angle (Pradhananga, unpublished). This module is based on the routine developed by Bernhardt and Schulz (2010), where snow slides given a threshold snow depth (H_d) and slope angle (S_m). The suggested value for minimum snow holding depth is 50 mm and minimum slope angle is 25°. The avalanche module uses the regression line fitting the curve of H_d [m] and S_m [°]:

$$H_d = 3178.4{S_m}^{-1.998} \tag{3.9}$$

- The infiltration module, *frozenAyers*, estimates rainfall infiltration into unfrozen soil following the work of Ayers (1959), which considers soil texture and ground cover. Infiltration into frozen soils uses Gray's parametric snowmelt infiltration algorithm (Zhao and Gray, 1999).

- The wind module, *Walmsley_wind*, relies on Walmsley et al., 1989, where a simple parametric model is used to estimate wind speed variation generated by small scale topographic features. It adjusts wind speed due to topography and is based on a wind ratio between the adjusted wind speed and the reference wind speed. Topographic features include 2D and 3D hills, 2D escarpments, 2D rolling terrain, 3D rolling terrain, and flat terrain.

- The routing module, *netroute*, uses the lag and route method described by Clark (1945) to manage the routing of surface, subsurface, and HRU routing.

3.5.2 Spatial Delineation

Hydrological Response Units (HRUs) represent the spatial distribution of hydrological processes, parameters, and driving meteorology. The basin is discretized according to characteristics including elevation, land cover type, slope, aspect, sky view factor, and the firn limit. This section will describe the spatial data used to define the HRU boundaries, and will present the final representation of HRUs for the Bologna Glacier basin.

3.5.2.1 Multi-spectral Imagery

Satellite imagery from the Landsat missions was found using the USGS Global Visualization Viewer (http://glovis.usgs.gov) and acquired from the USGS EarthExplorer (http://earthexplorer.usgs.gov). To determine the glacier margins and surface cover configuration, imagery had to be captured during the late-summer snow free period at the end of the melt season (August), and had to have minimal cloud cover and good resolution. Two images were found 30 years apart (1984 and 2014). The first image was acquired from Landsat 5 Thematic Mapper (TM) mission path 55, row 17 (Worldwide Referencing System-2 WRS-2) captured on August 3, 1984 (http://earthexplorer.usgs.gov/metadata/3119/ LT50550171984216PAC00). Landsat 5 was launched in March 1984 and Band 1 through 5 and 7 have a resolution of 30 m. Band 6 (thermal infrared band) was acquired at a resolution of 120

m but was resampled to 30 m. This image had cloud cover of 0.01% and an image quality of 9 (Excellent – no quality issues or errors detected). The second image was acquired from Landsat 8 Operational Land Imager (OLI) mission path 54, row 17 captured on August 15, 2014 (http://earthexplorer.usgs.gov/metadata/8704/LC80540172014227LGN00) and had cloud cover of 1.38% and image quality 9. Landsat 8 was launched in February 2013 and all bands have a resolution of 30 m (Bands 1 – 7 and 9), with the exception of the panchromatic band (Band 8), which has a resolution of 15m. Both scenes were processed with the Standard Terrain Correction (Level 1T).

3.5.2.2 Digital Elevation Model (DEM)

The DEM used to determine the basin boundary, elevation range, slope, and aspect was the Canada DEM (CDEM). It was retrieved from Natural Resource Canada's Geogratis (http://geogratis.gc.ca/geogratis). The CDEM is derived from the Canadian Digital Elevation Data (CDED), which was extracted from National Topographic Data Base (NTDB) maps at a scale of 1:50 000, in addition to the Geospatial Database (GDB) and other remotely sensed imagery and positional data acquired by provinces and territories (Natural Resources Canada, 2013). The resolution of this DEM is 16 m. The accuracy of the CDEM product is defined in the product specifications, which provide the range of precision over the area of each 1:50 000 NTDB map sheet. The Bologna Glacier lies on the boundary between two of these map sheets: 105-I/1, which has an accuracy of 10 to 15 m, and 95-L/4, which has an accuracy of 5 to 10 m. Both of these map sheets were published in 1985. A comparison was done between the CDEM and the surveyed points on the glacier from 2015. The difference was taken between the CDEM values and each survey point. It was determined that between 1985 and 2015 the glacier surface decreased in elevation by an average of 42 m. The CDEM elevation, slope, and aspect are shown in Figure 3.41 for the Bologna Glacier basin. Assuming that the glacier surface changed negligibly between 1984 and 1985, the DEM can also provide a reasonable representation of elevation for the 1984 glacier configuration (the same year for which Landsat imagery exists), which can then be adjusted for the contemporary glacier configurations in 2014 and 2015.

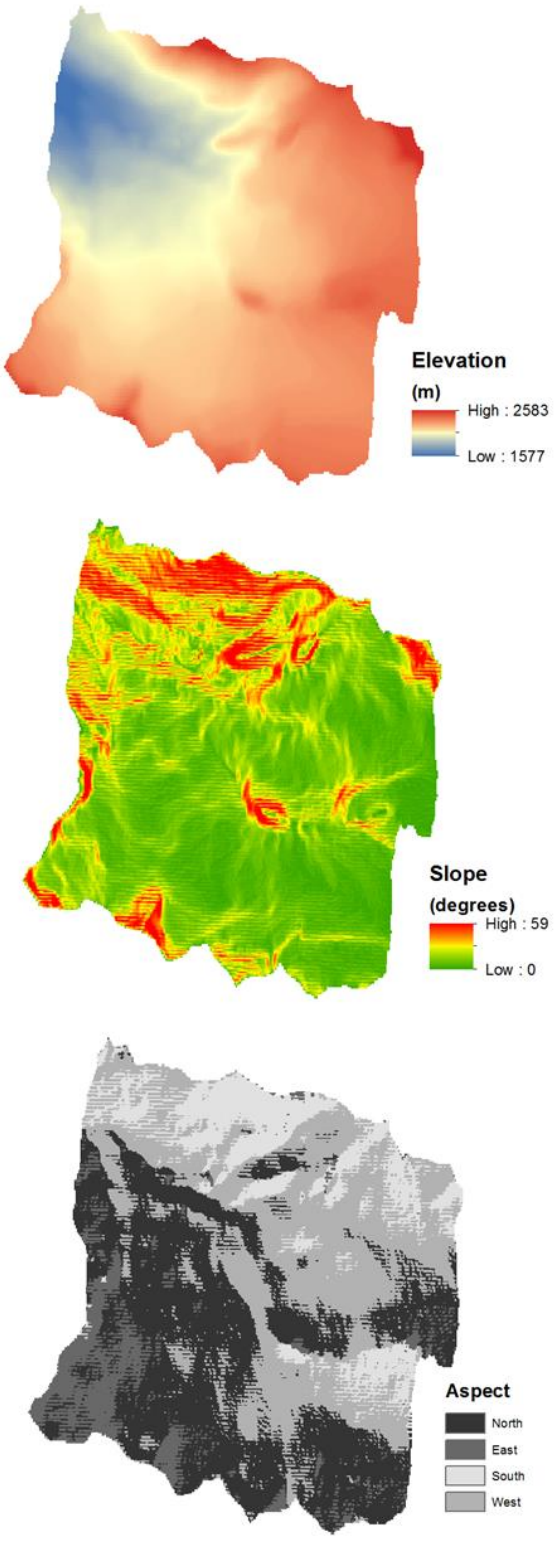

Figure 3.41: Elevation, slope, and aspect maps of the Bologna Glacier basin from the CDEM product

3.5.2.3 HRU Delineation

Five basin characteristics were considered in the delineation of HRUs for the Bologna Glacier basin: elevation, land cover type, firn limit, slope, and aspect. An important consideration in the delineation of the HRUs is that they had to represent either the 1984, 2014, or 2015 basin configuration, depending on how the model parameters are set. It is important that HRU boundaries remain constant for consistency in modelling. In some parts of the basin, areas once covered by glacier ice are now exposed land. For other parts of the basin, areas that were once covered by firn are now covered by exposed ice. When the model is run, parameters will be adjusted such that the appropriate land cover is represented.

Watershed boundary demarcation: The basin boundary was delineated in ArcGIS using the DEM and is shown by the red line in Figure 3.42. The basin outflow point was calculated so as to include the entire glacier but to exclude ice cover in neighbouring basins, such as the Butterfly Glacier, to the west of the Bologna Glacier. The same watershed is used for all three glacier configurations. Most of the boundary falls along alpine ridges, which are assumed to be at a constant elevation over the 30 year period. Since the Bologna Glacier is one of two main outlet glaciers of the Brintnell-Bologna Icefield, the division between the two glaciers was simply defined as the highest point between the two glaciers. This is also assumed to remain constant in the horizontal plane over 30 years, although it is likely to have lowered vertically as the glacier has lost mass over time.

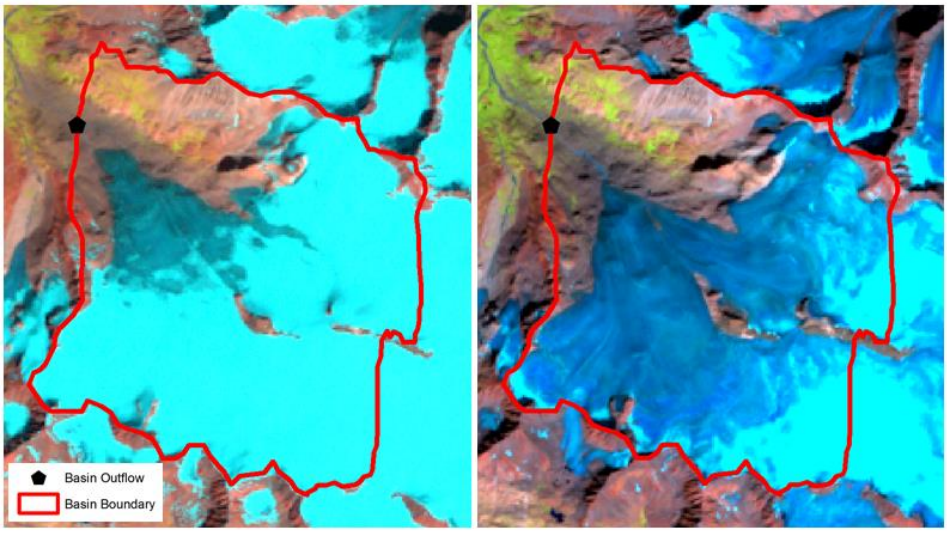

Figure 3.42: Watershed delineation of the Bologna Glacier in 1984 (L) and 2014 (R)

Elevation bands: The model scales temperature, precipitation, and vapour pressure according to elevation. The magnitude of the scaling must be taken into consideration when selecting the range of elevation bands. The basin has a relief of 1003 m. The temperature lapse rate for the model is taken to be the environmental lapse rate of 0.65°C per 100 m. Precipitation is adjusted in CRHM according to the equation

$$P = P_0 \left(1 + \frac{0.01 \Delta E}{100}\right) \tag{3.10}$$

where P is the adjusted precipitation, P_0 is the observed precipitation, and ΔE is the elevation difference from the HRU to the station. Given the elevation difference between the highest and lowest parts of the basin, there will be 10% more precipitation at the upper part of the basin, according to the equation. This is equivalent to roughly 60 mm. Considering the lapse rate and the precipitation scaling, it was determined that four elevation bands of 250 m, as shown in Table 3.8, would be adequate to capture the variations in temperature (1.625°C per 250 m) and precipitation (15 mm per 250 m) throughout the basin. These four levels are referred to as Bottom, Lower, Mid, and Upper in the HRU naming conventions.

Table 3.8: Elevation bands for HRU delineation

Band	Elevation Range	Band Width	Naming Convention
1	1550 – 1800 m	250 m	Bottom
2	1800 – 2050 m	250 m	Lower
3	2050 – 2300 m	250 m	Mid
4	2300 – 2550 m	250 m	Upper

Land cover type: Supervised land cover classification was used to delineate areas of firn, ice, and bare land. ArcGIS was used to select "training areas" from the satellite imagery – areas most representative of each land cover class. Subsequent ArcGIS tools then used these training areas to delineate areas of firn, ice, and bare land. Imagery delineation used false colour band selections, which can help to distinguish the boundary between snow and ice (Hall et al., 1987). The results of the supervised land cover classification are shown in Figure 3.43. There were

some minor issues with shadowing and the classification was manually adjusted to correct these issues.

From the satellite imagery shown in Figure 3.42, it is apparent that the boundary between firn and ice in the 1984 configuration is easily discernible. However, in the 2014 configuration, the boundary is not as clear – particularly in the northeast corner of the basin, the ice and firn seem to be integrated, with a slightly lower albedo than the firn areas at the west end of the basin. To accurately represent these areas in the model, they are classified as firn. The glacier module handles firn as layers, and these areas are represented with fewer firn layers than that of the higher-albedo firn areas.

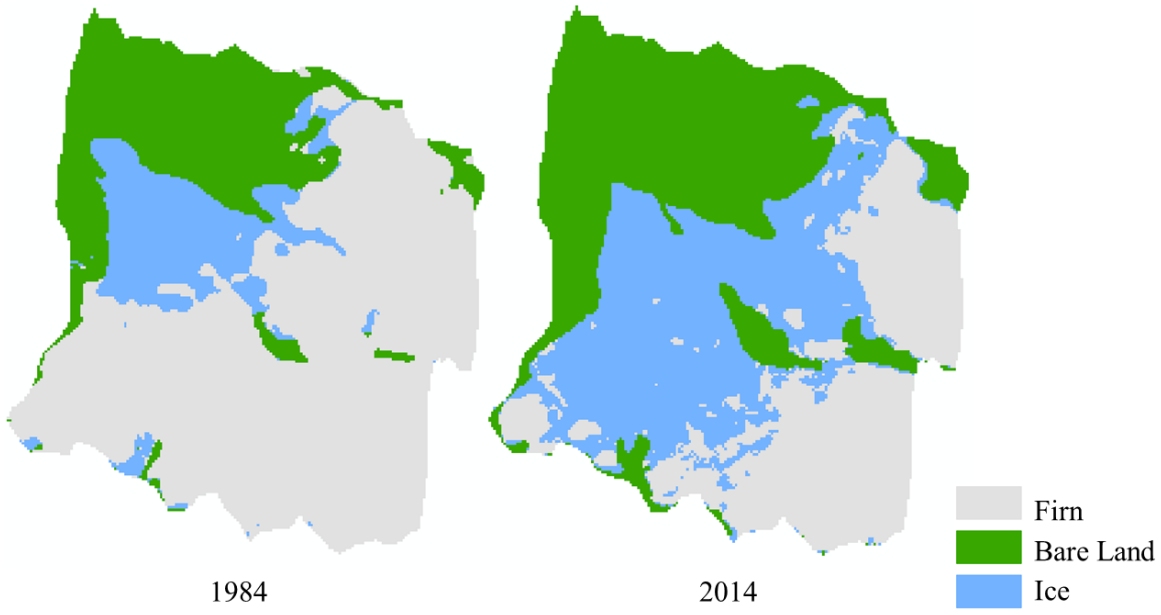

Figure 3.43: Supervised land cover classification of firn, bare land, and ice for two configurations of glacier coverage

Firn limit: On an annual basis, the firn limit divides the area of exposed ice and firn. The boundary was found for each glacier configuration by determining the closest elevation contour to the division between ice and firn as determined by supervised land cover classification. The boundaries for the 1984 and 2014 glacier configurations were determined to be 2050 m and 2250 m, respectively. Because the contour bands of 250 m did not align with the firn limit for the 2014 configuration, Band 3 was sub-divided into two bands: 2050-2250 m and 2250-2300 m.

Slope and aspect: Slope and aspect divisions were grouped together. Slope categories were considered as level (less than 10°), moderate (10° to 45°), or steep (greater than 45°). It was determined that less than 1% of the basin had a slope greater than 45% so this class was combined with the moderate slopes. Aspect classes considered were east/west, north and south. Level terrain and east-west facing slopes were grouped together (level/EW). The remaining terrain was then grouped into moderate south-facing (mod/S) and moderate north-facing (mod/N) classes. To constrain the number of divisions, slope and aspect were considered where the band/land cover area exceeded 5% of the basin area. Further, if a slope/aspect classification exceeded 90% of the band/land cover area, the area was not divided according to slope and aspect.

Sky view factor: An analysis of sky view factor was done using the GIS program System for Automated Geoscientific Analysis (SAGA). It was determined that the basin is largely unobscured by the surrounding terrain. There were some areas near the basin boundary that experienced some shading. Because these regions tended to have the steepest slopes, they were accounted for within the slope and aspect considerations. No separate HRUs were created specifically considering the sky view factor, but the shading was accounted for in the model parameterization.

Hydrological Response Units: The intersection of the terrain properties – elevation, land cover type, firn limit, and slope and aspect – resulted in 19 HRUs to describe the spatial distribution of hydrologically relevant characteristics in the basin. These are shown in Figure 3.44. It is important to note that a single HRU can represent changing land cover types over time (ice, firn, or land) so the naming is generalized to represent all configurations. This set of HRUs can represent the basin in three configurations, as shown in Figure 3.45. The 1984 configuration has significant firn cover, and the glacier covers a larger portion of the basin. The 2014 configuration shows a smaller glacier coverage and a reduction in the area of firn. The 2015 glacier area is approximated as equal in area to the 2014 coverage, but in this configuration there is no firn, as was observed in the field in August, 2015. Properties of each HRU including the land cover type, area, elevation, slope, and aspect of each HRU are given in Table 3.9.

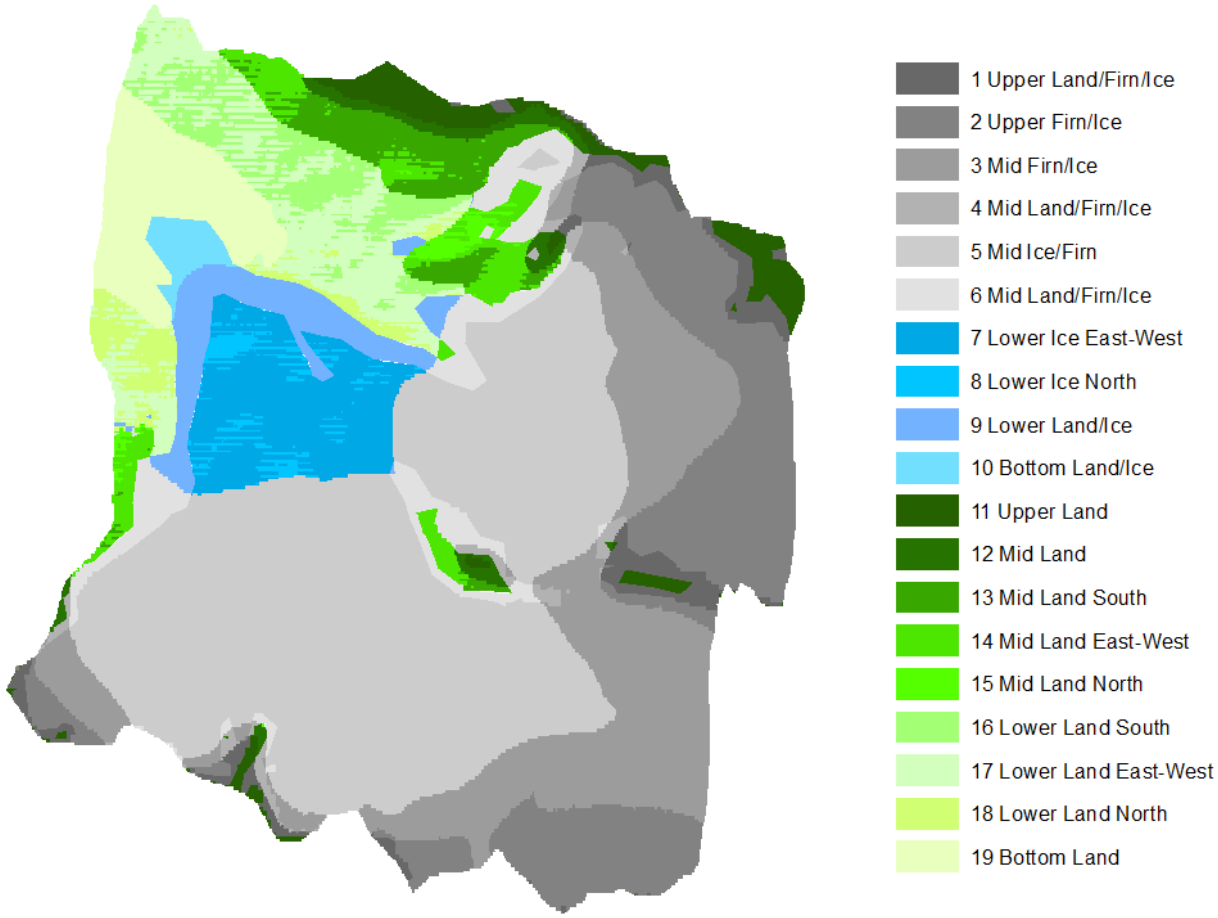

Figure 3.44: Hydrological Response Units for the Bologna Glacier basin

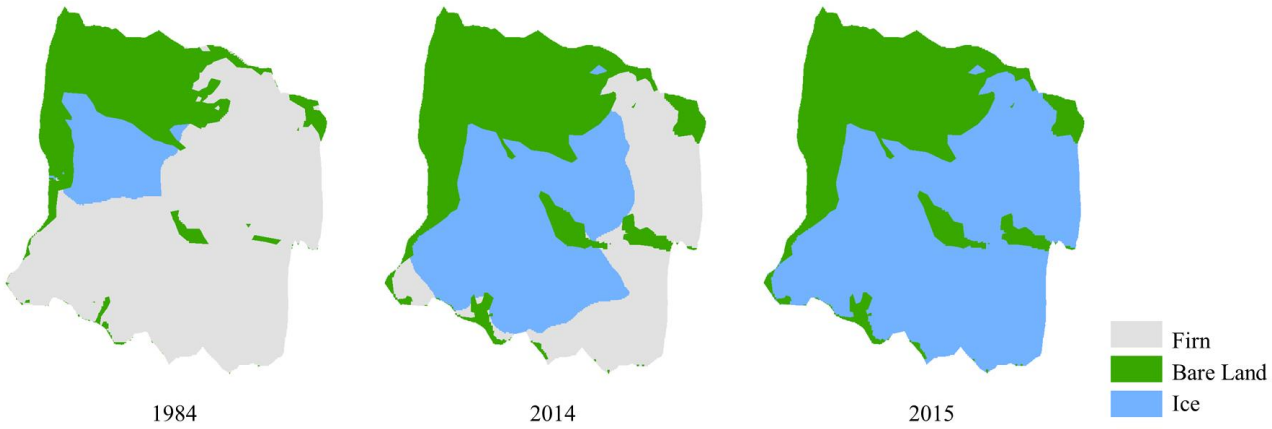

Figure 3.45: HRU configuration for 1984/2014/2015 model configurations

Table 3.9: HRU properties

HRU Number	HRU Land cover Type			Area (km^2)	Area (% of basin)	Mean elevation (m a.s.l.)	Mean aspect (°)	Mean slope (°)
	1984	2014	2015					
1	Firn	Land	Land	0.57	2.4	2354	212	19
2	Firn	Firn	Ice	3.13	13.1	2330	170	8
3	Firn	Firn	Ice	3.41	14.3	2274	176	8
4	Firn	Land	Land	0.21	0.9	2273	130	24
5	Firn	Ice	Ice	7.95	33.3	2169	123	7
6	Firn	Land	Land	0.93	3.9	2147	167	17
7	Ice	Ice	Ice	1.26	5.3	1988	66	7
8	Ice	Ice	Ice	0.22	0.9	1965	72	15
9	Ice	Land	Land	0.75	3.2	1934	65	14
10	Ice	Land	Land	0.2	0.9	1744	53	17
11	Land	Land	Land	0.65	2.7	2399	279	29
12	Land	Land	Land	0.27	1.1	2277	240	30
13	Land	Land	Land	0.67	2.8	2148	280	29
14	Land	Land	Land	0.63	2.6	2137	203	23
15	Land	Land	Land	0.12	0.5	2111	70	27
16	Land	Land	Land	0.7	2.9	1944	296	24
17	Land	Land	Land	1.28	5.4	1928	230	17
18	Land	Land	Land	0.38	1.6	1912	97	21
19	Land	Land	Land	1.06	4.5	1710	207	17

3.5.3 Model Parameterization

Table 3.10 lists the parameter values used in the model, specified for the three land cover types. A full list of model parameters and other CRHM specifications can be found in Appendix D. Where a parameter varies for a single land cover type, a range is specified. Parameters were set based on either past studies in similarly situated basins or from field observations. To account for the glacier configuration changes (1984/2014/2015), the parameters were adjusted such that the appropriate land cover type was represented. Parameters that changed between glacier configurations were populated in the model using R tools built by Shook (2016a) in the package "CRHMr". These include: elevation, firn depth, ice depth, soil texture and moisture properties, aerodynamic roughness heights, and others.

Shared parameters are those used by several modules. While the glacier ice and firn are non-vegetated, the vegetation height describes the surface conditions and is used by the blowing snow module. A height of 0.5 m was selected for the ice and firn HRUs, to capture the surface conditions, which include undulating ice and crevasses. A height of 0.3 m was selected for the land HRUs to capture both the vegetation as well as debris cover. Maximum depression storage is set to 0 for the glacier HRUs and 2 to 5 mm for the land HRUs, as ponding was evident, including a small lake adjacent to the glacier (present only in contemporary configurations). Maximum soil moisture and recharge are set to 0 for the glacier HRUs as it is assumed the glacier covers bedrock. Maximum soil moisture and recharge are estimated for land HRUs at relatively low values (125 mm and 25 mm, respectively), given the observed soil conditions.

Albedo parameters were set according to Gray and Landine (1987) and DeBeer and Pomeroy (2010).

The fraction to ground flux in *Evap* was set according to Granger (1999), who found that the mid-summer soil ground flux is typically 10% of the net radiation for alpine sites.

Parameters for soil infiltration in *frozenAyers* including the environment coefficient, C, surface saturation, S_o, were set following Zhao and Gray (1999), Gray et al. (2001), and Dornes et al. (2008a); initial soil saturation, S_i, was assumed to be 50% of saturation. Initial soil temperature was based on a measurement in the Marmot Creek Research Basin in Alberta (DeBeer and

Table 3.10: Parameter values used for CRHM project modules for three land cover types in the Bologna Glacier basin

Module	Parameter	Firn	Ice	Land
Shared	Vegetation height (m)	0.5	0.5	0.3
Shared	Maximum depression storage (mm)	0	0	2-5
Shared	Maximum soil moisture (mm)	0	0	125
Shared	Maximum soil recharge (mm)	0	0	25
Albedo	Initial albedo for bare ground (-)	0.17	0.17	0.17
Albedo	Initial albedo for snow cover (-)	0.85	0.85	0.85
evap	Fraction to ground flux (-)	0.1	0.1	0.1
frozenAyers	Groundcover (-)	Bare soil	Bare soil	Bare soil
frozenAyers	Texture (-)	Coarse/medium over coarse	Coarse/medium over coarse	Soil over shallow bedrock
frozenAyers	Environment coefficient (C, -)	2	2	2
frozenAyers	Surface saturation (S_o, mm^3/mm^3)	1	1	1
frozenAyers	Initial soil saturation (S_i, mm^3/mm^3)	0.5	0.5	0.5
frozenAyers	Initial soil temperature (K)	269.1	269.1	269.1
Glacier	Firn lag delay (h)	-	4	-
Glacier	Firn storage constant (d)	-	2	-
Glacier	Firn albedo (-)	-	0.5	-
Glacier	Ice lag delay (h)	1	-	-
Glacier	Ice storage constant (d)	0	-	-
Glacier	Ice albedo (-)	0.35	-	-
Glacier	Initial water equivalent of glacier ice (m)	100-500	-	-
Glacier	Snowmelt lag delay (h)	24	24	24
Glacier	Snowmelt storage constant (d)	1	1	1
Glacier	Convert any SWE to firn on Julian day	274	274	274
Global	Solar time offset from local time (h)	1.6	1.6	1.6
longVt	Terrain view factor	0.01-0.05	0.01-0.05	0.01-0.05
Netroute	Runoff storage constant (d)	0.1	0.1	0.1
Netroute	Runoff lag delay (h)	2	2	2
obs	Lapse rate	0.65	0.65	0.65
pbsmSnobal	Fetch distance (m)	Varies	Varies	Varies
SnobalCRHM	Roughness height (m)	0.001	0.003	0.01
SnobalCRHM	Maximum active layer thickness (m)	0.1	0.1	0.1
SnobalCRHM	Maximum liquid water content (m^3/m^3)	0.01	0.01	0.01
SnobalCRHM	Thermal conductivity of wet sand ($Jm^{-1}s^{-1}K^{-1}$)	1.65	1.65	0.08
Soil	Coverage type	Bare soil (no evaporation)	Bare soil (no evaporation)	Crops (recharge layer)
Soil	Soil withdrawal function	Clay	Clay	Sand
SWESlope	Minimum SWE holding depth (mm)	50	50	50

Pomeroy, unpublished). Groundcover and texture were determined from field observations. It was assumed that the glacier sits on bedrock.

Glacier firn and ice albedo was set according to Mölg et al. (2012) and Naz et al. (2014). Water flow through the glacier was informed by the work of Fountain and Walder (1998). The values for melt storage were set as two days for firn, one day for snow, and zero days for ice. The values for melt delay were set as four hours for firn, 24 hours for snow, and one hour for ice. The relative values of storage for firn (more storage capacity), snow (moderate storage capacity), and ice (little to no storage capacity) are well supported in the literature (Seaberg et al., 1988; Fountain, 1989; Fountain, 1996; Schneider, 2000). The role of weathering crust generation and decay in the uppermost layer of glacier ice has also been shown to play an important role in glacier drainage during the melt season (Müller and Keeler, 1969; Schuster, 2001). Shuster (2001) found that weathering crust development can dampen discharge by storing meltwater in the late morning, which then drains overnight. Decaying crust during the nighttime compounds nocturnal drainage.

Initial water equivalent of glacier thickness was determined using the method described by Frey et al. (2014). This method uses the elevation range and average slope of the glacier to determine average basal shear stress, which governs ice thickness. Mean ice thickness was determined for the central flow line and for the entire glacier and was used to estimate ice thickness for glacier HRUs (see Appendix A). On October 1 of each year, any remaining snow cover is converted to firn.

Global solar time offset from local time was found using the National Oceanic and Atmospheric Administration (NOAA) Solar Calculator (http://www.esrl.noaa.gov/gmd/grad/solcalc), which calculates the offset time based on the position and time zone.

The terrain view factor for calculating longwave radiation in module *longVt* was found using SAGA GIS. The north and south boundaries experience some shading from the topography but the basin is largely unaffected by shading. The values chosen for each HRU describe conditions found in the analysis.

Parameters in *Netroute*, the routing module, were estimated based on field observations. The runoff storage constant was set to 0.1 days and the lag delay was set to 2 hours. The subsurface runoff storage constant was set to two days and the subsurface lag delay was set to 5 hours. All groundwater runoff was routed to surface.

The module *obs* uses the lapse rate to scale temperature with elevation. The microclimate created by glaciers will produce katabatic wind flow, where an air parcel cools as it descends, counteracting adiabatic warming (Oerlemans, 2010). This produces a lapse rate less than that of the average environmental lapse rate of 6.5°C per kilometer. However, Pradhananga (unpublished) found an average lapse rate of 7.5°C per kilometre based on measurements in the Peyto Glacier basin and used a monthly lapse rate in modelling work with the CRHM Platform. Because the elevation difference of the two stations is only 51 m, this same calculation cannot be done for the Bologna Glacier. Therefore, it was determined that the environmental lapse rate would be used in the model.

Fetch, a parameter in *pbsmSnobal*, is the downwind distance over which snow can travel uninterrupted over uniform terrain; a longer fetch will promote higher sublimation per unit area (Li and Pomeroy, 2000). This distance was determined by measuring the length of each HRU in the prevailing wind direction, determined from the Ice Station wind rose (Appendix C). The value varies from 300 m (the minimum allowable value) to 2300 m.

SnobalCRHM parameters were set according to Marks et al. (2008), DeBeer and Pomeroy (2010), and calculated values. Van den Broeke (1997) calculated a roughness height of 4.4×10^{-3} m for the ablation zone and 2.3×10^{-3} m for the accumulation zone of the Pasterze Glacier in Austria. The aerodynamic roughness height, z_0, was calculated for the ablation zone (Appendix A) and was set to 3×10^{-3} m for the ice HRUs, which is consistent with the literature. A roughness height of 1×10^{-3} m was used for the firn HRUs, given that the accumulation zone is comparatively smoother than the ablation zone.

For the parameters in *soil*, non-glacier HRU soil coverage is set to having a recharge layer to represent the thin soil layer observed in the field. Glacier HRUs area assumed to have no evaporation; therefore, the coverage type is set to bare soil.

SWESlope parameters were set according to Bernhardt and Schulz (2010).

3.5.4 Model Assumptions

Assumption 1: The late summer snow line or the firn limit (whichever is lower) delineates the location of the firn and ice areas.

Each HRU must be classified as one of the three land cover types (land, ice, or firn) when the model is initialized. The boundary between ice and firn is not a dynamic feature of the model. An assumption was made that the firn limit could be delineated from satellite imagery, and that it could be approximated to one specific contour line. Any glacier HRUs above the line were initialized with firn coverage; glacier HRUs below the line were initialized as exposed glacier ice.

Assumption 2: Model re-sets every year to compensate for lack of ice dynamics

The model does not simulate ice flow, and therefore it cannot move ice from upslope to downslope HRUs. Ice flow is a significant process in glaciology. If the model is run continuously over an extended period of time, the accumulation area will accumulate a falsely high volume of snow, which will then be densified into firn and ice. The ablation zone, which would normally be fed by ice flow from the upper elevations, would melt too quickly. To resolve this issue, the model is re-set to initial conditions on an annual basis (October 1). The primary goal of the analysis is to quantify the components of snow, ice, and firn melt over a significant time period, and even when the glacier is reset every year, volumes of ice, firn, and snowmelt are still accounted for. The limitation of this assumption is that any leftover snowfall converted to firn, or any net melt of glacier ice in a year are not taken into account for the subsequent year of the model run.

Assumption 3: Calculating rainfall and snowmelt runoff

The water budget and mass balance analysis for this project were quantified on an annual basis. It is assumed that over this length of time, there are no changes in the groundwater storage and no net soil moisture storage change. Therefore, on an annual basis, rainfall and snowmelt runoff are assumed as equal to:

$$Rainfall\ runoff = Rainfall - ET \tag{3.11}$$

$$Snowmelt\ runoff = Snowmelt \tag{3.12}$$

3.5.5 Model Evaluation

The model was evaluated by comparing modelled results to the field observations, downstream discharge measurements, and satellite imagery. These available data were used to draw reasonable conclusions about the accuracy of the model.

First, it was observed in the field and from satellite imagery that the glacier is decreasing in area and that the surface facies configuration has changed drastically over the study period. Therefore, the model results should indicate negative glacier mass balance due to glacier wastage over the modelled time period.

Second, discharge measurements are available for the South Nahanni River at Virginia Falls, approximately 100 km downstream of the glacier. Because the glacier covers 0.1% of the South Nahanni River basin, the discharge contribution from the glacier should be a fraction of total volume of the South Nahanni River.

Last, volume-area scaling was used to calculate the volume change of the glacier between 1984 and 2014. It is recognized that errors in V-A scaling are high when the relationship is applied to a single glacier. Bahr et al. (2015) note, however, that the application of V-A scaling to a single glacier can accurately provide an order-of-magnitude estimate. For example, using the average global value for the scaling parameter, *c*, produces potentially 34% error in volume. This value does not include surface area measurement errors. By comparing the modelled glacier volume loss to the calculated volume change, it can be determined whether the model output is within a reasonable order of magnitude.

3.6 Firn Limit Analysis

The firn limit of the Bologna Glacier was assessed over 30 years (1984-2014) by assembling a set of late-summer satellite imagery for interim years where there was imagery with sufficiently low cloud cover and high resolution, similar to methods of other studies (Østrem, 1973; Østrem, 1975). The firn limit is defined as the average elevation of the boundary between the ice and firn at the end of a mass balance year. In this analysis, the firn limit is found rather than the equilibrium line altitude (ELA). The ELA is where snow accumulation is balanced by glacier ablation (Benn and Lehmkuhl, 2000) and is determined using the location of the late summer snowline (LSS) at the end of each mass balance year. It is an indicator of glacier response to climate change. With the available Landsat imagery, however, it is not possible to differentiate late summer snow from previous years' firn cover after the late summer snowline rises above the firn limit. In this study, the firn limit will be used as a supplementary indicator of glacier response to climate change. The firn limit is similar to the ELA and will be used to show the evolution of glacier surface facies over the study period. It is a low-pass filtered indicator of the state of the glacier: the location of the firn limit will determine if the next year's LSS supports the potential for negative annual mass balance for that year.

This analysis allows an evaluation of whether the firn limit experienced a monotonic rise over the study period and whether change accelerated in recent years. Imagery details are provided in Table 3.11. Eight images met the criteria (late-summer imagery with low cloud cover and high resolution) and are reasonably distributed over the study period, with the longest gap between images being seven years. The firn limit was found by taking the average elevation of the boundary between the ice and firn, which were classified using supervised landcover classification. Establishing this boundary allowed for the calculation of the firn area and the total glacier area, which can be used to determine the firn area ratio, as shown in equation 3.13. The firn limit, firn area ratio, and the total glacier area were tested for temporal trends to determine whether there has been a statistically significant change over the study period.

$$Firn\ Area\ Ratio = \frac{Firn\ Area}{Total\ Glacier\ Area} \tag{3.13}$$

Table 3.11: Satellite imagery metadata for firn limit analysis

Year	Acquisition Date	Path, Row	Product	Cloud Cover (%)
1984	August 3	55, 17	TM L1T	0
1991	August 7	55, 17	TM L1T	1
1993	August 21	54, 17	TM L1T	0
1998	August 3	54, 17	TM L1T	8
2004	August 18	55, 17	TM L1T	1
2009	August 1	54, 17	TM L1T	5
2010	August 3	55, 17	ETM+ L1T	0
2014	August 15	54, 17	OLI TIRNS L1T	1

3.7 Statistical Analysis

3.7.1 Statistical Indices

Statistical indices were used to assess how well the reanalyses matched observations. These were the coefficient of determination, R^2, mean bias error, MBE, and root mean square error, RMSE. R^2 is found using the package "base" included in R (R Core Team, 2015). MBE and RMSE were found using the package "hydroGOF" by Zambrano-Bigiarini (2014) as shown by the following equations:

$$MBE = \frac{1}{N}\sum_{i=1}^{N}(O_i - P_i) \tag{3.14}$$

$$RMSE = \sqrt{\frac{1}{N}\sum_{i=1}^{N}(O_i - P_i)^2} \tag{3.15}$$

where O_i and P_i represent the observed and predicted values, respectively, and N represents the number of observed and predicted value pairs.

3.7.2 Trend Tests

Both the meteorological data and the model output were tested for significant trends at varying time scales using the nonparametric rank-based Mann-Kendall (MK) statistical trend test.

Originally developed by Mann (1945) and Kendall (1975), this test has been shown to be robust in handing seasonality, non-normal distributions, and missing values – issues frequently encountered with hydrological time series (Hirsch and Slack, 1984). This test has been widely applied in hydrological studies (Yue et al., 2002). Before applying the MK trend test, a dataset must be tested for autocorrelation, which is the cross-correlation of between values at different points in a time series. Where autocorrelation is present, there can be a significant influence on trend test results (Yue et al., 2002). Trends were considered significant under the MK test at $p < 0.05$. The autocorrelation test and the MK trend test were done using the R packages "R Stats" (R Core Team, 2012) and "Kendall" (McLeod, 2011), respectively. Where trends were present, the slope was computed using a Thiel-Sen estimate of slope for a vector using the R package "zyp" (Bronaugh and Werner, 2013).

The approach for the MK test described here is obtained from Yue et al. (2002) and Sheikh and Bahremand (2011). The null hypothesis H_0 declares the data $(X_1, X_2 \ldots, X_n)$ are independent and identically distributed. The alternative hypothesis H_1 declares a monotonic trend exists in the data. The test statistic, S, is calculated for a dataset of length n by:

$$S = \sum_{i=1}^{n-1} \sum_{j=i+1}^{n} sgn(X_j - X_i) \tag{3.16}$$

where X_j and X_i represent the sequential data and for $\theta = X_j - X_i$:

$$sng(\theta) = \begin{cases} 1 \; if \; \theta > 0 \\ 0 \; if \; \theta = 0 \\ -1 \; if \; \theta < 0 \end{cases} \tag{3.17}$$

Which states that a positive S indicates an upward trend and a negative S indicates a downward trend.

The variance of S is calculated using the following equation. The mean of S is zero.

$$Var(S) = \frac{n(n-1)(2n+5) - \sum_{i=1}^{m} t_i(i)(i-1)(2i+5)}{18} \tag{3.18}$$

where m is the number of tied groups, which each have t_i tied observations.

The standardized test statistic Z is determined by:

$$Z = \begin{cases} \frac{S-1}{\sqrt{Var(S)}} & if\ S > 0 \\ 0 & if\ S = 0 \\ \frac{S+1}{\sqrt{Var(S)}} & if\ S < 0 \end{cases} \quad (3.19)$$

If $|Z| < Z_{1-\alpha/2}$, H_0 should be accepted.

3.8 Teleconnections to Atmospheric Variability

Climate teleconnections to spatially and temporally large-scale ocean-atmosphere circulation patterns including the Pacific Decadal Oscillation (PDO), Arctic Oscillation (AO) (or Northern Hemisphere Annular Mode, NAM), and the Southern Oscillation Index (SOI) have been shown to exert influence on hydroclimatic variables including temperature, precipitation, glacier mass balance, and streamflow in the northwestern regions of North America (Moore and McKendry, 1996; Spence, 2002; Meier et al., 2003; Woo and Thorne, 2003; Fleming et al., 2006; Demuth and Keller, 2006; Burn, 2008; Demuth et al., 2008; Whitfield et al., 2010; Fleming and Dahlke, 2014).

The PDO is characterized by decadal-scale shifts in atmospheric circulation manifested by the covariability between the North Pacific sea surface temperature and sea level pressure patterns (Mantua et al., 1997). A positive PDO index, the "warm phase", is produced by above-average-temperatures in the equatorial Pacific and below-average temperatures in the North Pacific. The opposite occurs when the PDO index is negative. PDO phases can last for 20 to 30 years, with the most recent shift to the positive phase occurring in the mid-1970s. The PDO index was obtained from the Joint Institute for the Study of the Atmosphere and Ocean (JISAO) (http://research.jisao.washington.edu/pdo/PDO.latest).

The SOI, which measures the strength of the El Niño Southern Oscillation, is based on the observed sea level pressure differences between Darwin, Australia and Tahiti (Trenberth, 1976). The SOI index was obtained from NOAA (http://www.cpc.ncep.noaa.gov/data/indices/soi). Positive PDO and negative SOI is correlated with decreased snow accumulation, decreased streamflow, decreased precipitation, and increased air temperature. Negative PDO and positive

SOI is correlated with increased precipitation, increased streamflow, and decreased air temperatures (Whitfield et al., 2010).

The AO is characterized by the symmetric wind fields between the polar cap region and a latitude of 45°N (Lorens, 1951; Wallace and Thompson, 1998). The AO manifests as below-average temperatures in the Arctic during the positive phase and above-average temperatures in the Arctic during the negative phase. The AO index was obtained from NOAA (http://www.cpc.ncep.noaa.gov/products/precip/CWlink/daily_ao_index/monthly.ao.index.b50.current.ascii.table). Monthly values of climate indices were obtained on July 12, 2016 from the websites given.

This analysis used corrected ERA-Interim reanalyses – temperature and precipitation from 1980 to 2015 – and model output to determine whether there are teleconnections with the PDO, SOI, and AO. This analysis followed the work of Bonsal et al. (2001), St. Jacques et al. (2010), and Harder et al. (2015). A Generalized Least Squares (GLS) model determined whether there was a correlation between a climate anomaly and hydro-meteorological data. Mean winter (November to March) indices were compared to the mean values for the subsequent year, the significance criterion was set at $p = 0.05$. This analysis used the R package for GLS, "nlme", by Pinheiro et al. (2012) and Theil-Sen "WRS" by Wilcox and Schönbrodt (2013).

3.9 Summary

The methods described in this section provide analyses to evaluate the impact of climate change, reduced glacier cover, and increased ice exposure on headwater streamflow generation in the Bologna Glacier basin. Outcomes include:

1. A corrected 36 year meteorological record for the Bologna Glacier;
2. Quantification of glacier area and surface facies change between 1984 and 2015;
3. A detailed assessment of the evolution of the firn limit and glacier area over time;
4. Trend identification in driving meteorology and hydro-glaciological outputs from the model over 36 years;
5. Identification of teleconnections with spatially and temporally large scale atmospheric variability including the PDO, AO, and SOI;
6. Basin water budget over 36 years for historical and contemporary glacier configurations;
7. Quantification of glacier wastage and melt contributions to streamflow;
8. An evaluation of how changes to glacier size and surface facies configuration affect water budget components;
9. Calculated annual and cumulative glacier mass balance over 36 years;
10. An analysis of whether glacier configuration affects the annual hydrograph; and
11. Quantification of glacier wastage and melt and their contribution to streamflow over the study period on the South Nahanni River at Virginia Falls.

These outcomes provide a comprehensive assessment of glacier change and corresponding hydrological change in a northern continental glacierized basin. They illustrate the sensitivity of the glacier-hydrological regime to changes in climate and allow for the exploration of whether the observed loss of firn has influenced melt rates and patterns. The satellite imagery analysis demonstrates whether the rise in the firn limit occurred gradually over time or if it rose rapidly in recent years.

4 RESULTS

4.1 Climate

The downscaled and bias corrected ERA-Interim reanalyses were evaluated to determine the average precipitation and temperature record over 36 years. The average annual daily maximum, mean, and minimum temperatures at the Bologna Glacier for 1980 to 2015 are -4.3°C, -6.6°C, and -8.6°C, respectively. To calculate these values, daily minimum, mean, and maximum temperature were averaged over the hydrological year spanning from October 1st to September 30th. The average monthly temperature is shown in Figure 4.1. Average annual precipitation was 583 mm, 28% falling as rain (161 mm) and 72% falling as snow (422 mm). These values are shown as monthly fractions in Figure 4.2.

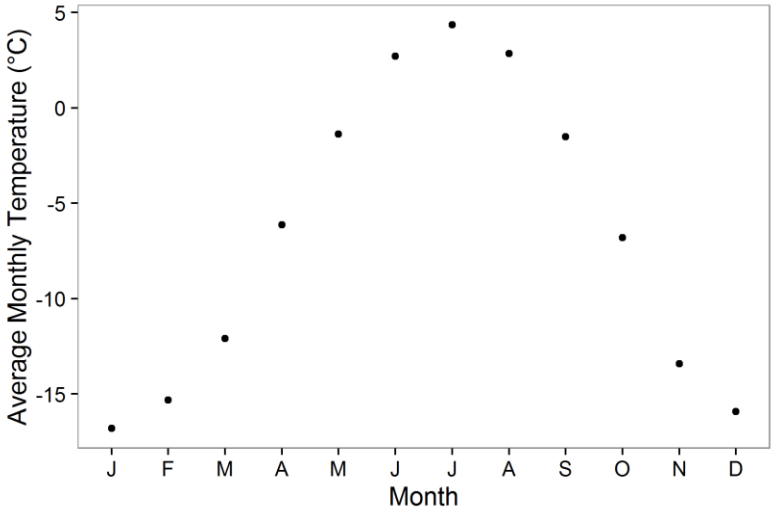

Figure 4.1: Average monthly temperature at the Bologna Glacier (1980 – 2015) from bias corrected ERA-Interim reanalyses

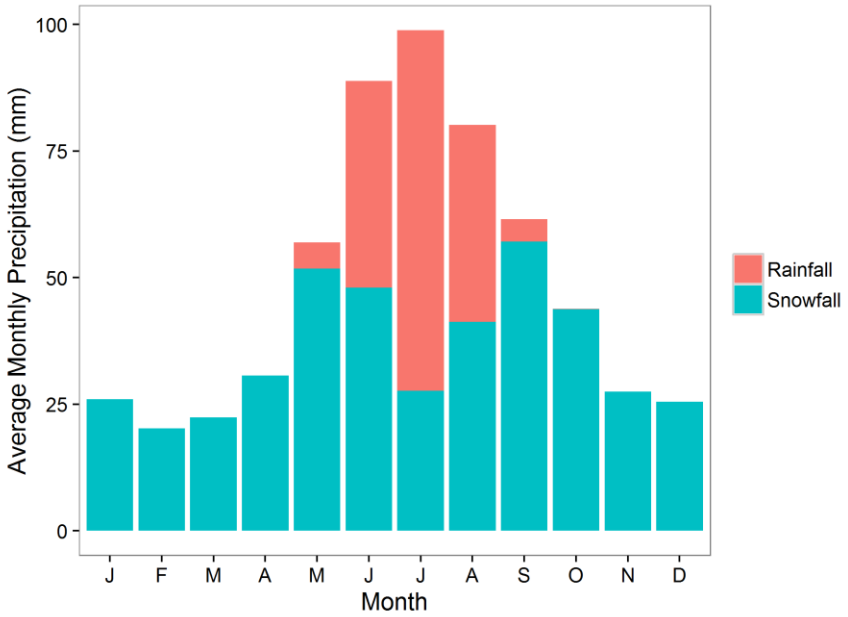

Figure 4.2: Average monthly precipitation at the Bologna Glacier (1980 – 2015) from bias corrected ERA-Interim reanalyses

4.1.1 Historical Variability of Select Hydroclimatic Variables

There were no statistically significant annual trends in the corrected ERA-Interim temperature or precipitation from 1980 to 2015. As shown in Figures 4.3 and 4.4, the *p*-values all exceed the significance criterion of 0.05 under the Mann-Kendall trend test. There were also no trends in the rainfall or snowfall components of precipitation. However, the rainfall ratio over the study period was found to be increasing significantly ($p = 0.018$), as shown in Figure 4.5. The blue line indicates a significant linear trend.

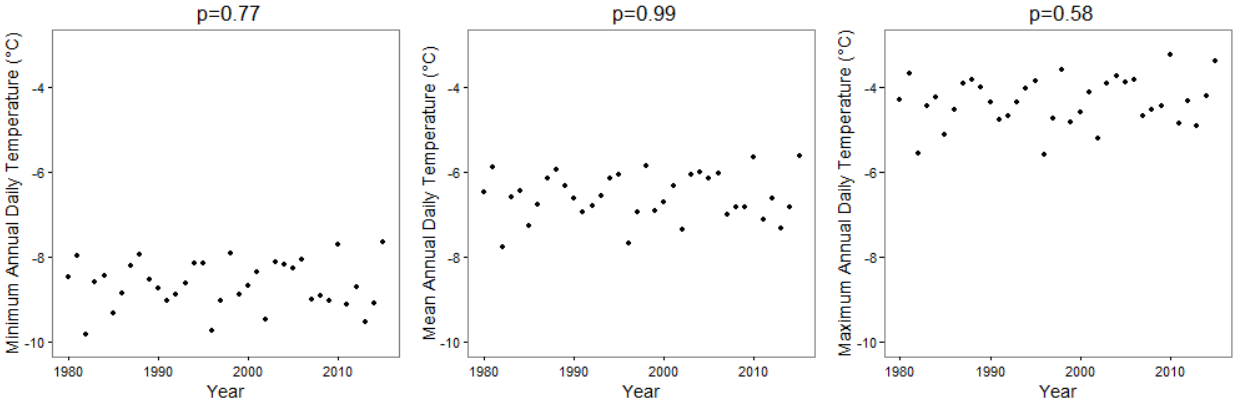

Figure 4.3: Minimum, mean, and maximum annual daily temperatures for the Bologna Glacier (hydrological years 1980-2015) from bias corrected ERA-Interim reanalyses

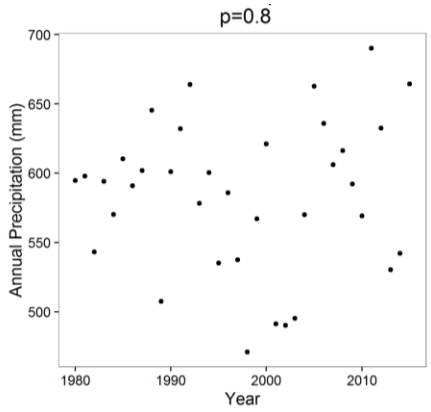

Figure 4.4: Annual precipitation at the Bologna Glacier (hydrological years 1980-2015) from bias corrected ERA-Interim reanalyses

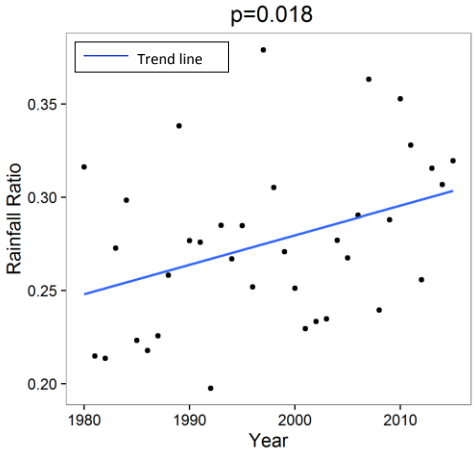

Figure 4.5: Rainfall ratio of annual precipitation at the Bologna Glacier (hydrological years 1980-2015) from bias corrected ERA-Interim reanalyses

Further testing for sub-annual trends revealed seasonal trends in temperature and precipitation. The average daily maximum summer (June, July, August) temperatures have increased by 0.54°C (p = 0.025), as shown in Figure 4.6. There were no trends in the average daily mean or average daily minimum summer temperatures. Total spring (March, April, May) precipitation has decreased by 24.0 mm (p = 0.027), as shown in Figure 4.7.

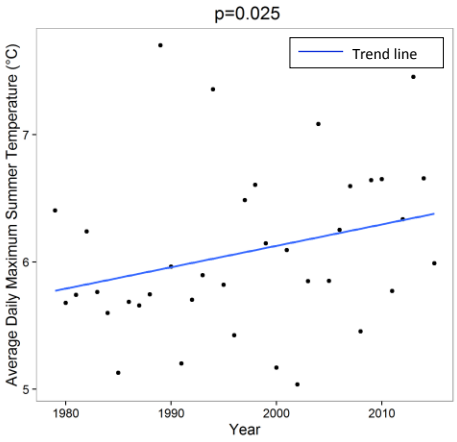

Figure 4.6: Average daily maximum summer (June, July, August) temperatures for 1979-2015 from bias corrected ERA-Interim reanalyses

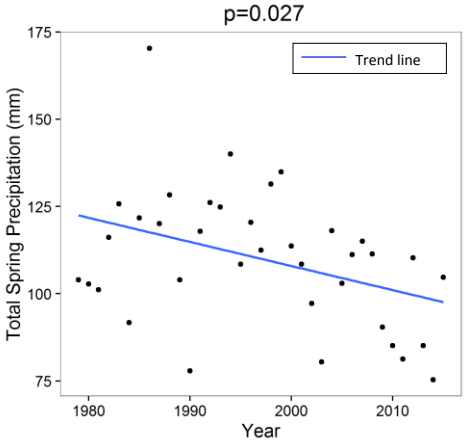

Figure 4.7: Total spring (March, April, May) precipitation for 1979-2015 from bias corrected ERA-Interim reanalyses

4.2 Glacier Change

4.2.1 Area and Surface Facies Change

Eight Landsat images, shown in Figure 4.8, were evaluated to determine how the glacier evolved over 30 years. Table 4.1 shows the glacier size, ice and firn coverage, firn limit, and firn ratio calculated using ArcMap 10.2.2 for each of the images. Because the 1985 DEM was used to calculate the average elevation of the firn limit for each year, these values are not representative of the true firn limit elevation since downwasting in the interim years could not be quantified. The Bologna Glacier's total area decreased by 14% from 1984 to 2014 from 18.7 km^2 to 16.0

km^2. The toe of the glacier receded 700 m horizontally and rose 190 m vertically. The area of firn decreased by 51% (7.9 km^2) and the exposed ice area increased by 158% (5.2 km^2) between 1984 and 2014. This significant change in the surface facies was concurrent with a rise in the firn limit of 204 m relative to the initial firn limit elevation. By comparing the on-glacier survey points collected in the field to the DEM from 1985, an approximate average decrease in the surface elevation of the glacier was found to be 42 m. The vertical accuracy of the DEM in this region is 5 to 15 m (Natural Resources Canada, 2013).

Table 4.1: Glacier area and firn limit determined from Landsat imagery

Year	Glacier Area (km^2)	Ice Area (km^2)	Firn Area (km^2)	% Firn Cover	Firn limit elevation from 1985 DEM (m)
1984	18.7	3.3	15.4	82.4	2057
1991	18.0	3.3	14.7	81.6	2109
1993	17.7	6.5	11.2	63.5	2186
1998	16.6	6.1	10.6	63.6	2180
2004	16.6	7.9	8.8	52.7	2220
2009	16.6	4.8	11.8	71.3	2172
2010	16.3	8.1	8.2	50.2	2235
2014	16.0	8.5	7.5	47.1	2261
2015*	16.0	16.0	0	0	-

*2015 values are estimated from 2014 – assuming no change in glacier area and accounting for the observed loss of firn

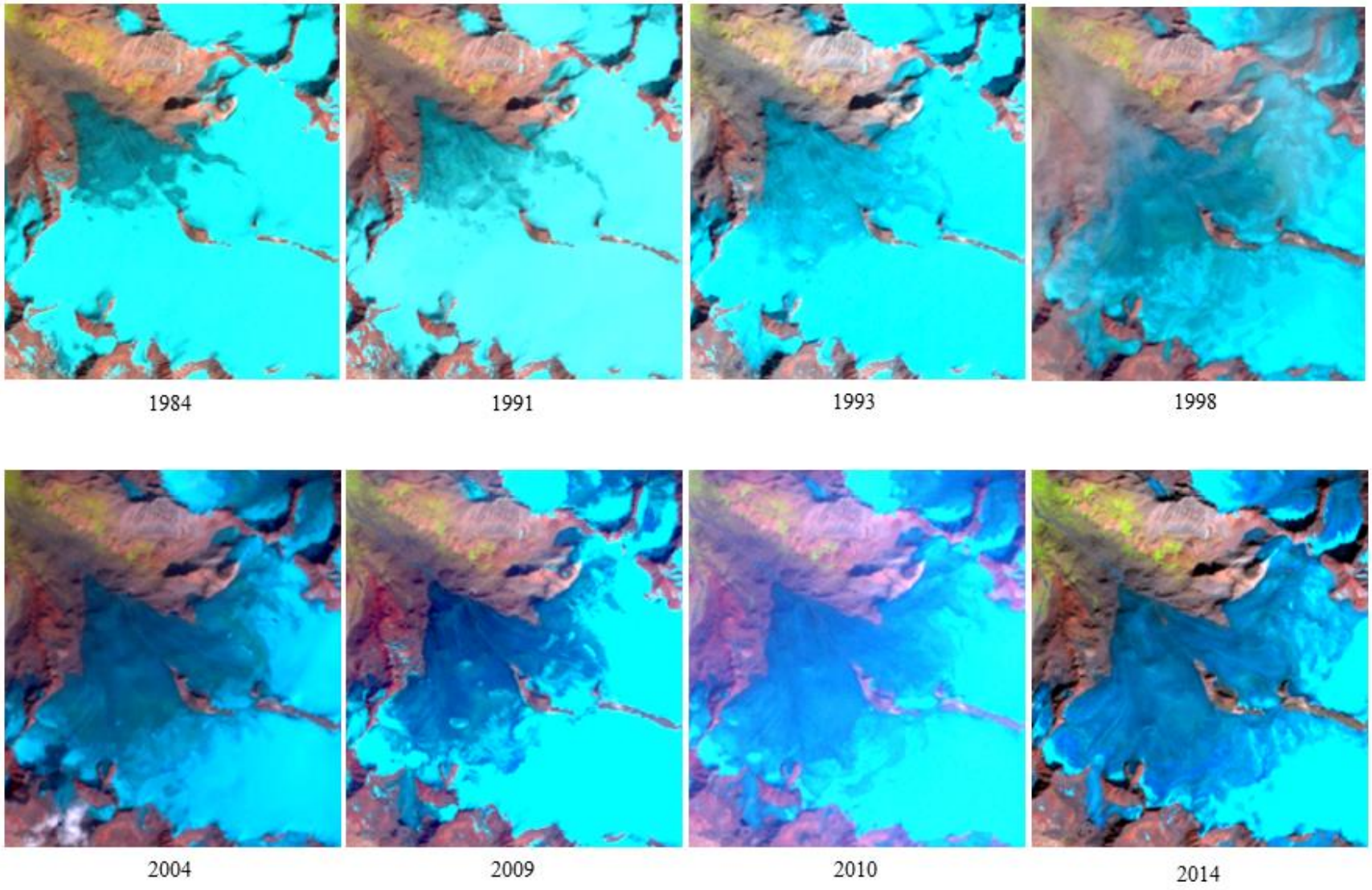

Figure 4.8: False colour Landsat imagery of the Bologna Glacier from 1984 to 2014 (NB: 2015 is not included as there is no satellite imagery available for this year but there was an observed total loss of firn via field observations)

Figure 4.9 shows that the glacier area is decreasing significantly at $p = 0.00037$. The majority of the area loss occurs between 1984 and 1998, followed by a period of constant glacier area between 1998 and 2009, after which the glacier continues to lose area.

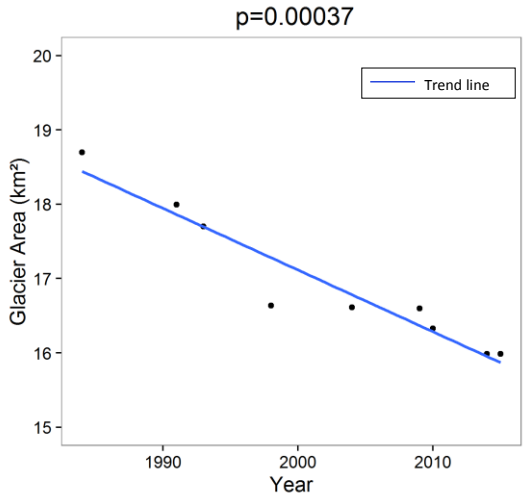

Figure 4.9: Glacier area calculated from Landsat imagery from 1984 to 2015

Figure 4.10 shows that the firn limit is increasing significantly at $p = 0.019$. The rise is not monotonic, as the firn limit decreases slightly between 1993 and 1998, and again between 2004 and 2009. Figure 4.11 shows that the firn area ratio is decreasing significantly at $p = 0.049$.

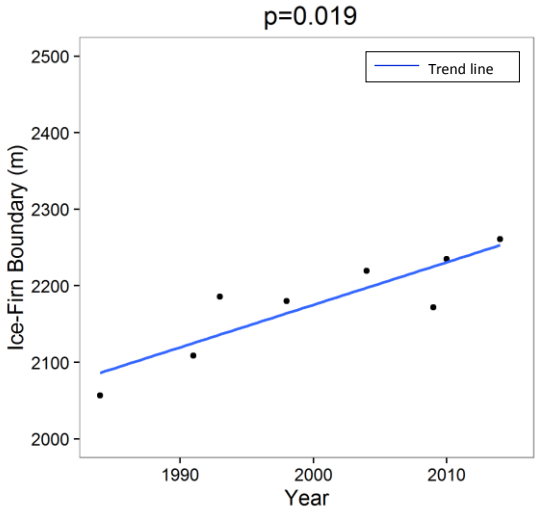

Figure 4.10: Firn limit elevation calculated from Landsat imagery from 1984 to 2015

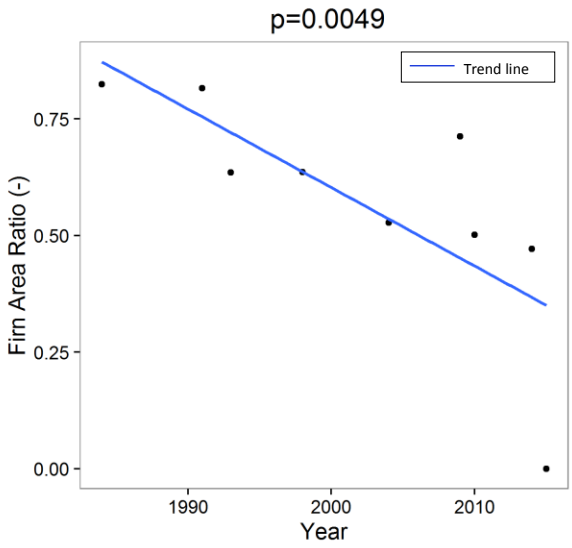

Figure 4.11: Firn area ratio calculated from Landsat imagery from 1984 to 2015

4.2.2 Volume Change

Glacier volume change was calculated using two methods: the first quantified glacier volume change in 1984 and 2014 using the volume-area scaling relationship (Section 2.4.2), the second quantified glacier volume change by running the model from 1984 to 2014 for each of the three model configurations. As noted in the literature review and methodology, the volume-area scaling relationship should typically be applied to an ensemble of glaciers, but can be applied to a single ice mass to determine an order of magnitude estimation (Bahr et al., 2015). The relationship is applied here to demonstrate that the model is producing results in a reasonable order of magnitude. Table 4.2 shows the results.

Table 4.2: Volume change from 1984 to 2014 for the Bologna Glacier, determined via V-A scaling and three model configurations

Method	Change in volume between 1984 and 2014 (10^6 m^3)
V-A Scaling	-310 ± 698
1984 Model Configuration	-257
2014 Model Configuration	-415
2015 Model Configuration	-491

The volume change calculated using volume-area scaling was -310 ± 698 x 10^6 m^3. The derivation of error in V-A scaling can be found in Appendix A. The volume change for the 1984, 2014, and 2015 model configurations was -257, -415, and -491 x 10^6 m^3, respectively. In each case, the glacier is shown to be losing mass, which corresponds with field observations and satellite imagery analysis. It is evident that the model results are of the same order of magnitude as volume change calculated from V-A scaling. The calculated volume change from V-A scaling falls within the range of modelled values.

4.3 Glacier Hydrology

4.3.1 Hydro-glaciological Trends

Model output was tested for trends over 36 years (hydrological years 1980-2015, inclusive) for the three model configurations, as shown in Figures 4.12, 4.13, and 4.14. Output tested included basin discharge, firn melt, ice melt, rainfall runoff, snowmelt, evapotranspiration, sublimation, and annual basin snow loss. Discharge increases significantly over the modelled time period for the 2014 and 2015 model configurations. Ice melt increases significantly over the modelled time period for the 1984 and 2014 model configurations. Evapotranspiration increases significantly in every model configuration. Annual peak volume and timing was also tested, with no significant trends found. In the 2015 configuration (Figure 4.14), firn melt is zero each year as there was no firn cover in that year.

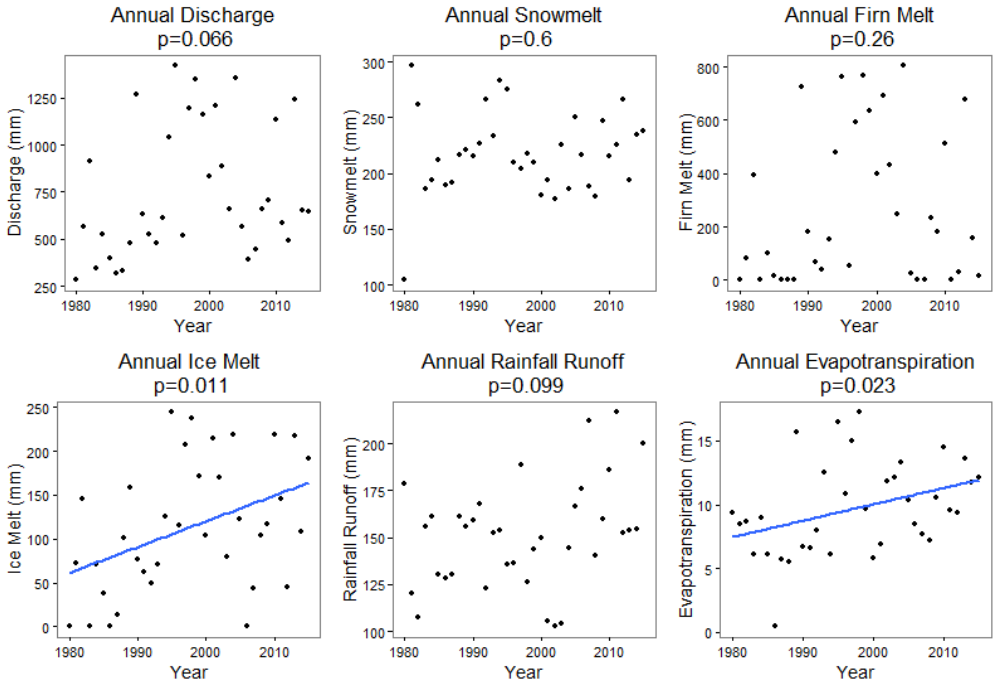

Figure 4.12: Model output for the 1984 model configuration with Mann Kendall p-values shown for each variable (y-axes vary)

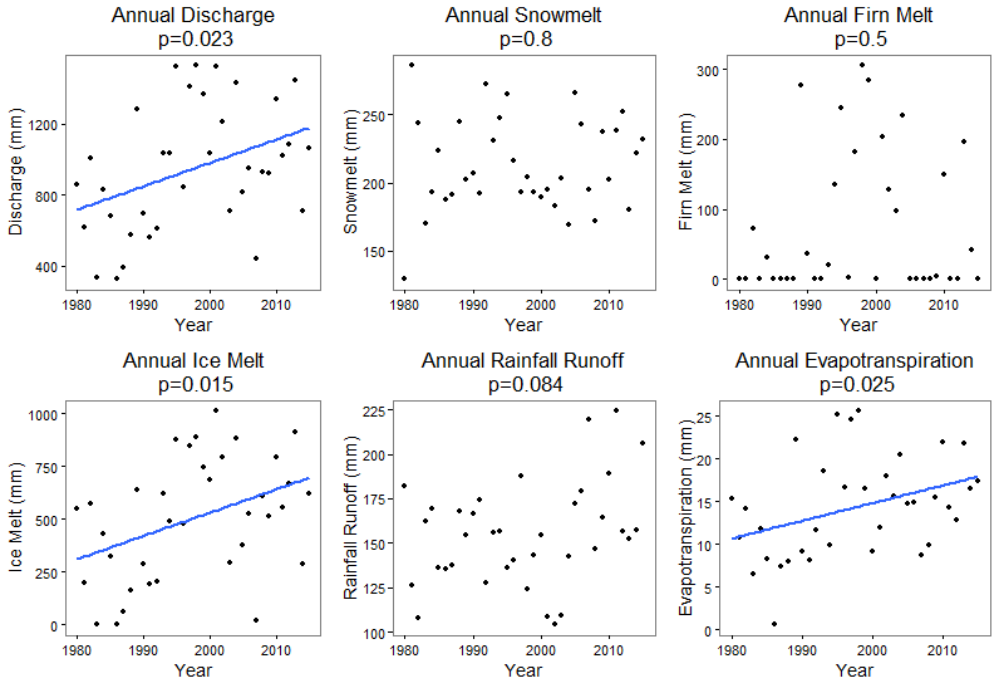

Figure 4.13: Model output for the 2014 model configuration with Mann Kendall p-values shown for each variable (y-axes vary)

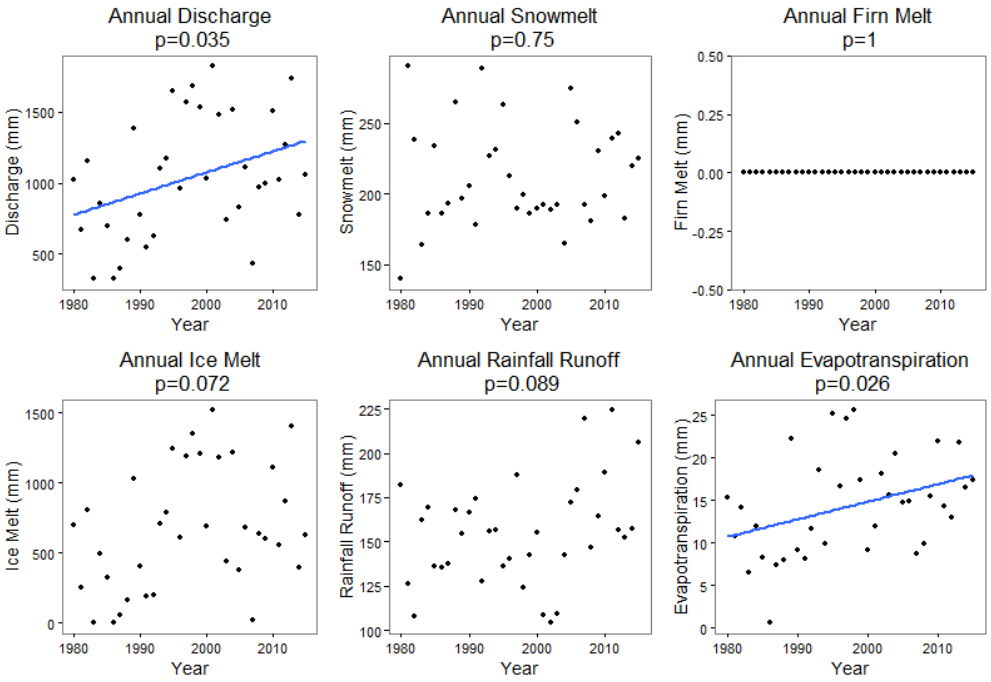

Figure 4.14: Model output for the 2015 model configuration (no firn) with Mann Kendall p-values shown for each variable (y-axes vary)

The annual fractions of snowmelt, ice melt, and firn melt contributions to discharge were calculated for each of the model configurations and were tested for trends. The fraction of ice melt compared to basin discharge was increasing significantly for the 1984 and 2014 model configurations (p = 0.0039 and p = 0.019), as shown in Figures 4.15, 4.16. The fraction of snowmelt compared to basin discharge was decreasing significantly for the 2014 model configurations (p = 0.0039), as shown in Figure 4.17.

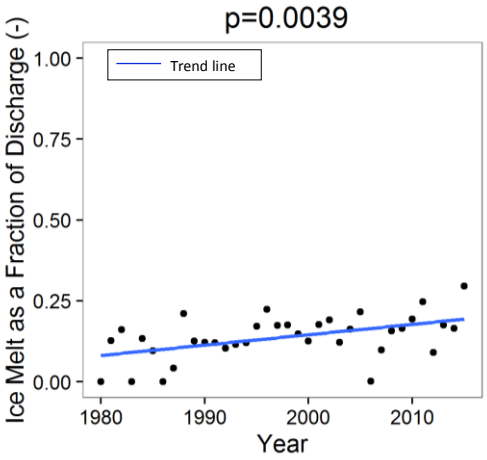

Figure 4.15: Fraction of ice melt compared to total basin discharge for 1984 model configuration

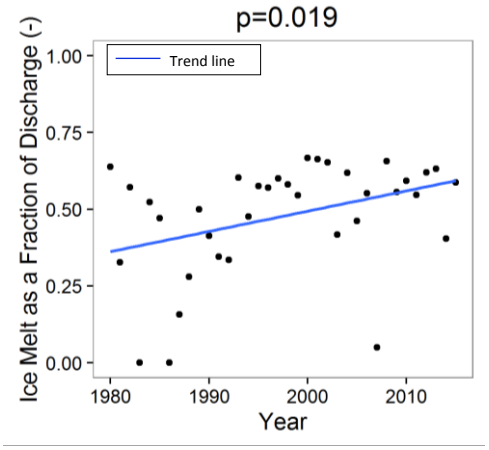

Figure 4.16: Fraction of ice melt compared to total basin discharge for 2014 model configuration

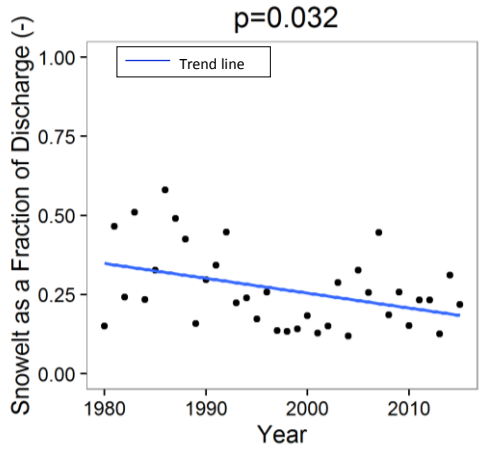

Figure 4.17: Fraction of snowmelt compared to total basin discharge for 2014 model configuration

4.3.2 Basin Water Budget

The average annual basin water budget was calculated from the output of the model run from hydrological years 1980 to 2015 (inclusive) for the 1984, 2014, and 2015 model configurations. Quantities of the water budget are shown in Table 4.3, where values are given as totals for the basin in millimetres as an annual average over 36 years. The water budget is shown schematically in Figure 4.18, where quantities are shown in the same units for the basin as well as for the *ice*, *firn*, and *land* cover types. In the 2015 configuration, there is no *firn* land cover type since there was an observed loss of firn in the August 2015 field season. It is also important to note that in the 1984 configuration, the *ice* HRUs receive more rainfall but less overall precipitation than the *land* HRUs. While intuitively it would seem that the *ice* HRUs should receive more precipitation and less rainfall than the *land* HRUs, on average, the elevation of the *ice* HRUs is lower than that of the *land* HRUs in this configuration. This is because the *ice* HRUs in this configuration are relatively small (2.43 km^2) and centralized in the basin whereas the *land* HRUs in this configuration are larger (5.76 km^2) and contain the steep slopes of the northern and western edges of the basin (see Figure E.7 in Appendix E).

In the 1984 model configuration, it is evident that the glacier is already in a state of negative annual balance, at -217 mm. This included a significant contribution from firn melt at 263 mm (35% of basin discharge) and a lesser contribution from ice melt at 113 mm (15% of basin discharge). Snowmelt runoff and rainfall runoff are also significant contributors to basin discharge at 218 mm (29%) and 151 mm (20%), respectively. Evapotranspiration, sublimation, and drift make up smaller fractions of the water budget at 10 mm, 44 mm, and 2 mm respectively.

Significant change in many of the model output components is evident in comparing results from the 1984 and 2014 configuration model runs. Percent difference was found by taking the difference between two values divided by the original value from the 1984 configuration run. The change in modelled output can be attributed to changes in the glacier configuration given that the input meteorology remained the same. The overall net basin water budget became more negative by 95%, resulting in a budget of -425 mm. Total discharge increased by 27%, firn melt decreased by 72%, ice melt increased by 347%, and evapotranspiration increased by 47%. Snowmelt runoff and rainfall runoff changed less than 5%. Rainfall runoff increased slightly and

snowmelt runoff decreased slightly. Sublimation and net drift did not change substantially between the two configurations. The contribution from firn melt to streamflow in the 2014 configuration averaged 8% of basin discharge whereas the contribution from ice melt was 53%.

By modelling the glacier in the 2015 configuration, where the glacier area is held constant to 2014 and all the firn is removed, there is change in the resulting model output. The basin water budget is increasingly negative, discharge and ice melt increase, and firn melt decreases significantly. Snowmelt runoff, rainfall runoff, evapotranspiration, sublimation, and basin net drift remain relatively constant compared to the 2014 configuration.

Table 4.3: Water budget components given in average depth per basin area per year for three model configurations

Flow per Basin Area (mm/year)	Model Configuration		
	1984	2014	2015
Net Basin	-217	-425	-515
Firn Melt	263	74	0
Ice Melt	113	504	668
Snowmelt Runoff	218	213	212
Rainfall Runoff	151	155	155
Evapotranspiration	10	14	14
Sublimation	44	43	43
Drift	2	2	2

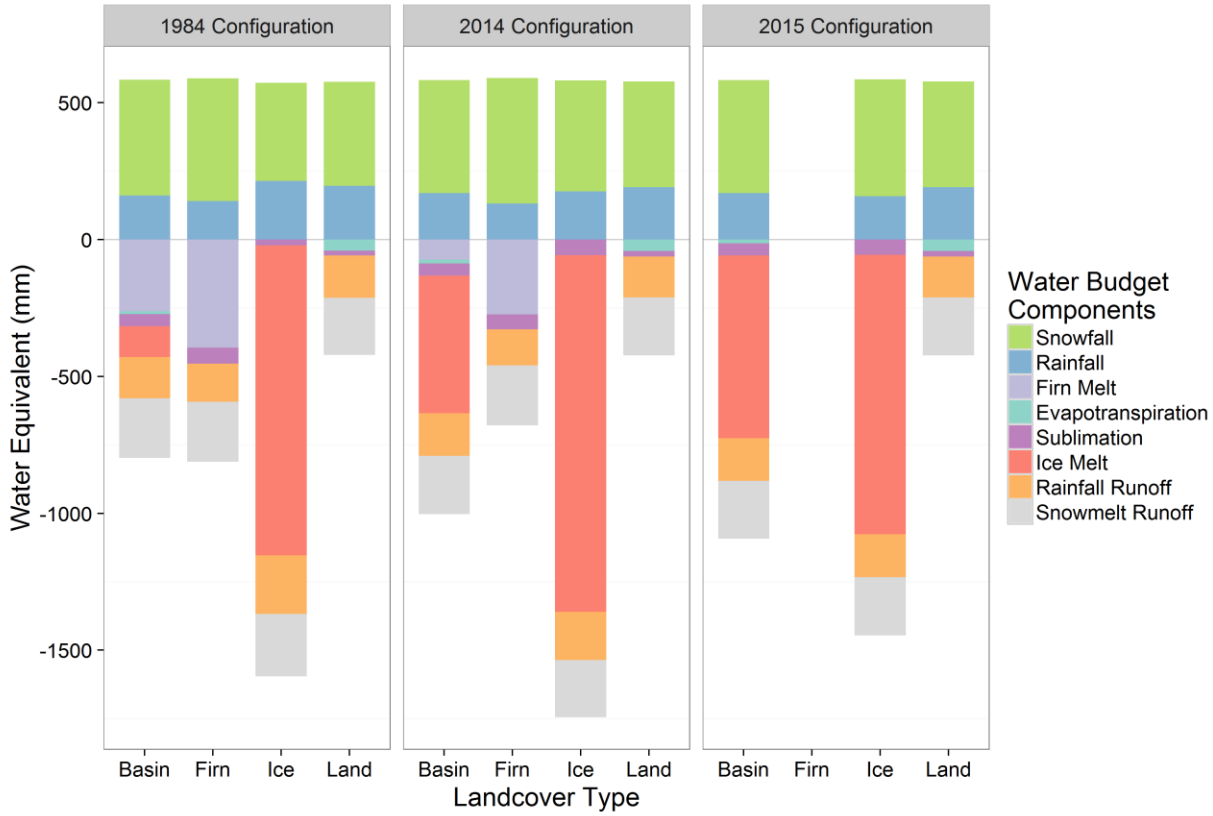

Figure 4.18: Average annual water budget for the 1984 model configuration, 2014 model configuration, and 2015 model configuration (no firn HRUs) for model run from 1980-2015; values are given as depth per HRU group (ice, firn, land) area of each configuration

4.3.3 Glacier Mass Balance

Annual net mass balance over 36 years is shown for each model configuration in Figure 4.19 and cumulative annual net mass balance is shown for each model configuration in Figure 4.20. The glacier's overall loss over the modelled time period is between 9.0 and 20.3 m water equivalent. The average mass balance for the 1984, 2014, and 2015 configurations are -0.25 m, -0.47 m, and -0.56 m, respectively. In the 1980s, there are a few years of positive mass balance for all model configurations. The most positive mass balance is in 1980, 1986, and 1983 for the 1984, 2014, and 2015 configurations, respectively. From 1990 onwards, net mass balance remains distinctly negative for all configurations with a few exceptions. Between 1993 and 1998 there is a pronounced acceleration in the negative balance, followed by a somewhat less negative pattern.

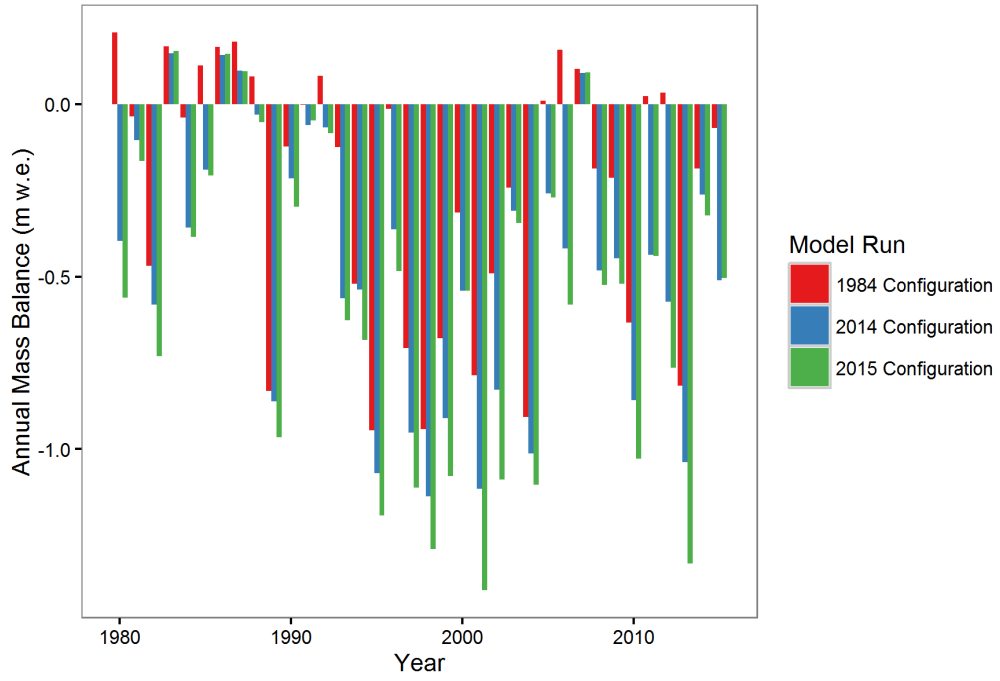

Figure 4.19: Annual mass balance for the Bologna Glacier in three configurations from 1980 to 2015

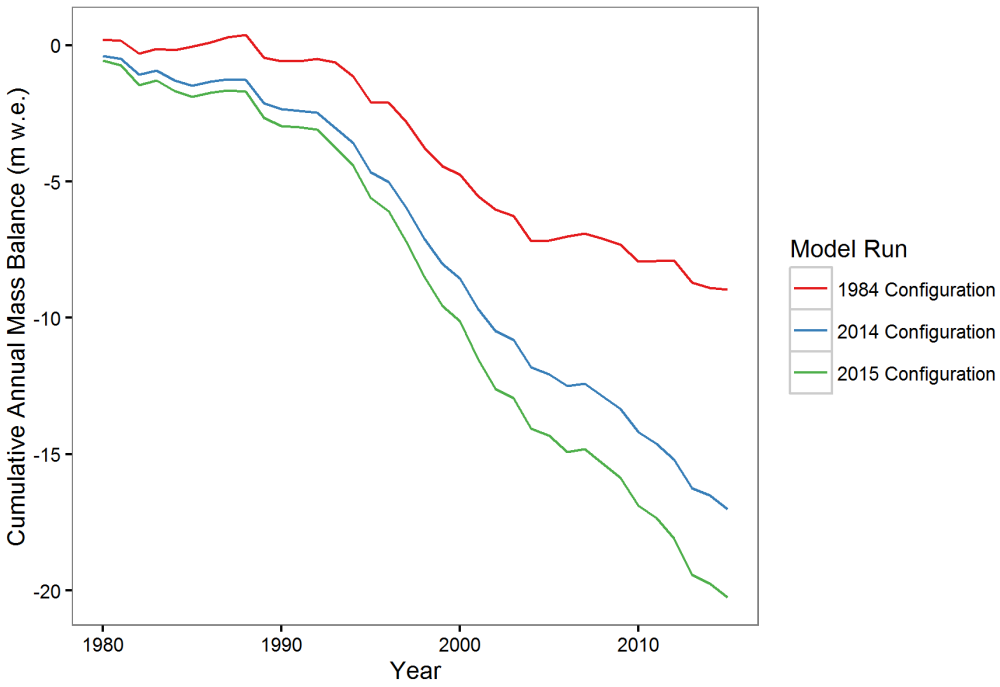

Figure 4.20: Annual cumulative mass balance for the Bologna Glacier in three configurations from 1980 to 2015

4.3.4 Glacier Wastage and Melt

Glacier wastage and melt were calculated according to Comeau et al. (2009), as described in Section 2.1.2. Table 4.4 quantifies the average annual basin discharge, wastage, and melt. Overall, wastage accounted for 35%, 48%, and 53% of the 1984, 2014, and 2015 configuration discharge over 36 years, respectively. Melt accounted for 13%, 13%, and 12% of the 1984, 2014, and 2015 configuration discharge over 36 years, respectively. Figure 4.21 shows annual wastage, melt, and storage as compared to annual basin discharge for the 1984, 2014, and 2015 model configurations. These figures illustrate the relative annual proportions of glacier contribution to streamflow. It is evident that in years of positive mass balance (e.g. 1983, and 1987), there is net storage into the system in each configuration. In years of negative mass balance, wastage is often a significant portion of the basin yield while melt comprises a smaller or negligible proportion (e.g. 1998).

Table 4.4: Total discharge, wastage, and melt contributions from the Bologna Glacier basin under three model configurations 1980 – 2015

	1984 Configuration	2014 Configuration	2015 Configuration
Average Basin Discharge (mm per basin area)	745	948	1038
Average Wastage (mm per basin area) (% discharge)	261 (35%)	454 (48%)	545 (53%)
Average Melt (mm per basin area) (% discharge)	97.5 (13%)	121 (13%)	121 (12%)

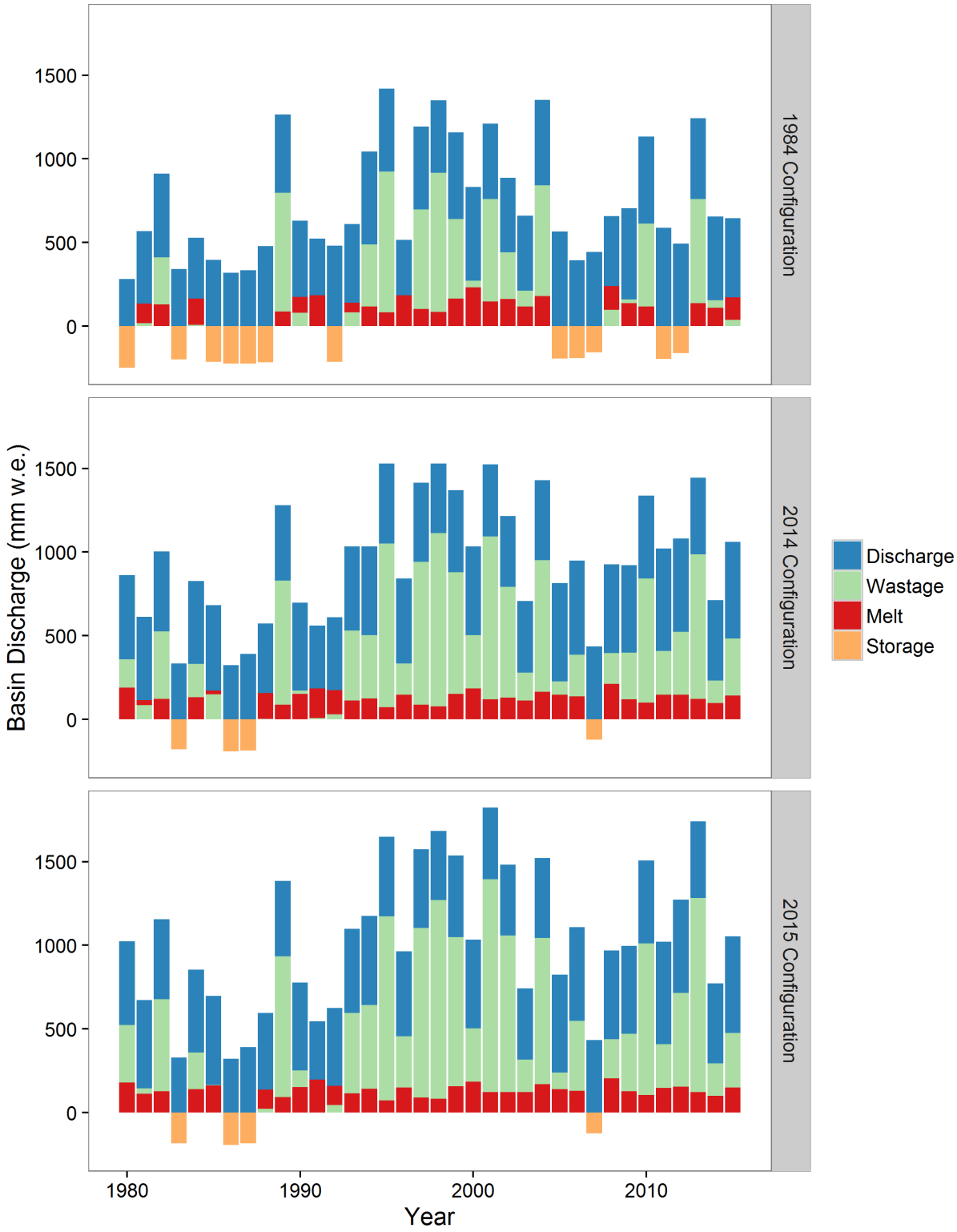

Figure 4.21: Annual basin yield with wastage, melt, and storage superimposed for three model configurations

4.3.5 Hydrographs

The daily hydrograph averaged over the study period for each model configuration is shown in Figure 4.22. The grey shading represents one standard deviation from the mean. It is evident that the 2014 and 2015 model configurations have more variation in volume and diurnal amplitude than the 1984 model configuration. Figures 4.23 and 4.24 show the annual hydrograph for the most positive mass balance year, 1987, and most negative mass balance year, 1998. The 1987 hydrograph remains essentially the same in all three configurations, whereas the 1998 hydrograph experiences vast changes in volume and diurnal amplitude between each of the three model configurations.

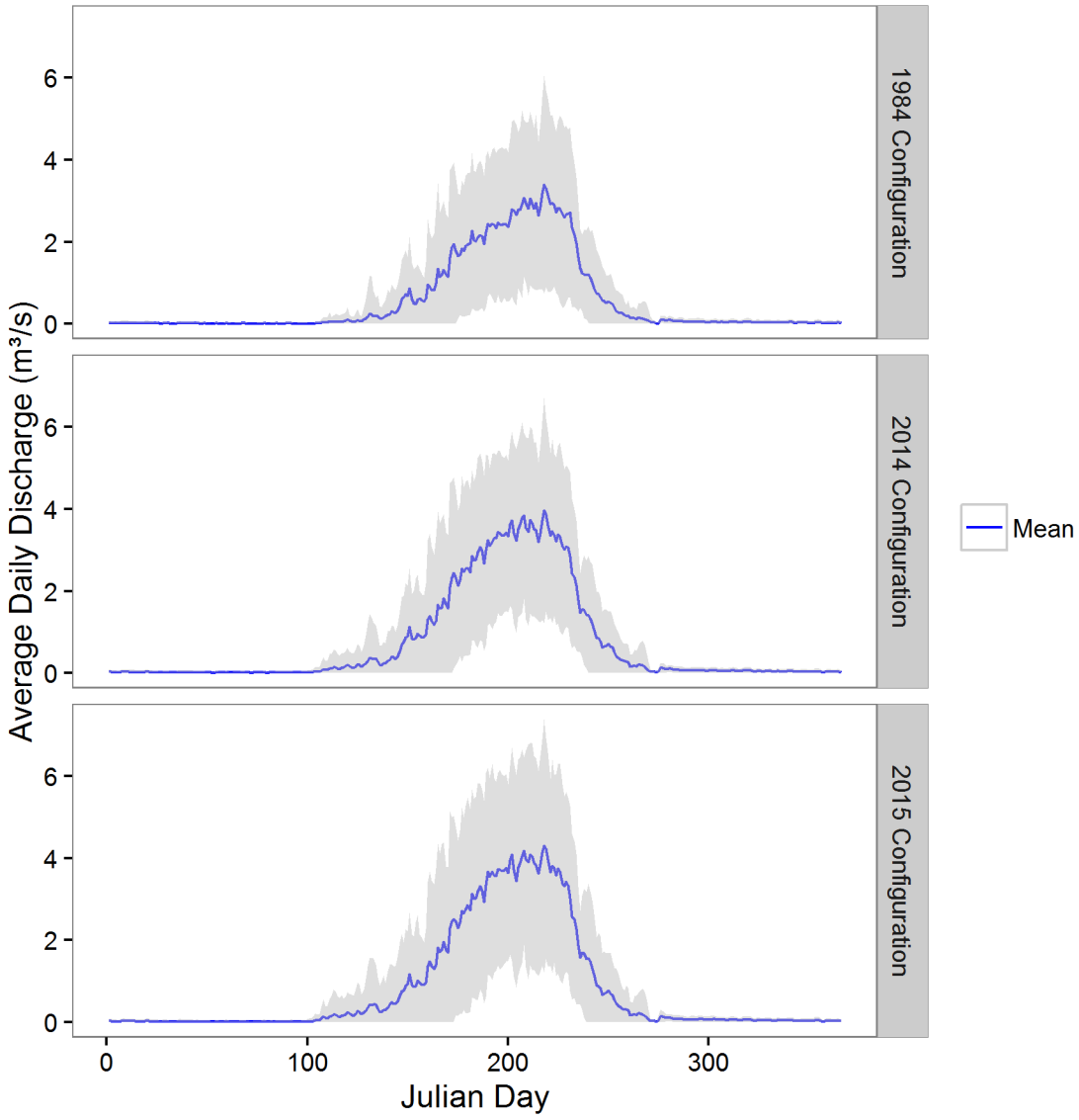

Figure 4.22: Average daily discharge from the Bologna Glacier basin by Julian day in three configurations; grey shading represents one standard deviation from the mean

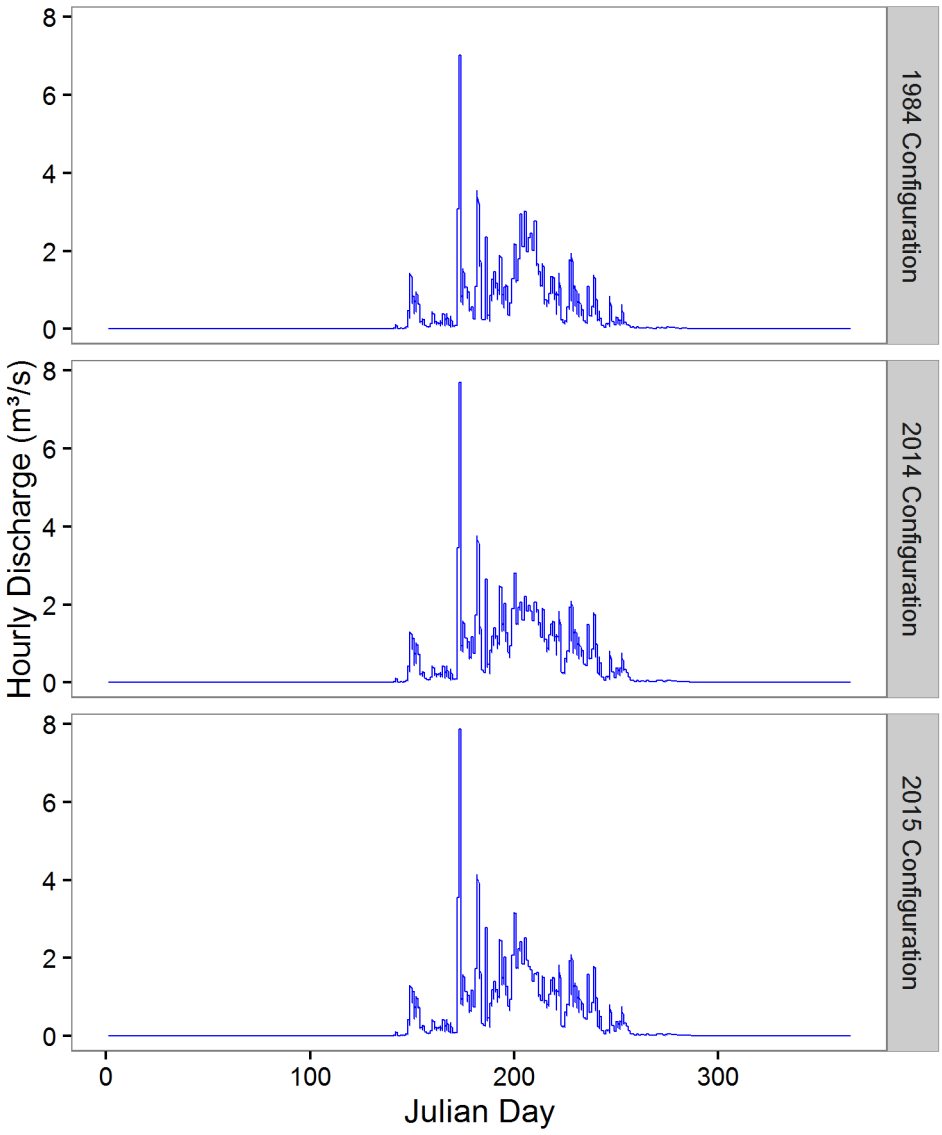

Figure 4.23: Hourly discharge from the Bologna Glacier basin in 1987 (positive annual mass balance) for three configurations

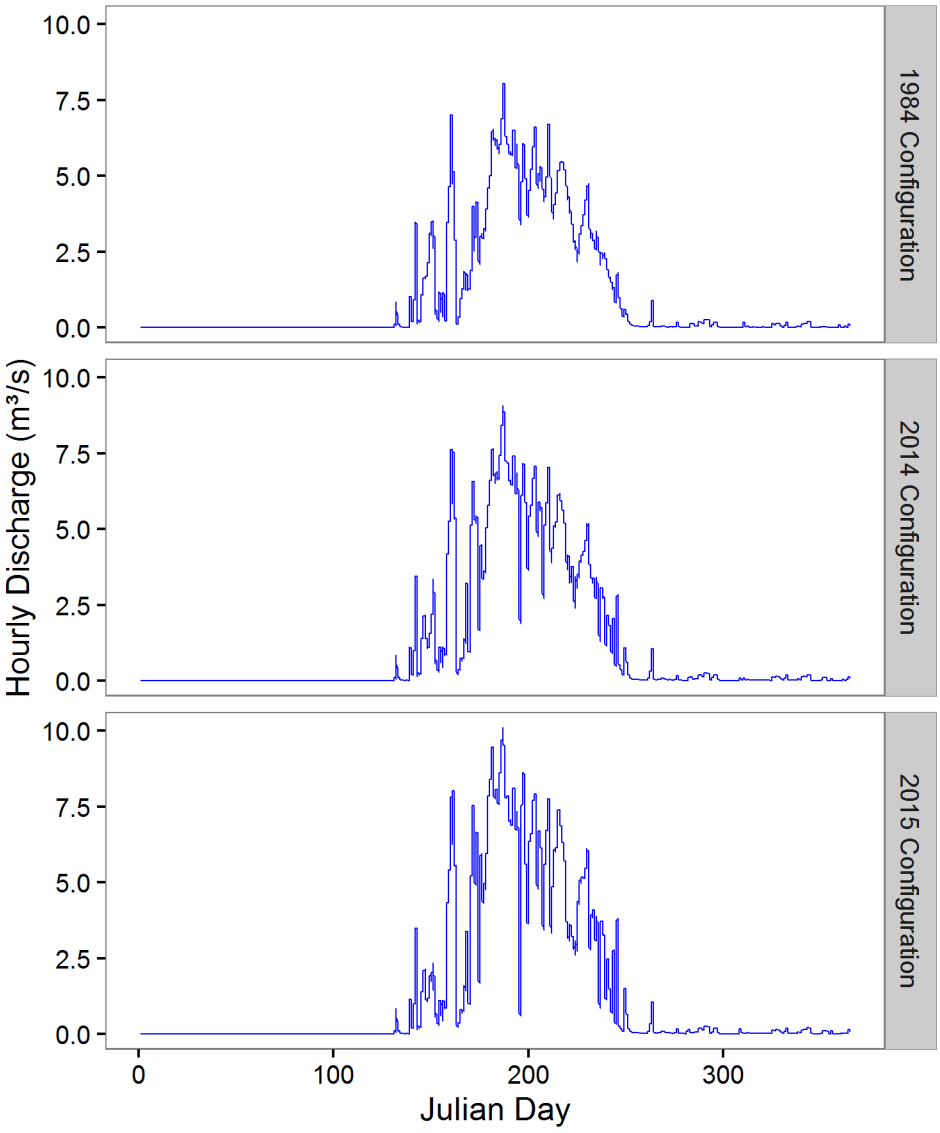

Figure 4.24: Hourly discharge from the Bologna Glacier basin in 1998 (negative annual mass balance) for three configurations

4.4 Contribution to South Nahanni River Basin Flow at Virginia Falls

Streamflow contribution to the South Nahanni River was quantified by comparing modelled discharge to the gauge measurements at Virginia Falls (map shown in Figure 3.2) from hydrological years 1980 to 2014, after which time Virginia Falls gauge measurements are unavailable. The Bologna Glacier covered 0.13% of the basin (14,500 km^2) in 1984 and 0.11% of the basin in 2014/2015. The contribution to streamflow was calculated for the basin discharge and for the components of glacier wastage and melt combined on both an annual basis and during the summer months. Results are shown in Table 4.5. Overall, the wastage and melt contributions from the Bologna Glacier contributed 4.0% to 7.3% of the summertime flow of the South Nahanni River at Virginia Falls.

Table 4.5: Average percentage contribution to streamflow simulated by CRHM for the Bologna Glacier for hydrological years 1980 – 2014 (inclusive) for three model configurations

Model Configuration	Basin Glacierized Area (%)	Percentage basin contribution to streamflow		Percentage wastage and melt contribution to streamflow		Percentage wastage contribution to streamflow	
		Annual	July – September	Annual	July – September	Annual	July - September
1984	0.13	6.0	7.6	2.9	4.0	2.2	2.9
2014	0.11	7.6	9.5	4.6	6.3	3.7	5.0
2015	0.11	8.4	10	5.4	7.3	4.4	6.0

4.5 Teleconnections to PDO, AO, and SOI

Temperature, precipitation, and model output (rainfall, snowfall, basin discharge, net basin drift, firn melt, mass balance, evapotranspiration, sublimation, ice melt, snowmelt, and rainfall runoff) for the basin value of each model configuration were tested for correlation with spatially and temporally large scale atmospheric anomalies. These included the Pacific Decadal Oscillation, Arctic Oscillation, Southern Oscillation Index, and an additional temporal trend test using the GLS method described in Section 3.8. It is important to note that the 36 years of meteorological input and model output are concurrent with the positive phase of the PDO (1977 to 2007) (Whitfield et al., 2010). The record may not be long enough to detect significant correlation to atmospheric anomalies. It was found that there were no teleconnections to temperature and precipitation. Rainfall and snowfall were also not correlated. None of the model outputs for each of the three configurations were correlated with any of the atmospheric anomalies.

5 DISCUSSION

The Bologna Glacier has experienced rapid reduction in area and change in surface facies configuration over recent decades. The 14% decrease in area, 42 m average decrease in surface elevation, and drastic reduction in surface cover and volume (Section 4.2) correspond to similar glacier change observed throughout the Canadian Cordillera (Meier et al., 2003; DeBeer and Sharp, 2007; Demuth et al., 2008; Marshall et al., 2011). Demuth et al., (2014) observed a 30% contraction in glacier cover in the Greater Nahanni Ecosystem between 1982 and 2008, noting that larger glaciers generally experienced lesser fractional area loss than smaller glaciers.

While the decrease in area of the Bologna Glacier is significant (p = 0.00037), the change in the surface facies over the study period is also drastic. The firn limit experienced a significant rise (p = 0.019) over the study period. The firn area ratio correspondingly experienced significant decline (p = 0.0049). Firn covered 82% of the glacier in 1984 and was reduced to 47% of the glacier in 2014. In August of 2015 and 2016 it was observed that there was no firn cover on the glacier. The firn limit rise can be approximated as 246 m, including approximately 42 m of downwasting over the 30 year period. An analysis of the firn limit progression over time (Table 4.1 and Figures 4.8 to 4.11) showed that it experienced a mainly monotonic rise throughout the study period.

The annual mass balance shown annually and cumulatively in Figures 4.19 and 4.20, respectively, illustrate that the glacier mass balance is in a primarily negative state in all three model configurations. The cumulative mass balance ranges between -9.0 m and -20.3 m water equivalent between configurations. This range provides an envelope estimate of the mass balance. These results are consistent with the regional annual glacier mass balance for Northwestern America (Figure 3.4), which shows the whole Cordillera region was in a state of strong negative mass balance from the late 1970s onwards, with the exception of slightly positive mass balance in 2000 and 2001. Modelled results are therefore in general agreement with the regional state of glacier mass balance for the Cordillera.

The volume change of the glacier between 1984 and 2014 was calculated as $-310 \pm 698 \times 10^6$ m^3 using volume-area scaling. The modelled volume change was -257, -415, and -491×10^6 m^3 for the 1984, 2014, and 2015 model configurations, respectively. While the error in the calculated

volume change is very high, it is evident that modelled results fall within this error, and that the model results are in the same order of magnitude of the calculated volume. While there are no long term direct discharge measurements with which to validate the model, this comparison indicates that the model is producing results within the actual range of the glacier volume change.

Modelled results showed an increasing trend in annual discharge in the 2014 and 2015 model configurations and an increasing trend in ice melt for the 1984 and 2014 model configurations (Section 4.3.1). Evapotranspiration was increasing significantly for each of the three model configurations. There were no temporal trends in any of the model configurations for firn melt, rainfall runoff, snowmelt, or sublimation. Trends in the driving meteorology (increasing maximum summer temperature, decreasing total spring precipitation, and increasing rainfall ratio) can help to explain trends in model results. Increasing maximum summer temperatures increase melt energy when ice exposure is at a maximum, therefore increasing ice melt and total discharge. Likewise, decreasing total spring precipitation and an increasing rainfall ratio cause earlier melt to snowpack on the glacier, leading to earlier ice exposure and a longer time period over which ice melt occurs. The same trends do not occur for firn melt, likely because firn has a higher albedo than ice and therefore firn requires more energy to melt than ice. The snowfall and rainfall volumes are not changing significantly, and therefore there are no trends in snowmelt or rainfall runoff reflected in the model results. However, the increasing trend in rainfall ratio and decreasing total spring precipitation indicate that the timing of the melt may be changing over the study period. Overall, the increase in ice exposure for the contemporary (2014, 2015) model configurations compared to the historical (1984) model configuration show the increasing hydrological sensitivity of the Bologna Glacier basin. The loss of firn and lower glacier albedo in the contemporary configurations can cause larger amplitude flows, more runoff, faster depletion of winter snow cover, and the lack of firn causes faster throughflow of water. Increased temperature and decreased precipitation will further exacerbate these consequences in the future.

While the model results indicate trends in ice melt and discharge in some of the model configurations, these trends are not observed consistently throughout each run. The modelling methods did not account for changing glacier coverage within the run: modelling the glacier in three configurations over 36 years allowed the determination of margin of model output, but not

the actual output itself. Because of the rapid increase in the firn line, it is likely that there was a corresponding trend in the actual discharge of the glacier. To further understand the glacier contribution to streamflow, the basin water budget and glacier mass balance were examined, as well an analysis of the melt and wastage contributions to discharge, similar to Hopkinson and Young (1998) and Comeau et al. (2009).

The basin water budget (Section 4.3.2) shows that the glacier was in a state of negative balance in the 1984 configuration. The budget became increasingly more negative with each subsequent model configuration. In the 1984 model configuration, the net basin budget was -217 mm/year. The 2014 and 2015 model configurations were -425 mm/year and -515 mm/year, respectively. This was concurrent with an increase in overall discharge, ice melt, evapotranspiration, decreasing firn melt, and relatively stable snowmelt runoff, rainfall runoff, sublimation, and drift between subsequent model configurations. Increased ice melt is caused by the greater area of exposed low-albedo ice, which accelerates melt rates. The increase in evapotranspiration is due to the increased land area: more vegetation and water ponding leading to increased ET. Firn melt decreased significantly between the model configurations, given the drastic reduction in the area of firn available for melting. In the 1984 configuration, there is a significantly higher contribution to flow from firn melt than ice melt, as compared to the 2014 configuration, where there is a significantly higher contribution from ice melt than firn melt. This shift is due to the rising firn limit and the increasing area of exposed ice. Snowmelt runoff, rainfall runoff, sublimation, and drift remained relatively the same throughout each model configuration. It is logical that these components remain the same throughout each model configuration because the driving meteorology – snowfall, rainfall, and wind – is the same throughout the configurations. While there may be some change in the timing of the snowmelt and rainfall runoff contributions, the totals are likely to remain roughly the same.

Glacier melt and wastage were calculated according to Comeau et al. (2009). By the definitions, melt is a storage term whereas wastage is ice loss due to any negative net mass balance. Figures 4.21 to 4.23 show that the quantity of wastage and melt can vary considerably year to year and depend on whether the glacier is in a state of positive or negative mass balance. In years of positive mass balance, the discharge is composed of neither wastage nor melt and the glacier stores snowfall in the system. Wastage alone is shown to be a significant contributor to total

basin discharge, ranging from 35 – 53% of basin discharge. This agrees with other studies that have found significant contributions from glacier wastage (Hopkinson and Young, 1998; Demuth et al., 2008; Comeau et al., 2009). Melt contributed a lesser amount to basin discharge, and remained a relatively constant percentage of basin discharge at 12 – 13%, which also agree with the literature. The wastage contributions increased significantly over time, while the melt contributions remained constant. This indicates that the driver behind the increasingly negative mass balance in the three configurations is due to the increased wastage contributions.

The analysis of the average daily hydrograph (Figures 4.24) and the annual hydrographs for a highly positive (1987) and a highly negative (1998) mass balance year (Figures 4.25, and 4.26) demonstrate the impact of glacier contributions on streamflow. The hydrographs from 1987 showed little difference in the three model configurations while the hydrographs from 1998 showed vast differences in the diurnal amplitude of discharge between model configurations. In the average daily hydrograph, it is evident that for the model configuration with the highest ice exposure (2015), there is more variability in streamflow than for the model configuration with the lowest ice exposure (1984). These hydrograph characteristics have been widely observed in the literature (Braun and Escher-Vetter, 1996; Hock et al., 2005; Schuster and Young, 2006). The change in amplitude and timing is a result of increased ice exposure and the efficient removal of meltwater due to a continuously developing drainage system (Singh and Singh, 2001; Schuster and Young, 2006).

To determine the overall impact of the Bologna Glacier on the South Nahanni River, the discharge volume of each model configuration was compared to the flow volume of the South Nahanni River at the Virginia Falls gauge over the study period. The margin of glacier contribution to streamflow is 6.0 – 8.4% annually and 7.6% – 10% during the summer months. The margin of contribution from wastage only is 2.2 – 4.4% annually and 2.9 – 6.0% during the summer months. This calculation assumes that all of the discharge from the Bologna Glacier basin is transported the full length of the South Nahanni River to the gauge at Virginia Falls. It is likely that a portion of this flow would be lost to groundwater given that this region is highly karstic (Ford, 2009). However, this groundwater flow would eventually reconnect with the South Nahanni River since long distance groundwater flow is negligible. Given that the glacier area comprises 0.11 – 0.13% of the South Nahanni River basin (14500 km^2), the Bologna Glacier

basin contribution to flow is high compared to contributions measured and published in the regional glaciological literature. Figure 5.1 is reproduced from Comeau et al. (2009). It shows the percentage wastage contribution to streamflow as a function of basin glacierized area for several glaciers of varying size throughout the North and South Saskatchewan River basins. Comeau et al. (2009) demonstrated that a glacier covering approximately 0.1% of a basin contributes less than 5% of the total streamflow from glacier wastage on both an annual and summer basis. Specifically, the Ram River basin is 0.2% glacierized and glacier wastage comprised 1.6% of summertime streamflow. The Highwood River basin is 0.1% glacierized and glacier wastage comprised 1.4% of summertime streamflow (Comeau et al., 2009). In this study, both the annual and summertime wastage contributions to streamflow fall below 5% for each model configuration, except the summertime wastage contribution for the 2015 model configuration falls above 5%. The modelled contributions from wastage are likely to be high due to the fact that neither firn nor melt is ever depleted in the model. Each year it is replenished so as to circumvent the lack of glacier dynamics. In reality, the firn layers would eventually disappear and the ice volume would decrease, limiting melt over time.

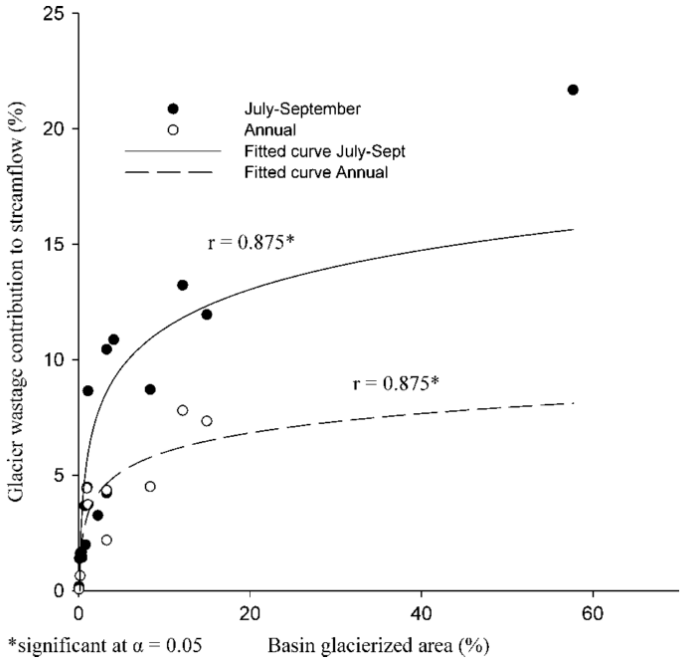

Figure 5.1: Percentage glacier wastage contribution to streamflow (1975–1998) compared to percentage basin glacierized area (average 1975 and 1998 area) (From Comeau et al., 2009, reproduced with permission of John Wiley and Sons. Copyright © 2009)

The teleconnections analysis demonstrated that there were no correlations found between the PDO, SOI, or AO and the temperature and precipitation record or the modelled results over the study period. The study period of 36 years (1980 – 2015) is concurrent with the positive phase of the PDO (1977 to 2007) (Whitfield et al., 2010). The record may not be long enough to detect significant correlation to atmospheric anomalies. Other regional and related glacier studies have found correlation of hydrological, climatological, and glaciological variables to atmospheric circulation patterns. Moore and Demuth (2001) found that the winter and net balances at Place Glacier in British Columbia were correlated with the PDO. Demuth and Keller (2006) noted that a reduction in winter snowfall occurred after the PDO shift, causing primarily negative net mass balance for Peyto Glacier in Alberta after 1976. Burn et al. (2004) investigated whether there were teleconnections of hydrological variables with the PDO in the Liard River basin, which is a non-glacierized basin just to the south of the South Nahanni River basin. They found that there was a relationship between the PDO and winter flows, the annual minimum flow, the timing of the spring freshet, and the timing of the spring maximum flow event. Regime shifts in both the PDO and AO have been observed in the mass balance time series for both the Gulkana and Wolverine Glaciers in Alaska (Hodge et al., 1998). Each of these studies used data from the 1960s, extending before the PDO shift occurred. Fleming et al. (2005) found that the annual glacier signal was correlated to the positive phase of the AO for glaciers in northern British Columbia and western Yukon. Gardner and Sharp (2007) found that the PDO had little to no effect on regional glacier mass balance in the Canadian High Arctic. They found no correlation between regional glacier mass balance and the AO but found the regional mass balance to be significantly correlated to the July AO.

Results discussed thus far can help to illustrate the complex interrelationships between the glacier area and surface facies, climate, and streamflow. The altitude of the ELA at the end of the ablation season is strongly linked to glacier mass balance (Braun and Escher-Vetter, 1996; Braithwaite and Raper, 2009) and several studies have linked the effects of the rising ELA on glacier meltwater production. While the firn limit established in this project is likely to be lower than the true ELA, similar melt patterns occur with a rising firn limit as with a rising ELA as both the ELA and firn limit are tools to quantify changing surface facies. Braun and Escher-Vetter (1996) observed decreasing firn coverage from 70% in the early 1980s to 10% in 1994, which coincided with a period of increased glacier runoff and sustained negative net mass

balance and a small decrease in glacier area. Moore and Demuth (2001) studied the effect of climate variability and change on glacier streamflow response. They observed a marked decrease in August runoff following significant firn depletion prior to the study period, and they suggested that the "transient response of glacier runoff to climatic fluctuations may be strongly conditioned by the initial extent of firn coverage". Increased streamflow from glaciers over several decades has been observed in numerous studies (Meier, 1984; Braun and Escher-Vetter, 1996; Hopkinson and Young, 1998) as well as decreasing streamflow from glaciers (Demuth and Pietroniro, 2003; Stahl and Moore, 2006; Rood et al., 2008). These later studies have shown that the ephemeral period of augmented glacier flow will eventually reach a threshold where area-wise reductions then limit meltwater production from the glacier, and meltwater volumes will continuously decline. The true discharge of the Bologna Glacier basin cannot be directly assessed from the model output; however, results indicate that over three decades, average annual basin discharge increases with each subsequent model configuration. Additionally, there were increasing trends in modelled discharge and ice melt. This suggests that glacier discharge is in the phase of rising discharge prior to being limited by the reduction in area. It is predicted that due to the complete loss of firn cover in the past two years (2015, 2016), flow from the glacier will eventually decline as the ice volume limits meltwater production.

The results from this study confirm and extend findings of recent research conducted on glacier hydrology in the Canadian Cordillera. However, there are some limitations of the study given the data available and the methodology. There were no trends in the total annual precipitation or average annual temperature in the corrected reanalyses. These findings are not supported by other research in the northern region: several studies have shown both temperature (IPCC, 2013; Liu et al., 2007; Vincent et al., 2015) and precipitation (IPCC, 2013; Vincent et al., 2015) to be increasing significantly. However, these studies used valley bottom stations at low elevations, which may experience different climate forcing than high altitude stations, such as those at the Bologna Glacier. The climate of alpine regions is highly complex due to interaction of the mountains and the circulation of the atmosphere. The interannual variability of temperature can be much higher for mountain regions and some studies have found little trend in precipitation in mountain regions (Beniston et al., 1997). While there were no trends in the average annual temperature or total annual precipitation, other trends were found in the driving meteorology. The rainfall ratio was found to be increasing significantly ($p = 0.021$) and two seasonal trends

found in the corrected reanalyses: maximum daily summer temperature increased significantly (p = 0.025) and total spring precipitation decreased significantly (p = 0.027). The warm summer temperatures are likely to accelerate albedo decay and melt. The lower spring precipitation is likely to cause early ablation and albedo decay of the spring snow cover resulting in exposure of ice. A precipitation regime with an increasing proportion of rainfall causes less solid precipitation to be stored in the glacier system.

Uncertainty in quantifying the firn limit is attributed to the relative ambiguity of the ice-firn boundary in the satellite imagery. For example, in in 1998 and 2004 (Figure 4.8), there is a wide band of the glacier where the area of firn and ice appear to be mixed. This is commonly seen where glaciers are in a state of negative mass balance, since a rising snowline tends to be more indistinct that than a descending snowline, especially when it rises above the firn limit. Using spectral bands which best differentiate snow and ice helps to differentiate these areas (Hall et al., 1987); however, there is still ambiguity. For the modelling set-up, these areas were classified as thinner layers of firn. To maintain consistency with the modelling analysis, these areas were classified as firn in the firn limit analysis.

Additional limitations in this project stem from the glacier module in the CRHM platform. The model does not include ice dynamics and so cannot dynamically evolve glacier geometry: the area does not change with respect to time, the firn limit remains in the same location, and ice cannot flow from one HRU to another. These are fundamental glacier processes and impact the response of a glacier undergoing changes in forcing meteorology. Many studies simply model glaciers in fixed configurations, which cannot accurately represent glacier discharge with respect to the changing glacier configuration. To partially overcome the limitations of the glacier module, the model was set up such that it represented the glacier in three configurations, and the driving meteorology remained constant for the three configurations. While this method cannot produce truly accurate discharge estimates, it does provide an envelope of discharge within which measured results should fall. An additional problem with running the model over decades in the same configuration is that the accumulation zone collects a falsely high volume of snowfall and the ablation zone continuously melts. The increase in snowfall in the accumulation zone is caused by incremental increases in elevation, leading to higher snowfall. The effect is minimal for short time scales but the error accumulates over time. In reality, the glacier flow will

redistribute ice from higher elevation areas to lower elevation areas due to basal sliding and ice deformation, essentially trying to maintain an equilibrium condition. To partially overcome this problem, the model is re-set every year to its original state. The key issue with this is the state of the glacier at the end of the hydrological year will have no effect on the following year, meaning that any compounding positive feedbacks will not be represented by the model. Any snowfall remaining on the glacier at the hydrological year's end will not be converted into firn and any net loss of ice will not be taken into account. Given that the glacier is predominantly in a state of net mass loss, it is unlikely that there would be a significant volume of firn added to the system over the study period. Because any ice and firn lost is replenished at the start of the next hydrological year, the volume of ice and firn available for melting may be falsely high, and will effectively never deplete, unless it does so within one hydrological year. Positive feedbacks are frequently seen in where melting ice is concerned: greater areas of exposed ice result in a lower albedo, which further accelerates melt, and so on. This feedback scenario cannot be represented by the model due to the lack of continuity and dynamic surface facies representation. This limitation is partially overcome by modelling the glacier in three configurations to provide an envelope of model output.

There is uncertainty in the driving meteorology that cannot be quantified due to the lack of long term meteorological records. However, testing of ERA-Interim reanalyses against AWS stations showed results that were consistent with those shown in the literature on the quality of ERA-Interim data (Betts et al., 2009; Krogh et al., 2015; Vuichard and Papale, 2015). Additionally, ERA-Interim assimilates upper air measurements that surround the Bologna Glacier basin at Norman Wells and Whitehorse, which allows for relatively accurate representations of downscaled climate data. The comparison of ERA-Interim temperature and long term meteorological observations at Macmillan Pass, YK (Environment Canada and Yukon Government stations) and Tungsten, NWT showed that ERA-Interim provides accurate hourly temperature (R^2 = 0.95, 0.94, and 0.96, respectively). This was similarly true of the short term hourly temperature observations at the Bologna Glacier (R^2 = 0.87), in addition to vapour pressure (R^2 = 0.87) and shortwave radiation (R^2 = 0.77), as shown in Section 3.2.1. This is consistent with findings in the literature (Betts et al., 2009; Vuichard and Papale, 2015). However, agreement for wind speed (no statistical correlation at the hourly time step) and precipitation (no statistical correlation at the daily time step) tends to be poor, as noted in other

studies of reanalyses against field observations (Krogh et al., 2015; Vuichard and Papale, 2015). Testing ERA-Interim reanalyses against other stations with long term precipitation observations showed that ERA-Interim provides fairly accurate precipitation on an annual basis (R^2 = 0.79, 0.85, and 0.49, for Macmillan Pass YG, EC, and Tungsten, respectively). However, these R^2 values are likely affected by the challenges and limitations of collecting high quality precipitation measurements in remote locations. Especially at Tungsten, there were a high percentage of observations missing and the gauge type was undocumented, which made wind undercatch corrections impossible. Overall, ERA-Interim was shown to be a suitable option for this site, given the lack of any long term meteorological observations with which to drive the model.

6 CONCLUSIONS

Dramatic changes to the size and surface configuration of the Bologna Glacier since the 1980s have had a significant impact on headwater streamflow generation in the basin. The complex inter-relationships between the glacier area and changing surface facies, climate, and streamflow have been examined via remote sensing, hydrological modelling, and statistical analysis.

The effect of climate change, reduced glacier cover, and increased ice exposure on headwater streamflow generation at the Bologna Glacier has been substantial. Glacier area decreased by 14% from 1984 to 2014 (30 years). Firn coverage was reduced from 82% to 47% over the same time period, and disappeared entirely by 2015. There was a shift in discharge contribution from substantial firn melt contributions to substantial ice melt contributions between the 1984 and 2014/2015 model configurations. The glacier was in a state of net negative mass balance in the 1984 configuration and became increasingly negative with each subsequent model configuration, concurrent with an increase in total basin discharge. Overall, there was a substantial contribution to streamflow from glacier wastage in all three configurations. The summertime wastage contribution to streamflow at the Virginia Falls gauge in the South Nahanni River ranged from 2.9 to 6.0% from 1980 to 2014. The results indicate that the glacier was in a state of ephemeral increasing discharge as the firn limit rose. It is predicted that because the firn has disappeared completely, the glacier area will eventually limit the amount of meltwater produced, and a continuous decline in glacier discharge will occur over the next decades.

Short-term in situ meteorological observations were used to bias correct and downscale a climate reanalysis product to construct a 36 year meteorological record at a remote northern mountain site. There were no significant trends in the reconstructed data for annual average maximum, mean, and minimum temperature or for annual total precipitation. However, both the rainfall ratio and the average daily maximum summer temperatures were found to be increasing significantly over the study period. Total spring precipitation was found to be decreasing significantly over the study period. The trends in driving meteorology were, in some cases, reflected in the modelled basin discharge and ice melt but not in the modelled firn melt, snowmelt, rainfall runoff, sublimation, or drift. There were no teleconnections with large scale atmospheric circulation patterns including those described by the SOI, AO, and PDO.

6.1 Recommendations for Further Work

The Bologna Glacier is a recent addition to the glacier monitoring and assessment reference network operated by Natural Resources Canada/Geological Survey of Canada and their partner agencies. It is an important contribution towards the study of energy and water fluxes in Canada's northern continental regions. Given that this glacier is a new addition to the network and its location in a remote and inaccessible basin, there have been few measurements made within the basin and region. The main limitation in this study was the lack of long term hydrometric and spatial data for parameterising, driving, and validating the model. The most beneficial contributions of data for this purpose would be to acquire LiDAR data to generate a contemporary high resolution DEM, to acquire glacier-thickness measurements using ground-penetrating radar, and the initiation of streamflow measurements supplemented by tracer studies to determine how groundwater moves within the basin.

Limitations in the glacier module could be overcome by including the capability to dynamically readjust the glacier geometry. This would limit the need for the steps taken to account for the static glacier configuration including running the model in three configurations and resetting the model to the original glacier configuration each subsequent year. Rather than providing an envelope of output between two configurations, as in this study, incorporating glacier dynamics would allow for a continuous estimation of model output.

REFERENCES

Agnew T, Brown R, Burgess M, Cogley G, Demuth M, Duguay C, Flato G, Goodison B, Koerner R, Melling H, O'Neill D, Prowse T, Ramsay B, Sharp M, Smith S, Walker A. 2002. National Plan for Cryospheric Monitoring: A Canadian Contribution to the Global Climate Observing System. Brown R, O'Neill D (eds). Unpublished Manuscript, Meteorological Service of Canada: Downsview, Ontario; 81 pp.

Arendt AA, Echelmeyer KA, Harrison WD, Lingle CS, Valentine VB. 2002. Rapid wastage of Alaska glaciers and their contribution to rising sea level. *Science* **297**: 382–386. doi: 10.1126/science.1072497.

Arendt A, Echelmeyer K, Harrison W, Lingle C, Zirnheld S, Valentine V, Ritchie B, Druckenmiller M. 2006. Updated estimates of glacier volume changes in the western Chugach Mountains, Alaska, and a comparison of regional extrapolation methods. *Journal of Geophysical Research* **111**: F03019. doi: 10.1029/2005JF000436.

Ayers H. 1959. Influence of soil profile and vegetation characteristics on net rainfall supply to runoff. *Proceedings of Hydrology Symposium* **1**: 198–205.

Bahr B, Meier F, Peckham SD. 1997. The physical basis of glacier volume-area scaling. *Journal of Geophysical Research* **102**: 20355–20362.

Bahr DB, Pfeffer WT, Kaser G. 2015. A review of volume-area scaling of glaciers. *Review of Geophysics* **53**: 95–140. doi:10.1002/2014RG000470.

Barnett TP, Adam JC, Lettenmaier DP. 2005. Potential impacts of a warming climate on water availability in snow-dominated regions. *Nature* **438**: 303–309. doi: 10.1038/nature04141.

Barrand NE, Sharp MJ. 2010. Sustained rapid shrinkage of Yukon glaciers since the 1957-1958 International Geophysical Year. *Geophysical Research Letters* **37**: L07501. doi: 10.1029/2009GL042030.

Beniston M, Diaz HF, Bradley RS. 1997. Climatic change at high elevations: An overview. *Climatic Change* **36**: 233–251. doi:

Benn DI, Evans DJA. 1998. Glaciers and Glaciation. Oxford University Press Inc.: New York, New York; 734 pp.

Benn DI, Lehmkuhl F. 2000. Mass balance and equilibrium-line altitudes of glaciers in high-mountain environments. *Quaternary International* **65/66**: 15–29. doi: 10.1016/S1040-6182(99)00034-8.

Bergström S. 1976. Development and application of a conceptual runoff model for Scandinavian catchments. Swedish Meteorological and Hydrological Institute (SMHI): Norrköping, Sweden.

Bernhardt M, Schulz K. 2010. SnowSlide: A simple routine for calculating gravitational snow transport. *Geophysical Research Letters* **37**: 1–6. doi: 10.1029/2010GL043086.

Berrisford PD, Dee D, Poli P, Burgge R, Fielding K, Fuentes M, Kållberg P, Kobayashi S, Uppala S, Simmons A. 2011. The ERA-Interim archive. *ERA Report Series* **2**: 1–16.

Betts AK, Köhler M, Zhang Y. 2009. Comparison of river basin hydrometerology in ERA-Interim and ERA-40 reanalyses with observations. *Journal of Geophysical Research* **114**: 1–12. doi: 10.1029/2008JD010761.

Beven K, Freer J. 2001. Equifinality, data assimilation, and uncertainty estimation in mechanistic modelling of complex environmental systems using the GLUE methodology. *Journal of Hydrology* **249**: 11–29.

Bolch T, Buchroithner M, Pieczonka T, Kunert A. 2008. Planimetric and volumetric glacier changes in the Khumbu Himal, Nepal, since 1962 using Corona, Landsat TM and ASTER data. *Journal of Glaciology* **54**: 592–600. doi: 10.3189/002214308786570782.

Bonsal BR, Shabbar A, Higuchi K. 2001. Impacts of low frequency variability modes on Canadian winter temperature. *International Journal of Climatology* **21**: 95–108. doi: 10.1002/joc.590.

Bostock H. 1948. Physiography of the Canadian Cordillera, with Special Reference to the Area North of the Fifty-fifth Parallel. GSC Memoir 247. Geological Society of Canada, Canada Department of Mines and Resources: Ottawa, Canada; 106 pp.

Braithwaite RJ, Zhang Y. 1999. Modelling changes in glacier mass balance that may occur as a result of climate changes. *Geografiska Annaler* **81**: 489–496.

Braithwaite RJ, Raper SCB. 2009. Estimating equilibrium-line altitude (ELA) from glacier inventory data. *Annals of Glaciology* **50**: 127–132. doi: 10.3189/172756410790595930.

Braun LN, Escher-Vetter H. 1996. Glacial discharge as affected by climate change. *Tagungspublikation* **1**: 65–74.

Braun LN, Weber M, Schulz M. 2000. Consequences of climate change for runoff from Alpine regions. *Annals of Glaciology* **31**: 19–25. doi: 10.3189/172756400781820165.

Bronaugh D, Werner A. 2013. Pacific Climate Impacts Consortium. zyp: Zhang + Yue-Pilon trends package. R package version 0.10-1. http://CRAN.R-project.org/package=zyp.

Burn DH, Cunderlik JM, Pietroniro A. 2004. Hydrological trends and variability in the Liard River basin. *Hydrological Sciences Journal* **49**: 53–67. doi: 10.1623/hysj.49.1.53.53994.

Burn DH. 2008. Climatic influences on streamflow timing in the headwaters of the Mackenzie River Basin. *Journal of Hydrology* **352**: 225–238. doi: 10.1016/j.jhydrol.2008.01.019.

Carslaw DC, Ropkins K. 2015. openair: Open-source tools for the analysis of air pollution data. R package version 1.6.7. http://CRAN.R-project.org/package=openair.

Centre for Hydrology. 2016. Cold Regions Hydrological Model Platform Modules Library.

Chen J, Ohmura A. 1990a. Estimation of Alpine glacier water resources and their change since the 1870s. *IAHS Publication* **193**: 127–136.

Chen J, Ohmura A. 1990b. On the influence of Alpine glaciers on runoff. *IAHS Publication* **193**: 117–126.

Clark CO. 1945. Storage and the unit hydrograph. *Proceedings of the American Society of Civil Engineers* **69**: 1333–1360.

Clarke GK, Berthier E, Schoof CG, Jarosch AH. 2009. Neural networks applied to estimating subglacial topography and glacier volume. *Journal of Climate* **22**: 2146–2160. doi: 10.1175/2008JCLI2572.1.

Church JA, Clark PU, Cazenave A, Gregory JM, Jevrejeva S, Levermann A, Merrifield MA, Milne GA, Nerem RS, Nunn PD, Payne AJ, Pfeffer WT, Stammer D, Unnikrishnan AS. 2013. Sea Level Change. In: Climate Change 2013: The Physical Science Basis. Contribution of Working Group I to the Fifth Assessment Report of the Intergovernmental Panel on Climate Change, Stocker TF, Qin D, Plattner G-K, Tignor M, Allen SK, Boschung J, Nauels A, Xia Y, Bex V, Midgley (eds). Cambridge University Press, Cambridge, United Kingdom and New York, NY, USA.

Cogley JG, Adams WP. Mass balance of glaciers other than the ice sheets. *Journal of Glaciology* **44**: 315–325.

Cogley JG, Hock R, Rasmussen LA, Arendt AA, Bauder A, Braithwaite RJ, Jansson P, Kaser G, Möller M, Nicholson L, Zemp M. 2011. Glossary of glacier mass balance and related terms. *IHP-VII Technical Documents in Hydrology* **86**: 965.

Collier EP. 1958. Glacier variation and trends in run-off in the Canadian Cordillera. *IAHS Publication* **46**: 344–357.

Collins DN. 2008. Climatic warming, glacier recession and runoff from Alpine basins after the Little Ice Age maximum. *Annals of Glaciology* **48**: 119–124. doi: 10.3189/172756408784700761.

Comeau LEL, Pietroniro A, Demuth MN. 2009. Glacier contribution to the North and South Saskatchewan Rivers. *Hydrological Processes* **23**: 2640–2653. doi: 10.1002/hyp.7409.

Cuffey KM, Paterson WSB. 2010. The Physics of Glaciers, 4th edition. Academic Press: Amsterdam; 704 pp.

DeBeer CM, Sharp MJ. 2007. Recent changes in glacier area and volume within the southern Canadian Cordillera. *Annals of Glaciology* **46**: 215–221.

DeBeer CM, Pomeroy JW. 2010. Simulation of the snowmelt runoff contributing area in a small alpine basin. *Hydrology and Earth System Science* **14**: 1205–1219.

Dee DP, Uppala SM, Simmons AJ, Berrisford P, Poli P, Kobayashi S, Andrae U, Balmaseda MA, Balsamo G, Bauer P, Bechtold P, Beljaars ACM, van de Berg L, Bidlot J, Bormann N, Delsol C, Dragani R, Fuentes M, Geer AJ, Haimberger L, Healy SB, Hersbach H, Hólm EV, Isaksen L, Kållberg P, Köhler M, Matricardi M, McNally AP, Monge-Sanz BM, Morcrette J-J, Park B-K, Peubey C, de Rosnay P, Tavolato C, Thépaut J-N, Vitart F. The ERA-Interim reanalysis: Configuration and performance of the data assimilation system. *Quarterly Journal of the Royal Meteorological Society* **137**: 553–597. doi: 10.1002/qj.828.

Demuth MN. 1998. The Canadian Glacier Variations Monitoring and Assessment Network Status and Future Perspectives. In Long-term Monitoring of Glacier Fluctuations in North America and Northwestern Europe (USGS Open-File Report 98-31), Williams RS Jr., Ferringo JG (eds). Environment Canada, National Hydrology Research Institute: Saskatoon, Saskatchewan; 37–51.

Demuth, MN, Pietroniro A. 2003. The impact of climate change on the glaciers of the Canadian Rocky Mountain eastern slopes and implications for water resource-related adaptation in the Canadian prairies, Phase I – Headwaters of the North Saskatchewan River Basin. *Geological Survey of Canada Open File 4322*; 96 pp.

Demuth MN, Keller R. 2006. An assessment of the mass balance of Peyto Glacier (1966-1995) and its relation to recent and past-century climatic variability. In Peyto Glacier: One Century of Science, Demuth MN, Munro DS, Young GJ (eds). National Hydrology Research Institute Science Report No. 8: Saskatoon; 83–132. ISBN: 0-660-17683-1.

Demuth M, Pinard V, Pietroniro A, Luckman B, Hopkinson C, Dornes P, Comeau L. 2008. Recent and past-century variations in the glacier resources of the Canadian Rocky Mountains: Nelson River system. *Terra Glacialis* **11**: 27–52.

Demuth MN, Haggerty D, Wilson P. 2014. The glaciers of Nahanni National Park Reserve, NT, Canada. In Global Land Ice Measurements from Space, Kargel J, Raup B (eds). Springer: Berlin, Germany; 375–383.

Derksen C, Smith SL, Sharp M, Brown L, Howell S, Copland L, Mueller DR, Gauthier Y, Fletcher CG, Tivy A, Bernier M, Bourgeois J, Brown R, Burn CR, Duguay C, Kushner P, Langlois A, Lewkowicz AG, Royer A, Walker A. 2012. Variability and change in the Canadian cryosphere. *Climatic Change* **115**: 59–88. doi: 10.1007/s10584-012-0470-0.

Dornes PF, Pomeroy JW, Pietroniro A, Carey SK, Quinton WL. 2008a. Influence of landscape aggregation in modelling snow-cover ablation and snowmelt runoff in a sub-arctic mountainous environment. *Hydrological Sciences Journal* **53**: 725–740. doi: 10.1623/hysj.53.4.725.

Dornes PF, Pomeroy JW, Pietroniro A, Verseghy DL. 2008b. Effects of spatial aggregation of initial conditions and forcing data on modeling snowmelt using a land surface scheme. *Journal of Hydrometeorology* **9**: 789–803. doi: 10.1175/2007JHM958.1.

Dornes PF, Tolson BA, Davison B, Pietroniro A, Pomeroy JW, Marsh P. 2008c. Regionalisation of land surface hydrological model parameters in subarctic and arctic environments. *Physics and Chemistry of the Earth* **33**: 1081–1089. doi: 10.1016/j.pce.2008.07.007.

Dyurgerov MB, Meier MF. 2000. Twentieth century climate change: Evidence from small glaciers. *Proceedings of the National Academy of Sciences* **97**: 1406–1411.

Dyurgerov M, Meier MF, Bahr DB. 2009. A new index of glacier area change: A tool for glacier monitoring. *Journal of Glaciology* **55**: 710–716.

Ellis CR, Pomeroy JW. 2007. Estimating sub-canopy shortwave irradiance to melting snow on forested slopes. *Hydrological Processes* **21**: 2581–2593. doi: 10.1002/hyp.

Ellis CR, Pomeroy JW, Brown T, MacDonald J. 2010. Simulation of snow accumulation and melt in needleleaf forest environments. *Hydrology and Earth System Sciences* **14**: 925–940. doi: 10.5194/hess-14-925-2010.

Escher-Vetter H. 1985. Energy balance calculations for the ablation period 1982 at Vernagtferner, Oetztal Alps. *Annals of Glaciology* **6**: 158–160.

Fang XJ, Pomeroy JW, Westbrook CJ, Guo X, Minke AG, Brown T. 2010. Prediction of snowmelt derived streamflow in a wetland dominated prairie basin. *Hydrology and Earth System Sciences* **14**: 1–16. doi: 10.5194/hess-14-1-2010.

Fang XJ, Pomeroy JW, Ellis CR, MacDonald MK, DeBeer CM, Brown T. 2013. Multi-variable evaluation of hydrological model predictions for a headwater basin in the Canadian Rocky Mountains. *Hydrology and Earth System Science* **17**: 1635–1659. doi: 10.5194/hess-17-1635-2013.

Farinotti D, Huss M. 2013. An upper bound estimate for the accuracy of glacier volume-area scaling. *The Cryosphere* **7**: 1707–1720. doi: 10.5194/tc-7-1707-2013.

Fisher D, Osterberg E, Dyke A, Dahl-Jensen D, Demuth M, Zdanowicz C, Bourgeois J, Koerner RM, Mayewski P, Wake C, Kreutz K, Steig E, Zheng J, Yalcin K, Goto-Azuma K, Luckman B, Rupper S. 2008. The Mt Logan Holocene – late Wisconsinan isotope record: tropical Pacific –Yukon connections. *The Holocene* **18**: 667-677. doi: https://doi.org/10.1177/0959683608092236.

Fleming SW, Clarke GKC. 2003. Glacial control of water resource and related environmental responses to climatic warming: empirical analysis using historical streamflow data from northwestern Canada. *Canadian Water Resources Journal* **28**: 69–86. doi: 10.4296/cwrj2801069.

Fleming SW, Clarke GKC. 2005. Attenuation of high-frequency interannual streamflow variability by watershed glacial cover. *Journal of Hydraulic Engineering* **131**: 615–618. doi: 10.1061/(ASCE)0733-9429(2005)131:7.

Fleming SW, Moore RD, Clarke GKC. 2006. Glacier-mediated streamflow teleconnections to the Arctic Oscillation. *International Journal of Climatology* **26**: 619–636. doi: 10.1002/joc.1273.

Fleming SW, Dahlke HE. 2014. Modulation of linear and nonlinear hydroclimatic dynamics by mountain glaciers in Canada and Norway: results from information-theoretic polynomial selection. *Canadian Water Resources Journal* **39**: 324–341. doi: 10.1080/07011784.2014.942164.

Foken T. 2008. Micrometeorology. Edited by CJ Nappo. Springer-Verlag: Berlin Heidelberg; 308 pp.

Ford D. 2009. Mapping known and potential karst areas in the Northwest Territories, Canada. Environment and Natural Resources; 66 pp.

Fountain AG, Tangborn WV. 1985. The effect of glaciers on streamflow variations. *Water Resources Research* **21**: 579–586. doi: 10.1029/WR021i004p00579.

Fountain AG. 1989. The storage of water in, and hydraulic characteristics of, the firn of South Cascade Glacier, Washington State, USA. *Annals of Glaciology* **13**: 69–75.

Fountain AG. 1996. Effect of snow and firn hydrology on the physical and chemical characteristics of glacial runoff. *Hydrological Processes* **10**: 509–521.

Fountain AG, Walder JS. 1998. Water flow through temperate glaciers. *Reviews of Geophysics* **36**: 299–328.

Frey H, Machguth H, Huss M, Huggel C, Bajracharya S, Bolch T, Kulkarni A, Linsbauer A, Salzmann N, Stoffel M. 2014. Estimating the volume of glaciers in the Himalayan–Karakoram region using different methods. *The Cryosphere* **8**: 2313–2333. doi: 10.5194/tc-8-2313-2014.

Gardner AS, Sharp MJ. 2007. Influence of the Arctic circumpolar vortex on the mass balance of Canadian High Arctic glaciers. *Journal of Climate* **20**: 4586–4598. doi: 10.1175/JCLI4268.1.

Gardner AS, Moholdt G, Wouters B, Wolken GJ, Burgess DO, Sharp MJ, Cogley JG, Braun C, Labine C. 2011. Sharply increased mass loss from glaciers and ice caps in the Canadian Arctic Archipelago. *Nature* **473**: 357–360. doi: 10.1038/nature10089.

Garnier BJ, Ohmura A. 1968. A method of calculating the direct shortwave radiation income of slopes. *Journal of Applied Meteorology* **7**: 796–800.

Gascoin S, Kinnard C, Ponce R, Lhermitte S, MacDonell S, Rabatel A. 2011. Glacier contribution to streamflow in two headwaters of the Huasco River, Dry Andes of Chile. *Cryosphere* **5**: 1099–1113. doi: 10.5194/tc-5-1099-2011.

Goodison BE, Louie PYT, Yang D. 1998. WMO solid precipitation measurement intercomparison. *World Meteorological Organization Report No. 67;* 212 pp.

Granger RJ. 1999. Partitioning of energy during the snow-free season in the Wolf Creek research basin. In Wolf Creek Research Basin – Hydrology, Ecology, Environment (Proc. workshop held in Whitehorse, Yukon, Canada, 5-7 March, 1998). NHRI publication 37–121/1999E, Saskatoon, Saskatchewan, Canada; 33–44.

Granger RJ, Gray DM. 1989. Evaporation from natural nonsaturated surfaces. *Journal of Hydrology* **111**: 21–29.

Granger RJ, Gray DM. 1990. A net radiation model for calculating daily snowmelt in open environments. *Nordic Hydrology* **21**: 217–234.

Gray DM, Landine PG. 1987. Albedo model for shallow prairie snow covers. *Canadian Journal of Earth Sciences* **24**: 1760–1768.

Gray DM, Landine PG. 1988. An energy-budget snowmelt model for the Canadian Prairies. *Canadian Journal of Earth Sciences* **25**: 1292–1303.

Gray DM, Toth B, Zhao L, Pomeroy JW, Granger RJ. 2001. Estimating areal snowmelt infiltration into frozen soils. *Hydrological Processes* **15**: 3095–3111. doi: 10.1002/hyp.320.

Haeberli W, Hoelzle M. 1995. Application of inventory data for estimating characteristics of regional climate-change effects on mountain glaciers: a pilot study with the European Alps. *Annals of Glaciology* **21**: 206–212.

Haeberli W, Hoelzle M, Paul F, Zemp M. 2007. Integrated monitoring of mountain glaciers as key indicators of global climate change : the European Alps. *Annals of Glaciology* **46**: 150–160.

Hall DK, Ormsby JP, Bindschadler RA, Siddalingaiah H. 1987. Characterization of snow and ice reflectance zones on glaciers using Landsat Thematic Mapper data. *Annals of Glaciology* **9**: 104–108. doi: https://doi.org/10.3198/1987AoG9-1-104-108.

Halliwell DR, Catto S. 2003. How and why is aquatic quality changing at Nahanni National Park Reserve, NWT, Canada? *Environmental Monitoring and Assessment* **88**: 243–281. doi: 10.1023/A:1025577325352.

Hannah D, Gurnell A, McGregor G. 2000. Spatio-temporal variation in microclimate, the surface energy balance and ablation over a cirque glacier. *International Journal of Climatology* **20**: 733–758.

Harder P, Pomeroy JW, Westbrook CJ. 2015. Hydrological resilience of a Canadian Rockies headwaters basin subject to changing climate, extreme weather, and forest management. *Hydrological Processes* **29**: 3905–3924. doi: 10.1002/hyp.10596.

Herron MM, Langway CC. 1980. Firn densification: an empirical model. *Journal of Glaciology* **25**: 373–385.

Hirsch RM, Slack JR. 1984. A nonparametric trend test for seasonal data with serial dependence. *Water Resources Research* **20**: 727–732.

Hock R. 2003. Temperature index melt modelling in mountain areas. *Journal of Hydrology* **282**: 104–115. doi: 10.1016/S0022-1694(03)00257-9.

Hock R. 2005. Glacier melt: a review of processes and their modelling. *Progress in Physical Geography* **29**: 362–391.

Hock R, Jansson P. 2005. Modeling glacier hydrology. In Encyclopedia of Hydrological Sciences, Anderson MG (ed). John Wiley & Sons, Ltd.; 2647-2655.

Hock R, Jansson P, Braun LN. 2005. Modelling the response of mountain glacier discharge to climate warming. In Global Change and Mountain Regions (A State of Knowledge Overview), Huber UM, Bugmann HKM, Reasoner MA (eds). Springer: Dordrecht, Netherlands; 243–252.

Hock R, de Woul M, Radić V, Dyurgerov M. 2009. Mountain glaciers and ice caps around Antarctica make a large sea-level rise contribution. *Geophysical Research Letters* **36**: L07501. doi: 10.1029/2008GL037020.

Hodge SM, Trabant DC, Krimmel RM, Heinrichs TA, March RS, Josberger EG. 1998. Climate variations and changes in mass of three glaciers in western North America. *Journal of Climate* **11**: 2161–2179. doi: 10.1175/1520-0442(1998)011<2161:CVACIM>2.0.CO;2.

Hodgkins R, Cooper R, Wadham J, Tranter M. 2009. The hydrology of the proglacial zone of a high-Arctic glacier (Finsterwalderbreen, Svalbard): atmospheric and surface water fluxes. *Journal of Hydrology* **378**: 150–160. doi: 10.1016/j.jhydrol.2009.09.020.

Hoinkes H. 1970. Methoden und Möglichkeiten von Massenhaushaltsstudien auf Gletschern. Ergebnisse der Messreihe Hintereisferner (Ötztaler Alpen) 1953-1968. *Zeitschrift für Gletscherkunde und Glazialgeologie* **6**: 37–90.

Holmgren B. 1971. Climate and energy exchange on a sub-polar ice cap in summer. Arctic Institute of North America Devon Island Expedition 1961-1963. Uppsala: Meteorologiska Institutionen. *Uppsala Universitet Meddelande* **107**: Part A–E.

Hopkinson C, Young GJ. 1998. The effect of glacier wastage on the flow of the Bow River at Banff, Alberta, 1951-1993. *Hydrological Processes* **12**: 1745–1762.

Hopkinson C, Demuth MN. 2006. Using airborne lidar to assess the influence of glacier downwasting on water resources in the Canadian Rocky Mountains. *Canadian Journal of Remote Sensing* **32**: 212–222.

Hopkinson C, Chasmer L, Munro S, Demuth N. 2010. The influence of DEM resolution on simulated solar radiation-induced glacier melt. *Hydrological Processes* **24**: 775–788. doi: 10.1002/hyp.7531.

Huss M. 2011. Present and future contribution of glacier storage change to runoff from macroscale drainage basins in Europe. *Water Resources Research* **47**: W75011. doi: 10.1029/2010WR010299.

Intergovernmental Panel on Climate Change (IPCC). 2013. Climate Change 2013: The Physical Science Basis. Contribution of Working Group I to the Fifth Assessment Report of the Intergovernmental Panel on Climate Change. Stocker T, Qin D, Plattner G-K, Tignor M, Allen SK, Boschung J, Nauels A, Xia Y, Bex V, Midgley PM (eds). Cambridge University Press: Cambridge, United Kingdom and New York, New York, USA; 317–382.

Intergovernmental Panel on Climate Change (IPCC). 2014. Climate Change 2014: Impacts, Adaptation, and Vulnerability. Part A: Global and Sectoral Aspects. Field CB, Barros VR, Dokken DJ, Mach KJ, Mastrandrea MD, Bilir TE, Chattergee M, Ebi KL, Estrada YO, Genova RC, Girma B, Kissel ES, Levy AN, MacCracken S, Mastrandrea PR, White LL (eds). Cambridge University Press: Cambridge, United Kingdom and New York, New York, USA; 243.

Jansson P, Hock R, Schneider T. 2003. The concept of glacier storage: a review. *Journal of Hydrology* **282**: 116–129. doi: 10.1016/S0022-1694(03)00258-0.

Jost G, Moore RD, Menounos B, Wheate R. 2012. Quantifying the contribution of glacier runoff to streamflow in the upper Columbia River Basin, Canada. *Hydrology and Earth System Sciences* **16**: 849–60. doi: 10.5194/hess-16-849-2012.

Kargel, JS, Leonard GJ, Bishop MP, Kaab A, Raup B (eds). 2014. Global Land Ice Measurements from Space. Springer; 876 pp. ISBN: 978-3-540-79817-0.

Kaser G, Hardy DR, Mölg T, Bradley RS, Hyera TM. 2004. Modern glacier retreat on Kilimanjaro as evidence of climate change: observations and facts. *International Journal of Climatology* **24**: 329–339. doi: 10.1002/joc.1008.

Kaser G, Cogley JG, Dyurgerov MB, Meier MF, Ohmura A. 2006. Mass balance of glaciers and ice caps: Consensus estimates for 1961-2004. *Geophysical Research Letters* **33**: L19501. doi: 10.1029/2006GL027511.

Kendall M. 1975. Rank Correlation Methods, 4th Ed. Charles Griffin: London.

Kessler MA, Anderson RS, Stock GM. 2006. Modeling topographic and climatic controls of east-west asymmetry in Sierra Nevada glacier length during the Last Glacial Maximum. *Journal of Geophysical Research* **111**: F02002. doi: 10.1029/2005JF000365.

Khromova TE, Dyurgerov MB, Barry RG. 2003. Late-twentieth century changes in glacier extent in the Ak-shirak Range, Central Asia, determined from historical data and ASTER imagery. *Geophysical Research Letters* **30**: 1–5. doi: 10.1029/2003GL017233.

Klok EJ, Nolan M, van den Broeke MR. 2005. Analysis of meteorological data and the surface energy balance of McCall Glacier, Alaska, USA. *Journal of Glaciology* **51**: 451–461. doi: 10.3189/172756505781829241.

Krogh SA, Pomeroy JW, McPhee J. 2015. Physically based mountain hydrological modeling using reanalysis data in Patagonia. *Journal of Hydrometeorology* **16**: 172–193. doi: 10.1175/JHM-D-13-0178.1.

La Frenierre J, Mark BG. 2013. A review of methods for estimating the contribution of glacial meltwater to total watershed discharge. *Progress in Physical Geography* **38**: 173–200. doi: 10.1177/0309133313516161.

Lafrenière M, Sharp M. 2003. Wavelet analysis of inter-annual variability in the runoff regimes of glacial and nival stream catchments, Bow Lake, Alberta. *Hydrological Processes* **17**: 1093–1118.

Lawrence MG. 2005. The relationship between relative humidity and the dewpoint temperature in moist air. *American Meteorological Society* **86**: 223–233. doi: 10.1175/BAMS-86-2-225.

Le Meur E, Vincent C. 2003. A two-dimensional shallow ice-flow model of Glacier de Saint-Sorlin, France. *Journal of Glaciology* **49**: 527–538.

Leavesley GH, Lichty RW, Troutman BM, Saindon LG. 1983. Precipitation-runoff modeling system: User's manual. *USGS Water-Resources Investigations Report* 83; 206 pp.

Letréguilly A. 1988. Relation between the mass balance of western Canadian mountain glaciers and meteorological data. *Journal of Glaciology* **34**: 11–18.

Liu J, Curry JA, Dai Y, Horton R. 2007. Causes of the northern high-latitude land surface winter climate change. *Geophysical Research Letters* **34**: L14702. doi: 10.1029/2007GL030196.

López-Moreno JI, Revuelto J, Gilaberte M, Morán-Tejeda E, Pons M, Jover E, Esteban P, García C, Pomeroy JW. 2013. The effect of slope aspect on the response of snowpack to climate warming in the Pyrenees. *Theoretical and Applied Climatology* **117**: 207–219. doi: 10.1007/s00704-013-0991-0.

López-Moreno JI, Boike J, Sanchez-Lorenzo A, Pomeroy JW. 2016. *Global and Planetary Change* **146**: 10–21. doi: 10.1016/j.gloplacha.2016.09.006.

Lorenz EN. 1951. Seasonal and irregular variations of the Northern Hemisphere sea-level pressure profile. *Journal of Meteorology* **8**: 52–59.

MacGregor KR, Anderson R, Anderson S, Waddington E. 2000. Numerical simulations of glacial-valley longitudinal profile evolution. *Geology* **28**: 1031–1034.

Mann HB. 1945. Non-parametric tests against trend. *Econometrica* **13**: 163–171.

Mantua NJ, Hare SR, Zhang Y, Wallace JM, Francis RC. 1997. A Pacific interdecadal climate oscillation with impacts on salmon production. *Bulletin of the American Meteorological Society* **78**: 1069–1079. doi: 10.1175/1520-0477(1997)078<1069:APICOW>2.0.CO;2.

Mark BG, Seltzer GO. 2003. Tropical glacier meltwater contribution to stream discharge: A case study in the Cordillera Blanca, Peru. *Journal of Glaciology* **49**: 271–281. doi: 10.3189/172756503781830746.

Marks D, Domingo J, Susong D, Link T, Garen D. 1999. A spatially distributed energy balance snowmelt model for application in mountain basins. *Hydrological Processes* **13**: 1935–1959.

Marks D, Reba M, Pomeroy J, Link T, Winstral A, Flerchinger G, Elder K. 2008. Comparing simulated and measured sensible and latent heat fluxes over snow under a pine canopy to improve an energy balance snowmelt model. *Journal of Hydrometeorology* **9**: 1506–1522. doi: 10.1175/2008JHM874.1.

Marshall SJ, White EC, Demuth MN, Bolch T, Wheate R, Menounos B, Beedle MJ, Shea JM. 2011. Glacier water resources on the eastern slopes of the Canadian Rocky Mountains. *Canadian Water Resources Journal* **36**: 109–134. doi: 10.4296/cwrj3602823.

McLeod AI. 2011. Kendall: Kendall rank correlation and Mann-Kendall trend test. R package version 2.2. http://CRAN.R-project.org/package=Kendall.

Meier MF, Tangborn WV. 1961. Distinctive characteristics of glacier runoff. *USGS Professional Paper* **424**: 14–16.

Meier MF. 1969. Glaciers and water supply. *American Water Works Association* **61**: 8–12.

Meier MF. 1984. Contribution of small glaciers to global sea level. *Science* **226**: 1418–1422.

Meier MF, Dyurgerov MB, McCabe GJ. 2003. The health of glaciers: recent changes in glacier regime. *Climatic Change* **59**: 123–135. doi: 10.1023/A:1024410528427.

Meier MF, Dyurgerov MB, Rick UK, O'Neel S, Pfeffer WT, Anderson RS, Anderson SP, Glazovsky AF. 2007. Glaciers dominate eustatic sea-level rise in the 21st century. *Science* **317**: 1064–1067. doi:10.1126/science.1143906.

Mernild SH, Lipscomb WH, Bahr DB, Radić V, Zemp M. 2013. Global glacier changes: a revised assessment of committed mass losses and sampling uncertainties. *The Cryosphere* **7**: 1565–1577. doi: 10.5194/tc-7-1565-2013.

Mölg T, Maussion F, Yang W, Scherer D. 2012. The footprint of Asian monsoon dynamics in the mass and energy balance of a Tibetan glacier. *The Cryosphere* **6**: 1445–1461. doi: 10.5194/tc-6-1445-2012.

Moore RD. 1992. The influence of glacial cover on the variability of annual runoff, Coast Mountains, British Columbia, Canada. *Canadian Water Resources Journal* **17**: 101–109. doi: 10.4296/cwrj1702101.

Moore RD, McKendry IG. 1996. Spring snowpack anomaly patterns and winter climatic variability, British Columbia, Canada. *Water Resources Research* **32**: 623–632. doi: 10.1029/95WR03640.

Moore RD, Demuth MN. 2001. Mass balance and streamflow variability at Place Glacier, Canada in relation to recent climate fluctuations. *Hydrological Processes* **15**: 3473–3486.

Moore RD, Fleming SW, Menounos B, Wheate R, Fountain A, Stahl K, Holm K, Jakob M. 2009. Glacier change in western North America: influences on hydrology, geomorphic hazards and water quality. *Hydrological Processes* **23**: 42–61. doi: 10.1002/hyp.7162.

Müller F, Keeler CM. 1969. Errors in short-term ablation measurements on melting ice surfaces. *Journal of Glaciology* **8**: 91–105.

Natural Resources Canada. 2013. Canada Digital Elevation Model: Product Specifications – Edition 1.1; 18 pp.

Naz BS, Frans CD, Clarke GKC, Burns P, Lettenmaier DP. 2014. Modeling the effect of glacier recession on streamflow response using a coupled glacio-hydrological model. *Hydrology and Earth System Sciences* **18**: 787–802. doi: 10.5194/hess-18-787-2014.

Oerlemans J, Knap WH. 1998. A 1 year record of global radiation and albedo in the ablation zone of Morteratschgletscher, Switzerland. *Journal of Glaciology* **44**: 231–238.

Oerlemans J. 1989. A projection of future sea level. *Climatic Change* **15**: 151–174. doi: 10.1007/BF00138850.

Oerlemans J. 2010. The Microclimate of Valley Glaciers. Utrecht Publishing & Archiving Services: Utrecht; 138 pp.

Ohmura A. 2001. Physical basis for the temperature-based melt-index method. *Journal of Applied Meteorology* **40**: 753–761.

Ommanney C. 1980. The inventory of Canadian glaciers: procedures, techniques, progress and applications. *IAHS Publication* **126**: 35–44.

Østrem G. 1973. The transient snow-line and glacier mass balance in southern British Columbia and Alberta, Canada. *Geografiska Annaler* **55**: 96–106.

Østrem G. 1975. ERTS data in glaciology, an effort to monitor glacier mass balance from satellite imagery. *Journal of Glaciology* **15**: 403–415.

Østrem G, Brugman M. 1991. Glacier Mass Balance Measurements: a Manual for Field and Office Work. National Hydrology Research Institute Science Report No. 4. National Hydrology Research Institute and the Norwegian Water Resources and Electricity Board; 224 pp.

Parks Canada. 2002. Nahanni National Park Reserve Natural and Cultural Guide to Nah'a Dehe. Parks Canada: Gatineau Quebec; 122 pp.

Parks Canada. 2004. Nahanni National Park Reserve of Canada Management Plan. 56 pp.

Parks Canada. 2009. Nahanni National Park Reserve of Canada Nah'a Dehe State of the Park Report 2009: Fort Simpson, NT. Parks Canada: Gatineau Quebec; 67 pp.

Paterson WSB. 1994. The Physics of Glaciers, 3rd edition. Elsevier: Oxford.

Paul F, Haeberli W. 2008. Spatial variability of glacier elevation changes in the Swiss Alps obtained from two digital elevation models. *Geophysical Research Letters* **35**: 1–5. doi: 10.1029/2008GL034718.

Petersen L, Pellicciotti F. 2011. Spatial and temporal variability of air temperature on a melting glacier: Atmospheric controls, extrapolation methods and their effect on melt modeling, Juncal Norte Glacier, Chile. *Journal of Geophysical Research* **116**: D23109. doi: 10.1029/2011JD015842.

Petts GE, Gurnell AM, Milner AM. 2006. Eco-hydrology: new opportunities for research on glacier-fed rivers. In Peyto Glacier: One Century of Science, Demuth MN, Munro DS, Young GJ (eds). National Hydrology Research Institute Science Report No. 8: Saskatoon; 255–278. ISBN: 0-660-17683-1.

Pinheiro J, Bates D, DebRoy S, Sarkar D, R, Development Core Team. 2012. Nlme: linear and nonlinear mixed effects models. R package version 3. 1-105.

Pomeroy JW, Hedstrom NR, Parvainian J. 1999. The snow mass balance of Wolf Creek, Yukon: effects of snow sublimation and redistribution. In Wolf Creek Research Basin – Hydrology, Ecology, Environment (Proc. workshop held in Whitehorse, Yukon, Canada, 5-7 March, 1998). NHRI publication 37–121/1999E, Saskatoon, Saskatchewan, Canada; 15-29.

Pomeroy JW, Li L. 2000. Prairie and arctic areal snow cover mass balance using a blowing snow model. *Journal of Geophysical Research* **105**: 26,619–26.634.

Pomeroy JW, Gray DM, Brown T, Hedstrom NR, Quinton WL, Granger RJ, Carey SK. 2007. The cold regions hydrological model: a platform for basing process representation and model structure on physical evidence. *Hydrological Processes* **21**: 2650–2667. doi:10.1002/hyp.6787.

Pomeroy JW, Fang X, Shook K, Whitfield PH. 2013. Predicting in ungauged basins using physical principals obtained using the deductive, inductive, and abductive reasoning approach. In Putting Prediction in Ungauged Basins into Practice, Pomeroy JW, Whitfield PH, Spence C (eds). Canadian Water Resources Association; 42–62.

Pomeroy JW, MacDonald MK, Dornes PF, Armstrong R. 2016. Water budgets in ecosystems. In A Biogeoscience Approach to Ecosystems, Johnson EA, Martin YE (eds). Cambridge University Press: Cambridge, United Kingdom; 88–132.

Preuger JH, Kustas WP. 2005. Aerodynamic methods for estimating turbulent flows. *Micrometeorology in Agricultural Systems* **18**: 407–436.

Priestley CHB, Taylor RJ. 1972. On the assessment of surface heat flux and evaporation using large-scale parameters. *Monthly Weather Review* **100**: 81–92.

Quick MC, Pipes A. 1977. UBC watershed model. *Hydrological Sciences Bulletin* **221**: 153–161.

Quincey D, Bishop MP, Kääb A, Berthier E, Flach B, Bolch T, Buchroithner M, Kamp U, Khalsa SJS, Toutin T, Haritashya UK, Racoviteanu A, Schroder JF, Raup BH. 2014. Digital terrain modeling and glacier topographic characterization. In Global Land Ice Measurements from Space, Kargel J, Raup B (eds). Springer: Berlin, Germany; 113–144.

R Core Team. 2015. R: A language and environment for statistical computing. R Foundation for Statistical Computing, Vienna, Austria. URL http://www.R-project.org/.

Rabatel A, Dedieu J-P, Vincent C. 2005. Using remote-sensing data to determine equilibrium-line altitude and mass-balance time series: Validation on three French glaciers, 1994-2002. *Journal of Glaciology* **51**: 539–546. doi: 10.3189/172756505781829106.

Radić V, Bliss A, Beedlow AC, Hock R, Miles E, Cogley JG. 2013. Regional and global projections of twenty-first century glacier mass changes in response to climate scenarios from global climate models. *Climate Dynamics* **42**: 37–58. doi: 10.1007/s00382-013-1719-7.

Radić V, Hock R. 2014. Glaciers in the Earth's hydrological cycle: assessments of glacier mass and runoff changes on global and regional scales. *Surveys in Geophysics* **35**: 813–837. doi: 10.1007/s10712-013-9262-y.

Rood SB, Pan J, Gill KM, Franks CG, Samuelson GM, Shepherd A. 2008. Declining summer flows of Rocky Mountain rivers: Changing seasonal hydrology and probably impacts on floodplain forests. *Journal of Hydrology* **349**: 397–410. doi: 10.1016/j.jhydrol.2007.11.012.

Schneider T. 2000. Hydrological processes in the wet-snow zone of glacier: a review. *Zeitschrift fur Gletscherkunde und Glazialgeologie* **36**: 89–106.

Schuster C. 2001. Weathering crust processes on melting ice (Alberta, Canada). *Theses and Dissertations (Comprehensive).* Paper 489.

Schuster C, Young GJ. 2006. The derivation of runoff from the Peyto Glacier catchment. In Peyto Glacier: One Century of Science, Demuth MN, Munro DS, Young GJ (eds). National Hydrology Research Institute Science Report No. 8: Saskatoon; 226–254. ISBN: 0-660-17683-1. ISBN: 0-660-17683-1.

Seaberg SZ, Seaberg JZ, Hooke R, Leb R, Wiberg DW. 1998. Character of the englacial and subglacial drainage system in the lower part of the ablation area of Storglaciaren, Sweden, as revealed by dye-trace studies. *Journal of Glaciology* **34**: 217–227.

Searcy JK, Hardison CH. 1950. Double-mass curves. In Manual of Hydrology: Part I, General Surface Water Techniques. *Geological Survey Water-supply Paper* **1541–B***: 31–66.*

Sharp M, Burgess DO, Cawkwell F, Copland L, Davis JA, Dowdeswell EK, Dowdeswell JA, Gardner AS, Mair D, Wang L, Williamson SN, Wolken GJ, Wyatt F. 2014. Remote sensing of recent glacier changes in the Canadian Arctic. In Global Land Ice Measurements from Space, Kargel JS, Leonard GJ, Bishop MP, Kääb A, Raup BH (eds). Springer-Verlag: Berlin, Germany; 205–228.

Sheikh V, Bahremand A. 2011. Trends in precipitation and stream flow in the semi-arid region of Atrak River Basin, North Khorasan, Iran. *Desert* **16**: 49–60.

Shook K. 2015. MSCr: a package for reading data from the Meteorological Service of Canada (MSC) webserver and producing obs files for the Cold Regions Hydrological Modelling (CRHM) platform. URL www.usask.ca/hydrology/RPkgs.php/.

Shook K. 2016a. CRHMr: pre- and post- processing for the Cold Regions Hydrological Modelling (CRHM) platform. URL www.usask.ca/hydrology/RPkgs.php/.

Shook K. 2016b. Reanalysis: Creates Cold Regions Hydrological Modelling (CRHM) platform observations files from reanalysis data. URL www.usask.ca/hydrology/RPkgs.php/.

Sicart JE, Pomeroy JW, Essery RLH, Bewley D. 2006. Incoming longwave radiation to melting snow: observations, sensitivity and estimation in northern environments. *Hydrological Processes* **20**: 3697–3708. doi: 10.1002/hyp.6383.

Sicart JE, Hock R, Ribstein P, Litt M, Ramirez E. 2011. Analysis of seasonal variations in mass balance and meltwater discharge of the tropical Zongo Glacier by application of a distributed energy balance model. *Journal of Geophysical Research* **116**: D13105. doi: 10.1029/2010JD015105.

Sicart JE, Litt M, Helgason W, Tahar VB, Chaperon T. 2014. A study of the atmospheric surface layer and roughness lengths on the high-altitude tropical Zongo glacier, Bolivia. *Journal of Geophysical Research: Atmospheres* **119**: 3793–3808. doi: 10.1002/2013JD020615.

Singh P, Singh VP. 2001. Snow and Glacier Hydrology. Kluwer Academic Publishers: Dordrecht, Netherlands; 742 pp.

Singh P, Arora M, Goel NK. 2006. Effect of climate change on runoff of a glacierized Himalayan basin. *Hydrological Processes* **20**: 1979–1992. doi: 10.1002/hyp.5991.

Smeets CJPP, van den Broeke, MR. 2008. Temporal and spatial variations of the aerodynamic roughness length in the ablation zone of the Greenland ice sheet. *Boundary-Layer Meteorology* **128**: 315–338. doi: 10.1007/s10546-008-9291-0.

Spence C. 2002. Streamflow variability (1965 to 1998) in five Northwest Territories and Nunavut rivers. *Canadian Water Resources Journal* **27**: 135–154. doi: 10.4296/cwrj2702135.

St. Jacques J-M, Sauchyn DJ, Zhao Y. 2010. Northern Rocky Mountain streamflow records: Global warming trends, human impacts or natural variability? *Geophysical Research Letters* **37**: L06407 1–5. doi: 10.1029/2009GL042045.

Stahl K, Moore RD. 2006. Influence of watershed glacier coverage on summer streamflow in British Columbia, Canada. *Water Resources Research* **42**: W06201. doi: 10.1029/2006WR005022.

Svobodo F, Paul F. 2009. A new glacier inventory on southern Baffin Island, Canada, from ASTER data: I. Applied methods, challenges and solutions. *Annals of Glaciology* **50**: 11–21. doi: 10.3189/172756410790595912.

Tangborn WV. 1984. Prediction of glacier derived runoff for hydroelectric development. *Geografiska Annaler* **66A**: 257–265.

Trenberth KE. 1976. Spatial and temporal variations of the Southern Oscillation. *Quarterly Journal of the Royal Meteorological Society* **102**: 639–653.

Trubilowicz JW, Shea JM, Jost G, Moore RD. 2016. Suitability of North American Regional Reanalysis (NARR) output for hydrologic modelling and analysis in mountainous terrain. *Hydrological Processes.* doi: 10.1002/hyp.10795.

Van den Broeke MR. 1997. Structure and diurnal variation of the atmospheric boundary layer over a mid-latitude glacier in summer. *Journal of Boundary Layer Meteorology* **83**: 183–205.

Verseghy, D. 1991. Class – A Canadian land surface scheme for GCMS. I. Soil model. *International Journal of Climatology* **11**: 111–133. doi: 10.1002/joc.3370110202.

Vincent LA, Zhang X, Brown RD, Feng Y, Mekis E, Milewska EJ, Wan H, Wang XL. 2015. Observed trends in Canada's climate and influence of low-frequency variability modes. *Journal of Climate* **28**: 4545–4560. doi: 10.1175/JCLI-D-14-00697.1.

Vuichard N, Papale D. 2015. Filling the gaps in meteorological continuous data measured at FLUXNET sites with ERA-Interim reanalysis. *Earth Systems Science Data* **7**: 157–171. doi: 10.5194/essd-7-157-2015.

Wallace JM, Thompson DWJ. 1998. The Arctic Oscillation signature in the wintertime geopotential height and temperature fields. *Geophysical Research Letters* **25**: 1297–1300. doi: 10.1029/98GL00950.

Walmsley JL, Taylor PA, Salmon JR. 1989. Simple guidelines for estimating wind speed variations due to small-scale topographic features – An update. *Climatological Bulletin* **23**: 3–14.

Walters RA, Meier, MF. 1989. Variability of glacier mass balances in western North America. *Geophysical Monograph Series* **55**: 365–374.

Wendler G, Weller G. 1974. A heat-balance study on McCall Glacier, Brooks Range, Alaska: a contribution to the International Hydrological Decade. *Journal of Glaciology* **13**: 13–26.

Whitfield PH, Moore RD, Fleming SW, Zawadzki A. 2010. Pacific Decadal Oscillation and the hydroclimatology of Western Canada – Reviews and prospects. *Canadian Water Resources Journal* **35**: 1–28. doi: 10.4296/cwrj3501001.

Wilcox R, Schönbrodt F. 2013. The WRS package for robust statistics in R. R package version 0.20.

Williams RS Jr., Ferrigno JG. 2002. Glaciers of Canada: Introduction. Satellite Image Atlas of Glaciers of the World, Vol. J: North America (USGS Survey Professional Paper 1386-J): J1– J26.

Woo MK, Thorne R. 2003. Streamflow in the Mackenzie Basin, Canada. *Arctic* **56**: 328–340.

World Glacier Monitoring Service (WGMS). 1998. Into the second century of worldwide glacier monitoring: prospects and strategies. Haeberli W, Hoezle M, Suter S (eds). UNESCO Studies and Reports in Hydrology 56, UNESCO: Paris; 227 pp.

Yang D, Goodison BE, Metcalfe JR. 1998. Accuracy of NWS 8" Standard nonrecording precipitation gauge: results and application of WMO intercomparison. *Journal of Atmospheric & Oceanic Technology* **15**: 54–68.

Yue S, Pilon P Phinney B, Cavadias G. 2002. The influence of autocorrelation on the ability to detect trend in hydrological series. *Hydrological Processes* **16**: 1807–1829. doi: 10.1002/hyp.1095.

Zambrano-Bigiarini M. 2014. hydroGOF: Goodness-of-fit functions for comparison of simulated and observed hydrological time series. R package version 0.3-8. http://CRAN.R-project.org/package=hydroGOF.

Zemp M, Armstrong R, Gärtner-Roer I, Haeberli W, Hoelzle M, Kääb A, Kargel JS, Khalso SJS, Leonard GJ, Paul F, Raup BH. 2014. Introduction: Global glacier monitoring – a long-term task integrating in situ observations and remote sensing. In Global Land Ice Measurements from Space, Kargel J, Raup B (eds). Springer: Berlin, Germany; 1–21.

Zhao L, Gray DM. 1999. Estimating snowmelt infiltration into frozen soils. *Hydrological Processes* **13**: 1827–1842.

Zhao Y, Ciais P, Peylin P, Viovy N, Longdoz B, Bonnefond JM, Rambal S, Klumpp K, Olioso A, Cellier P, Maignan F, Eglin T, Calvet JC. 2012. How errors on meteorological variables impact simulated ecosystem fluxes: A case study for six French sites. *Biogeosciences* **9**: 2537–2564. doi: 10.5194/bg-9-2537-2012.

Zhou J, Pomeroy JW, Zhang W, Cheng G, Wang G, Chen C. 2014. Simulating cold regions hydrological processes using a modular model in the west of China. *Journal of Hydrology* **509**: 13–24. doi: 10.1016/j.jhydrol.2013.11.013.

APPENDIX A: Equations and Derivations

Aerodynamic Roughness Height of Glacier Ice

The aerodynamic roughness height, z_0, of the glacier was calculated without (Method I) and with (Method II) a stability correction. For this analysis, a subset of the on-ice station observations were used. Hourly observations were analyzed and the analysis was performed on containing conventional wind and temperature profiles ($T_2 < T_1$ and $U_2 > U_1$), where T denotes hourly temperature, U denotes wind speed, and the subscripts 2 and 1 denote the upper and lower measurement locations, respectively. This left roughly 200 time steps for analysis.

Method I:

The Prandtl-von Kármán Wind Speed Profile is given by

$$u_z = \frac{u^*}{\kappa} \ln \frac{z - d_0}{z_0} \tag{A.1}$$

Where, u_z is the wind speed at height z, u^* is the friction velocity, κ is the von Kármán constant (0.4), d is the displacement height $0.67 \times h_{veg}$ (Prueger and Kustas, 2005), z_0 is the aerodynamic roughness height. The vegetation height, h_{veg}, was estimated to be 0.5 m, based on the observed glacier surface surrounding the on-ice meteorological station. For a mast with two wind measurement heights, this equation can also be written as

$$(u_2 - u_1) = \frac{u^*}{\kappa} ln \left(\frac{z_2 - d_0}{z_1 - d_0}\right) \tag{A.2}$$

Where the subscripts denote the upper (9.2 m) and lower (1.4 m) measurement heights.

Using the observations and an assumed d_0, the friction velocity was determined. The roughness height, z_0, was then calculated. Results are shown below.

Method II:

Flux Equations

The flux equations for friction velocity, u_* and sensible heat flux, $Q_H$with stability corrections are:

$$u_* = u\kappa\left[\ln\left(\frac{z-d_0}{z_{0m}}\right) - \Psi_m\right]^{-1} \quad \text{(A.3)}$$

Where u is wind velocity at the reference height, κ is the von Karman constant, d_0 is displacement height taken as $0.67 \times h_{veg}$ (Prueger and Kustas, 2005), and Ψ_m is the stability correction.

$$Q_H = -a_h\kappa u_*\rho c_p(T_2 - T_1)\left[ln\left(\frac{z_2-d_0}{z_1-d_0}\right) - \Psi_h\right]^{-1} \quad \text{(A.4)}$$

Where a_h and a_v are assumed to be 1, ρ is density of air at 1.2 kg/m^3, c_p is specific heat capacity of air at 1005 Jkg^{-1}K^{-1}, T_2 and T_1 (K) are the upper and lower measurement heights, respectively, and Ψ_h is the stability correction.

Monin-Obukhov Similarity Theory

From Prueger and Kustas (2005), Obukhov length, L, is given by

$$L = -\frac{T_r u_*^3 \rho c_p}{\kappa g Q_H} \quad \text{(A.5)}$$

Where g is acceleration due to gravity and the other variables have been previously defined.

The indicator of stability is given by

$$\zeta = \frac{z}{L} \quad \text{(A.6)}$$

If $\zeta < 0$, conditions are unstable, If $\zeta \approx 0$, conditions are neutral, and if If $\zeta > 0$, conditions are stable. For neutral conditions, there is no stability correction soΨ_m, Ψ_h, and Ψ_v are equal to zero.

For unstable conditions, corrections are found in Foken (2008), page 48:

$$\Psi_m(\zeta) = \ln\left[\left(\frac{1+x^2}{2}\right)\left(\frac{1+x^2}{2}\right)^2\right] - 2\tan^{-1}x + \frac{\pi}{2} \quad \text{(A.7)}$$

$$\Psi_h(\zeta) = 2\ln\left(\frac{1+y}{2}\right) \quad \text{(A.8)}$$

Where, $x = (1 - 19.3\zeta)^{1/4}$ and $y = 0.95(1 - 11.6\zeta)^{1/2}$ and it is assumed that $\Psi_h(\zeta) = \Psi_v(\zeta)$.

For stable conditions, corrections are found in Foken (2008):

$$\Psi_m(\zeta) = -6\zeta \quad \text{(A.9)}$$

$$\Psi_h(\zeta) = -7.8\zeta \quad \text{(A.10)}$$

Numerical Model

A numerical model was written in R. An iterative solution was used to solve for the Obukhov Length, L. For the iteration, initial conditions were set to be neutral and error tolerance was 10^{-3}. Model outputs are friction velocity, u_*, sensible heat flux, Q_H, latent heat flux, Q_E, and the Monin-Obukhov similarity indicator, ζ.

Results

Results of both methods are shown in Figures A.1 and A.2. Without the stability correction, the mean and median roughness heights were found to be 18 mm and 3.2 mm, respectively. With the stability correction, the mean and median roughness heights were found to be 48 mm and 15 mm, respectively. Sicart et al. (2011) used 10 mm at the Zongo glacier. Smeets et al. (2008) found a z_0 ranging from 0.1 mm to 10 mm for the ablation area of the Greenland ice sheet. Given the analysis and the values found in the literature, it was determined that a value of 3 mm would be used for the ablation zone in the model.

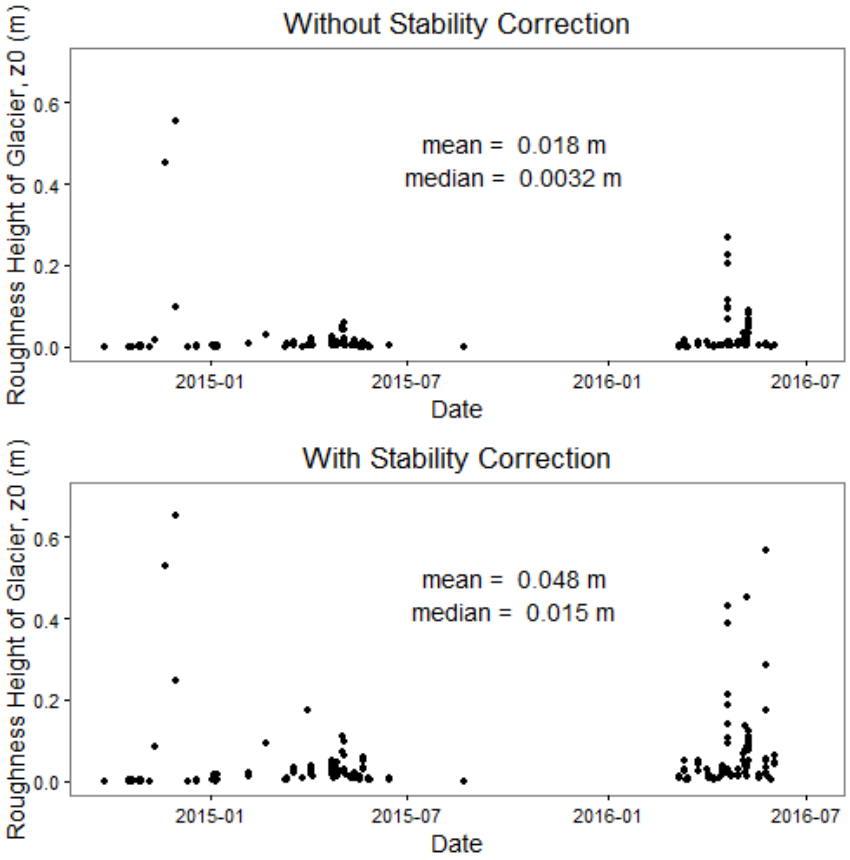

Figure A.1: Calculated roughness height of the glacier without (top) and with (bottom) the stability correction based on two measurement heights of temperature and wind speed at the on-ice meteorological station

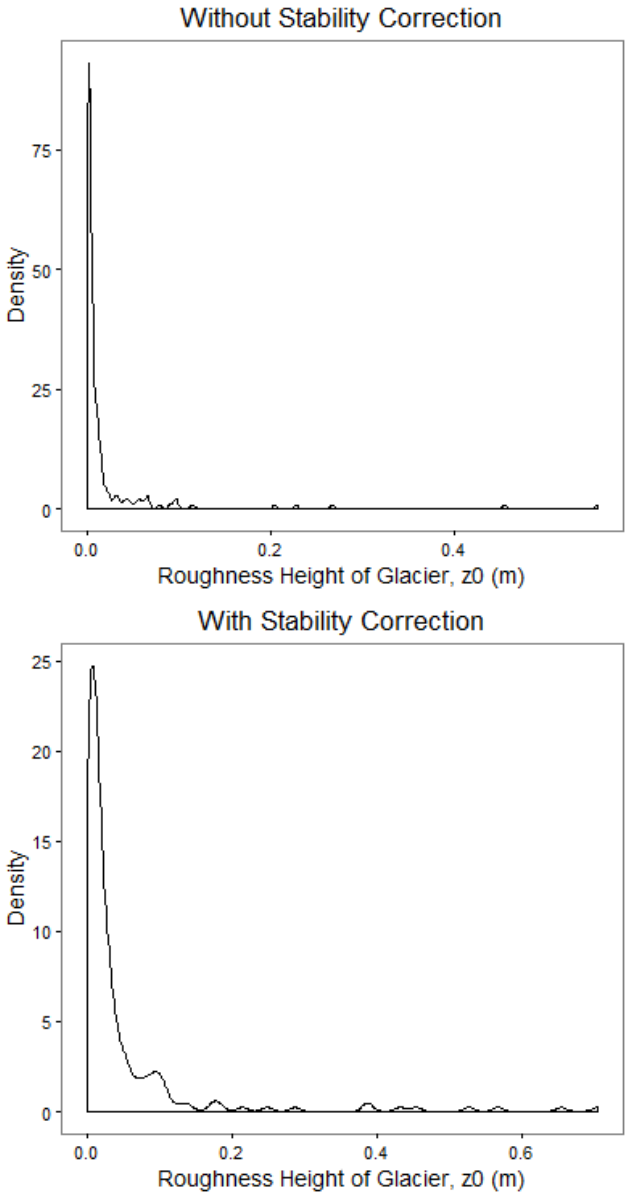

Figure A.2: Density of resulting roughness height calculations without (top) and with (bottom) the stability correction based on two measurement heights of temperature and wind speed at the on-ice meteorological station

Wind Undercatch Corrections

The Catch Ratios used in the undercatch corrections are from Table 3 in Goodison et al. (1998). The OTT Pluvio1 with Alter shield was approximated as the NWS 8" gauge with an alter shield (equations A.11 and A.13). The unshielded stand pipe gauge was approximated as the NWS 8" unshielded gauge (equations A.12 and A.14). Yang et al. (1998) defined mixed precipitation occurring when the average daily air temperature is between 0 and 3°C. The catch ratio is defined by the wind speed, W_s, in m/s. The corrections for solid precipitation are:

$$CR_{NWS\,8-Alter\,Shield} = \exp\left(4.61 - 0.04{W_s}^{1.75}\right) \quad \text{(A.11)}$$

$$CR_{NWS\,8-unshielded} = \exp\left(4.61 - 0.16{W_s}^{1.28}\right) \quad \text{(A.12)}$$

The corrections for mixed precipitation are:

$$CR_{NWS\,8-Alter\,Shield} = 101.04 - 5.62W_s \quad \text{(A.13)}$$

$$CR_{NWS\,8-unshielded} = 100.77 - 8.34W_s \quad \text{(A.14)}$$

Conversion to Vapour Pressure

From Lawrence (2005), the dew point temperature is converted to relative humidity using air temperature:

$$RH = 100 \times \frac{e^{\left(\frac{At_d}{B+t_d}\right)}}{e^{\left(\frac{At}{B+t}\right)}} \quad \text{(A.15)}$$

Where A = 17.625 and B = 243.04°C.

Ice Thickness Estimation

Ice thickness of the glacier was estimated according to Frey et al., 2014. The average basal shear stress, τ, along the central flow line, f, is calculated by:

$$\tau[kPa] = \begin{cases} 0.5 + 159.8\Delta H - 43.5(\Delta H)^2 : \Delta H \leq 1.6\ km \\ 150 : \Delta H > 1.6\ km \end{cases} \quad \text{(A.16)}$$

Where ΔH is the change in elevation over the glacier. The ice thickness along the central flowline, h_f, is calculated by Haeberli and Hoelzle (1995) as:

$$h_f = \frac{\tau}{f \rho g\, sin(\alpha)} \quad \text{(A.17)}$$

Where f is a shape factor of 0.8 for valley glaciers (Cuffey and Paterson, 2010), ρ is the density of the glacier ice (900 kg/m^3), g is acceleration due to gravity, and α is the average slope of the glacier. The mean ice thickness of the glacier, h_F, is then found by:

$$h_F = h_f \left(\frac{\pi}{4}\right) \quad \text{(A.18)}$$

Derivation of Error Estimation for V-A Scaling

The error in the volume estimation using the V-A scaling relationship is due to both the error in the scaling relationship and the area measurement error from delineating the glacier boundaries in ArcGIS. The error in the scaling relationship is 34% when it is applied to a single glacier (Bahr et al., 2015). The error in the area measurement is derived below:

Glacier volume, V (10^6 m^3), of an alpine valley glacier is related to its area, A (10^6 m^3), by:

$$V = cA^{\gamma}, \tag{A.19}$$

Where scaling parameters c and γ are equal to 28.5 and 1.375 (for valley glaciers). The error in volume due to measurement errors in the area is:

$$dV = \left(\frac{\delta V}{\delta A}\right) dA \tag{A.20}$$

$$dV = c\gamma A^{\gamma-1} dA \tag{A.21}$$

Where $\frac{\delta V}{\delta A}$ is the partial derivative of volume with respect to area and dA is the area in the measurement. The resolution of the Landsat imagery is 30 m and this value is taken to be the error in one dimension. Therefore, dA is taken to be (30 m)^2 or 900 m^2.

$$dV = (28.5)(1.375)A^{0.375}(0.0009 \times 10^6 m^2) \tag{A.22}$$

Table A.1 shows the calculations for the total error of the glacier volume for the 1984 area and the 2014 area.

Table A.1: Area in volume estimates for the Bologna Glacier

Year	Glacier area (x 10^6 m^2)	Glacier volume (x 10^6 m^2)	Error in volume from area measurements (x 10^6 m^3)	Error in scaling relationship from Bahr et al. (2015) (x 10^6 m^3)	Total error in volume (x 10^6 m^3)
1984	18.7	1598	0.106	543	543
2014	16.0	1288	0.100	438	438

Therefore, in 1984 the glacier volume is 1598 ± 543 x 10^6 m^3 and in 2014 the glacier volume is 1288 ± 438 x 10^6 m^3. The difference in volume between these two years is 310 x 10^6 m^3. The combined error in the difference is:

$$Total\ error = \sqrt{((543 \times 10^6 m^3)^2 + (438 \times 10^6 m^3)^2} \quad \text{(A.23)}$$

$$Total\ error = 698\ \times 10^6 m^3 \quad \text{(A.24)}$$

Therefore, the glacier volume change between 1984 and 2014 is 310 ± 698 x 10^6 m^3.

APPENDIX B: Reanalysis Comparison

Table B.1: Metadata of reanalysis options considered for this project

Product	Source	Years Available	Resolution	Lowest time step	File Format
ERA-Interim	ECMWF	1979 – 2016	0.125° x 0.125°	3 hourly	netCDF
NARR	NCEP	1979 – 2016	32 km	3 hourly	netCDF or GRIB
WFD	WATCH	1901 – 2001	0.5° x 0.5°	3 or 6 hourly	NC
WFDEI	WATCH	1979 – 2012	0.5° x 0.5°	3 hourly	NC

APPENDIX C: Wind Roses

Wind roses shown in Figures C.1 to C.4 were plotted using the R package "openair" (Carslaw and Ropkins, 2015).

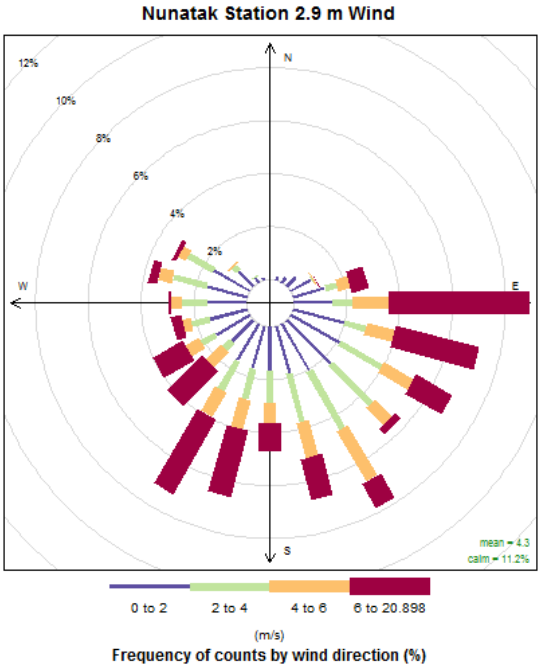

Figure C.1: Wind rose for Nunatak Station wind observations at 2.9 m

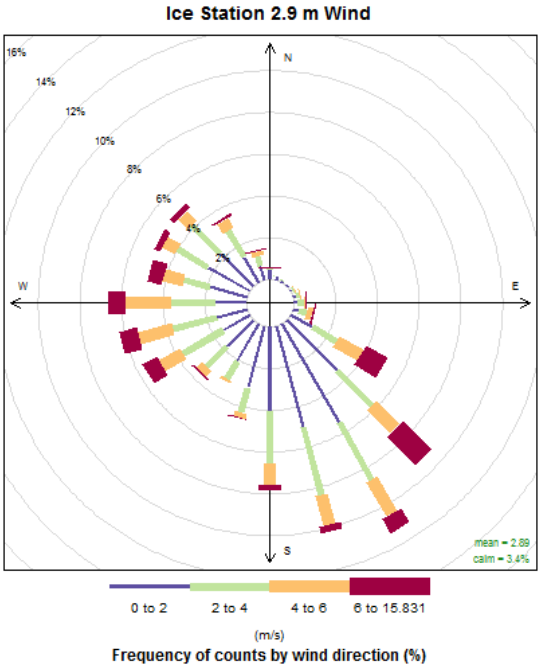

Figure C.2: Wind rose for Ice Station wind observations at 2.9 m

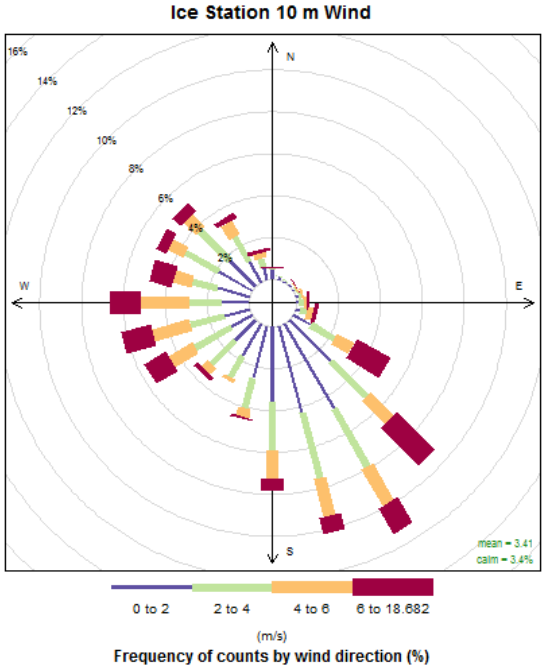

Figure C.3: Wind rose for Ice Station wind observations at 10 m

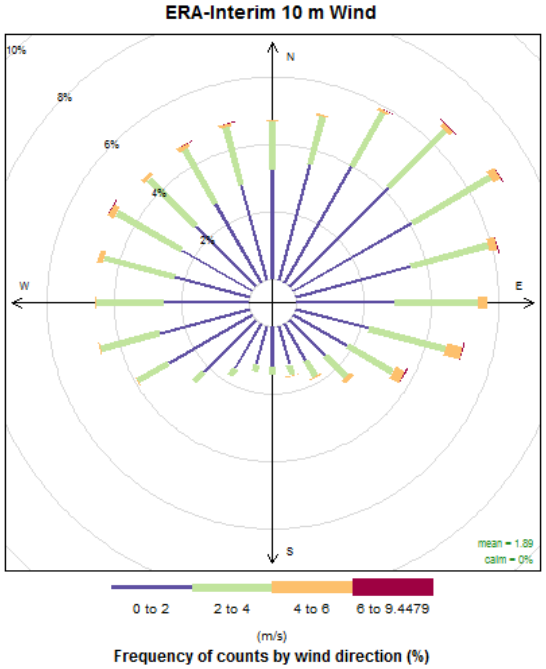

Figure C.4: Wind rose for uncorrected ERA-Interim data at 10 m

APPENDIX D: CRHM Specifications

CRHM version 01/30/2017 was used in this study. Module names and release dates are given in Table D.1. Model parameters are given in Table D.2.

Table D.1: Modules used in the Bologna Glacier basin CRHM

Module Process	Module Name	Release Date
Global radiation	global	04/19/13
Observations	obs	01/13/17
Basin specifications	basin	02/24/12
Sunshine hours	calcsun	10/01/13
Slope radiation	Slope_Qsi#1	07/14/11
Wind	walmsley_wind	07/30/08
Longwave radiation	longVt	02/10/16
All-wave radiation	netall	03/22/16
Evaporation	evap	09/26/13
Radiation under canopy	CanopyClearing#3	09/27/16
Albedo	albedo_Richard	03/19/15
Glacier	glacier#1	01/28/17
Snow Transport	pbsmSnobal#1	01/05/17
Avalanche	SWESlope	06/02/16
Snowmelt	SnobalCRHM#1	11/21/16
Soil infiltration	frozenAyers	08/02/16
Soil moisture	Soil	01/12/17
Routing	Netroute	11/26/15

Table D.2: Full set of parameters for the Bologna Glacier basin CRHM

Module	Parameter	Firn	Ice	Land
Shared	Basin area, basin_area (km^2)		24.4	
	HRU area, hru_area (km^2)		Refer to Table 3.10	
	HRU aspect, hru_ASL (°)		Refer to Table 3.10	
	HRU elevation, hru_elev (m)		Refer to Table 3.10	
	HRU slope, hru_GSL (°)		Refer to Table 3.10	
	HRU latitude, hru_lat (°)	62.11	62.11	62.11
	Vegetation height (m)	0.5	0.5	0.3
	Inhibit evaporation, inhibit_evap (-)	0	0	0
	HRU routing process order, order (-)		Varies	
	Maximum depression storage, Sdmax (mm)	0	0	2-5
	Maximum soil moisture, soil_moist_max (mm)	0	0	125
	Maximum soil recharge, soil_rechr_max (mm)	0	0	25
	Wind measurement height, Zwind (-)	10	10	10
Albedo	Albedo decay time constant for cold snow, a (s)	1.08e-7	1.08e-7	1.08e-7
	Albedo decay time constant for melting snow (s)	7.2e5	7.2e5	7.2e5
	Initial albedo for bare ground, Albedo_Bare (-)	0.17	0.17	0.17
	Initial albedo for snow cover, Albedo_Snow (-)	0.85	0.85	0.85
	Maximum albedo for fresh snow, amax (-)	0.84	0.84	0.84
	Minimum albedo for aged snow, amin (-)	0.5	0.5	0.5
	Minimum snowfall to refresh snow albedo, smin (mm/int)	5	7	10
Basin	Basin name, basin_name		Bologna1984, Bologna2014, Bologna2015	
	HRU names, hru_names		Varies	
Canopy Clearing	Canopy albedo, Alpha_c (-)	0.1	0.1	0.1
	Canopy enhancement parameter, B_canopy	0.038	0.038	0.038
	CanopyClearing (clearing – 1)	1	1	1
	Leaf area index, LAI (-)	0.1	0.1	0.1
	Maximum canopy snow interception load, Sbar (kg/m^2)	6.6	6.6	6.6
	If ice-bulb temp >= t: canopy snow is unloaded as snow, unload_t (°C)	1	1	1
	If ice-bulb temp >= t: canopy snow is unloaded as water, unload_t_water (°C)	4	4	4
	Roughness height of snow, z0snow (m)	0.01	0.01	0.01
	Temperature measurement height, Zref (m)	1.4	1.4	1.4
	Ventilation and wind speed height (z/Ht), Zvent (-)	0.75	0.75	0.75
Evap	Evaporation method, evap_type (Granger – 0)	0	0	0

	Fraction to ground flux (-)	0.1	0.1	0.1
Frozen Ayers	Environment coefficient, C (-)	2	2	2
	Groundcover (-)	Bare soil	Bare soil	Bare soil
	Initial soil temperature, hru_tsoil (K)	269.1	269.1	269.1
	Surface saturation, S_o (mm^3/mm^3)	1	1	1
	Initial soil saturation, $S_{i\,(}mm^3/mm^3$)	0.5	0.5	0.5
	Texture (-)	Coarse/medium over coarse	Coarse/medium over coarse	Soil over shallow bedrock
	Overnight minimum to cause ice lens after major melt, t_ice_lens (°C)	-20	-20	-20
Glacier	Inhibit melt until this Julian day, delay_melt (-)	0	0	0
	Adjust glacier surface elevation (1) / Do not adjust glacier surface elevation (0), Elev_Adj_glacier_surf	0	0	0
	Firn lag delay, firnLag (h)	-	4	-
	Firn storage constant, firnStorage (d)	-	2	-
	Firn albedo, firn_Albedo (-)	-	0.5	-
	Ice lag delay, iceLag (h)	1	-	-
	Ice storage constant, icestorage (d)	0	-	-
	Ice albedo, ice_Albedo (-)	0.35	-	-
	Density of glacier ice, ice_dens (kg/m^3)	900	-	-
	Initial water equivalent of glacier ice, ice_init (m)	100-500	-	-
	Mean annual accumulation of glacier SWE, SWEA (m/yr)	0.1-2	0.1	0.1
	Snowmelt lag delay, SWELag (h)	24	24	24
	Snowmelt storage constant, SWEstorage (d)	1	1	1
	Convert any SWE to firn on Julian day, SWE_to_firn_Julian (-)	274	274	274
	Mean annual temperature of glacier, TKMA (°C)	-5 - -3	-2 - -1	-1
Global	Solar time offset from local time (h)	1.6	1.6	1.6
LongVt	Terrain emissivity, epsilon_s (-)	0.98	0.98	0.98
	Terrain view factor, Vt (-)	0.01-0.05	0.01-0.05	0.01-0.05
Netroute	Groundwater storage constant, gwKstorage (d)	0	0	0
	Groundwater lag delay, gwLag (h)	0	0	0
	Destination of groundwater outflow, gwwhereto (surface basinflow – 100)	100	100	100
	Aggregated storage constant, Kstorage (d)	0	0	0
	Aggregated lag delay, Lag (h)	0	0	0
	Runoff storage constant, runKstorage (d)	0.1	0.1	0.1
	Runoff lag delay, runLag (h)	2	2	2

	Bypass depressional storage (no bypass – 0)	0	0	0
	Bypass recharge layer (no bypass – 0)	0	0	0
	Subsurface runoff storage constant, ssrKstorage (d)	2	2	2
	Subsurface runoff lag delay, ssrLag (h)	5	5	5
	Destination of surface water outflow, whereto (basin outflow – 0)	0	0	0
Obs	Precipitation under catch adjustment, catchadjust (-)	None	None	None
	Climate change control, ClimChng_flag (-)	Maintain RH	Maintain RH	Maintain RH
	Lapse rate, lapse_rate (°C/100 m)	0.65	0.65	0.65
	Measurement altitude, obs_elev (m)	2159	2159	2159
	Temporal precipitation distribution, ppt_daily_distrib	First interval	First interval	First interval
	Precipitation height adjustment, precip_elev_adj (1/100 m)	0.01	0.01	0.01
	Snow/rain determination, snow_rain_determination	Harder	Harder	Harder
PbsmSnobal	Stalk diameter, A_S (m)	0	0	0
	Distribution fractions, distrib (-)	1	1	1
	Fetch distance, fetch (m)	350-1100	350-1500	300-500
	Inhibit blowing snow (do not inhibit – 0)	0	0	0
	Inhibit sublimation (do not inhibit – 0)	0	0	0
	Vegetation number density, N_S (m^{-2})	1	1	1
Snobal CRHM	Ground flux used when observed ground flux not available, hru_F_g (W/m^2)	0	0	0
	Density of falling snow, hru_rho_snow (kg/m^3)	100	100	100
	Ground temperature when observed ground temperature not available, hru_T_g	0	0	0
	Thermal conductivity of wet sand, KT_sand($Jm^{-1}s^{-1}K^{-1}$)	1.65	1.65	0.08
	Maximum liquid water content, max_h2o_vol (m^3/m^3)	0.01	0.01	0.01
	Maximum active layer thickness, max_z_s_0 (m)	0.1	0.1	0.1
	Handle rain or snow, rain_soil_snow (-) (rain and snow when SWE > 0.02 m – 1)	0	0	0
	Ground flux, T_g_or_G_flux (calculate ground flux from ground temperature – 0)	0	0	0
	Roughness height, z_0 (m)	0.001	0.003	0.01
	Height of air temperature and vapour pressure measurement, z_T (m)	1.4	1.4	1.4
	Height of wind measurement, z_u (m)	10	10	10

Soil	Coverage type, cov_type (-)	Bare soil (no evaporation)	Bare soil (no evaporation)	Crops (recharge layer)
	Initial groundwater, gw_init (mm)	0	0	0
	Daily groundwater drainage from groundwater reservoir, gw_K (mm/d)	0	0	0
	Maximum available water holding capacity of groundwater reservoir, gw_max (mm)	0	0	0
	Daily subsurface runoff from soil column, lower_ssr_K (mm/d)	0.1	0.1	0.1
	Daily subsurface drainage from recharge, rechr_ssr_K (mm/d)	1	1	1
	Initial depression storage, Sdinit (mm)	0	0	0
	Daily depression storage groundwater drainage, Sd_gw_K (mm/d)	0	0	0
	Daily depression storage subsurface runoff drainage factor, Sd_ssr_K (mm/d)	0	0	0
	Maximum soil water excess routed to groundwater, soil_gw_K (mm/d)	0	0	0
	Initial soil water capacity, soil_moist_init (mm)	0	0	125
	Initial value for soil recharge zone, soil_rechr_init (mm)	0	0	25
	Soil column excess to interflow/runoff (interflow – 0)	0	0	0
	Soil withdrawal function	Clay	Clay	Sand
	Limit transpiration to recharge layer only (0)	0	0	0
SWESlope	Minimum SWE holding depth, Hd_min (mm)	50	50	50
	Density of snow, snow_density (kg/m^3)	100	100	100
	Use rho from Snobal, use_rho (1)	1	1	1
	Destination HRU of slides from this HRU		Varies	
Walmsley Wind	Coefficient for wind speed change due to topography, A (-) (2D escarpments – 2.5)	2.5	2.5	2.5
	Coefficient for wind speed change due to topography, B (-)(2D escarpments – 0.8)	0.8	0.8	0.8
	Upwind length at half height, L (m)	1000	1000	1000
	Walmsley height, Walmsley_Ht (m)	50	50	50

APPENDIX E: Study Site Photographs

Figure E.1: Surveying the glacier margins in August 2014 (reproduced with the permission of M. N. Demuth, Natural Resources Canada, 2015)

Figure E.2: Porcupine carcass found on the Bologna Glacier in August 2015 (reproduced with the permission of M. N. Demuth, Natural Resources Canada, 2015)

Figure E.3: Caribou skull found on the Bologna Glacier in August 2014

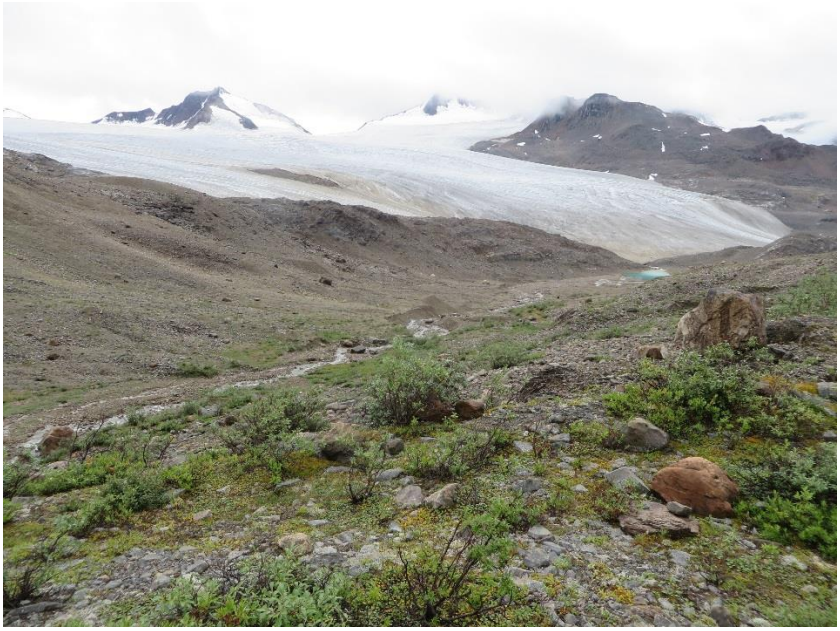

Figure E.4: Bologna Glacier pictured from the North

Figure E.5: Proglacial stream at the Bologna Glacier in August 2014

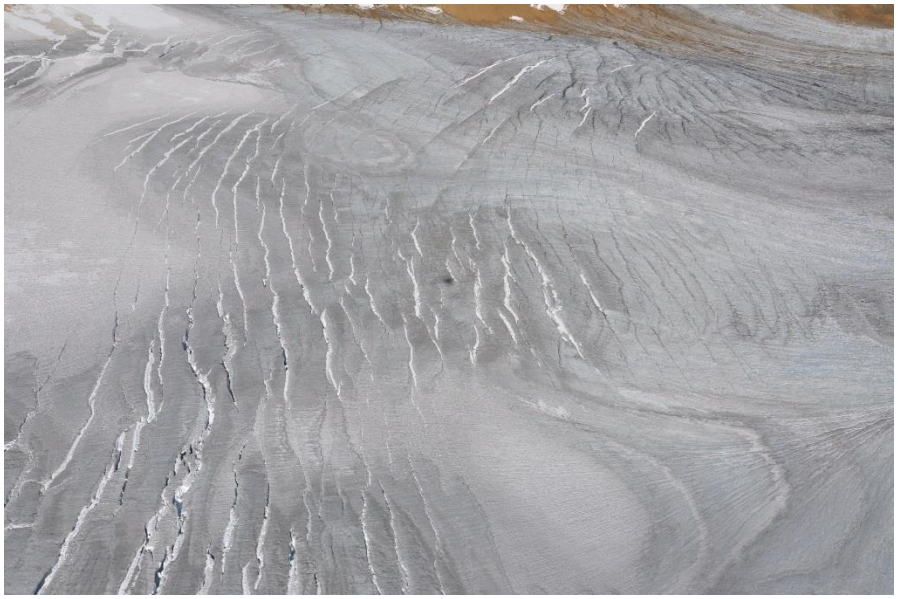

Figure E.6: Glacier surface taken from helicopter (reproduced with the permission of May Guan, 2014)

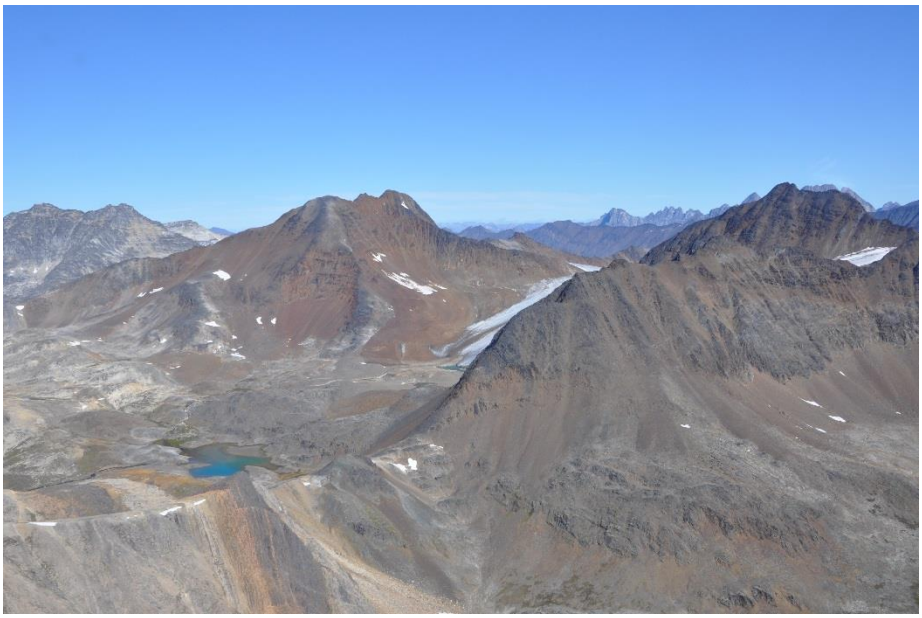

Figure E.7: Bologna Glacier basin from the west (reproduced with the permission of May Guan, 2014)